RTG Seminar: Continuum Mechanics

Michael Neunteufel

May 15, 2025

Contents

Introduction

This seminar on *Continuum mechanics* aims to derive and discuss models, finite elements, and numerical methods for problems arising in continuum mechanics, especially elasticity, beams, plates, and shells.

The first part is devoted to classical (nonlinear) elasticity. It will turn out that this approach has severe weaknesses when one of the domain dimensions is significantly smaller than the others. Thus, we perform a dimension reduction leading us to (linear) beams and plates, revealing several typical discretization problems for those problem classes. Non-standard finite elements like vector-valued tangential-continuous Nédélec and matrix-valued normal-normal-continuous Hellan–Herrmann–Johnson elements are used to construct robust discretization methods. Before going to shells, the "prima-donna" of structures, tools from so-called extrinsic differential geometry are repeated, where a surface is embedded in $\mathbb{R}^3$. We introduce the surface's fundamental forms and related quantities (e.g. metric and Weingarten tensor), (covariant) derivatives, and finite elements on surfaces. We end the seminar by discussing and simulating linear shells.

Chapter 1

Elasticity

This section introduces the equations of continuum mechanics (elasticity) to describe how an elastic body gets deformed in the presence of forces like gravity. For literature on (nonlinear) elasticity and continuum mechanics see e.g. [9, 21, 32, 5, 19].

1.1 Strain tensors

Let $\Omega \subset \mathbb{R}^d$ be an open and bounded domain in $d = 2, 3$ dimensions and let the boundary $\partial\Omega$ be sufficiently smooth. Then $\overline{\Omega}$ describes the reference configuration of a body, also called the undeformed configuration. The boundary is split into a Dirichlet and Neumann part Γ_D and Γ_N, respectively, with $\Gamma_D \cap \Gamma_N = \emptyset$ and $\overline{\Gamma_D} \cup \overline{\Gamma_N} = \partial\Omega$. Further, we assume that the measure of Γ_D is not zero, i.e., $|\Gamma_D| \neq 0$.

Applying external forces to the body leads to *deformation* represented by the function

$$\begin{aligned} \Phi : \overline{\Omega} &\to \mathbb{R}^d \\ x &\mapsto \Phi(x), \end{aligned} \tag{1.1.1}$$

which can be split additively into the identity function and the *displacement* u

$$\Phi = \mathrm{id} + u. \tag{1.1.2}$$

Next, we introduce the *deformation gradient*

$$\boldsymbol{F} := \boldsymbol{I} + \nabla u = \nabla\Phi, \tag{1.1.3}$$

where $\boldsymbol{I}$ denotes the identity matrix. A deformation is called *permissible* if the *deformation determinant* $J := \det(\boldsymbol{F})$ is greater than zero, $J > 0$, which entails that the material is non-interpenetrable, i.e., the orientation is preserved and volume elements with positive measure have also positive measure after the deformation.

To measure the quadratic change of lengths of the deformation, the (right) *Cauchy–Green strain tensor* is introduced as

$$\boldsymbol{C} := \boldsymbol{F}^\top \boldsymbol{F}. \tag{1.1.4}$$

It is also called *metric tensor* in the context of differential geometry and shells. There holds for $\Phi \in C^2(\Omega, \mathbb{R}^d)$ with Taylor's theorem for $\|\Delta x\| \to 0$

$$\begin{aligned} \frac{\|\Phi(x+\Delta x) - \Phi(x)\|^2}{\|\Delta x\|^2} &= \frac{\|\Phi(x) + \nabla\Phi\Delta x + \mathcal{O}(\|\Delta x\|^2) - \Phi(x)\|^2}{\|\Delta x\|^2} = \frac{\Delta x^\top \boldsymbol{F}^\top \boldsymbol{F}\Delta x + \mathcal{O}(\|\Delta x\|^3)}{\|\Delta x\|^2} \\ &= \frac{\Delta x^\top \boldsymbol{C}\Delta x}{\|\Delta x\|^2} + \mathcal{O}(\|\Delta x\|), \end{aligned} \tag{1.1.5}$$

i.e., it measures the change of lengths.

If $\boldsymbol{C} = \boldsymbol{I}$, the body does not get deformed; however, it could be rotated or translated. The following theorem states that these motions are precisely the kernel of $\boldsymbol{C} - \boldsymbol{I}$, so-called *rigid body motions* (or *Euclidean motion*).

Theorem 1.1.1 *Let Ω be a connected domain and $\Phi \in C^1(\Omega, \mathbb{R}^d)$. Then a deformation is a rigid body motion if and only if*

$$\Phi \in RB := \{\Psi(x) = a + \boldsymbol{Q}x \,|\, a \in \mathbb{R}^d,\, \boldsymbol{Q} \in \mathrm{SO}(d)\}, \tag{1.1.6}$$

where $\mathrm{SO}(d) := \{\boldsymbol{A} \in \mathbb{R}^{d\times d} \,|\, \det \boldsymbol{A} = 1$ and $\boldsymbol{A}^{-1} = \boldsymbol{A}^\top\}$ denotes the special orthogonal group.

Proof: See e.g., [9, Theorem 1.8-1]. □

This motivates the definition of the *Green strain tensor*

$$\boldsymbol{E} := \frac{1}{2}(\boldsymbol{C} - \boldsymbol{I}) \tag{1.1.7}$$

measuring the real strains induced by the deformation Φ. Its kernel is exactly the rigid body motions, $\ker \boldsymbol{E} = RB$. Inserting (1.1.3)–(1.1.4) yields the representation

$$\boldsymbol{E} = \frac{1}{2}\left(\nabla u^\top \nabla u + \nabla u^\top + \nabla u\right). \tag{1.1.8}$$

Assuming $\nabla u = \mathcal{O}(\varepsilon)$ with $1 \gg \varepsilon > 0$ small and neglecting all higher order terms gives the *linearized strain tensor*

$$\boldsymbol{\varepsilon}(u) := \frac{1}{2}\left(\nabla u^\top + \nabla u\right) = \operatorname{sym}(\nabla u) \tag{1.1.9}$$

used in linear elasticity.

Remark 1.1.2 (Engineering notation) *Objects in reference notation are frequently denoted by capital letters, e.g., X for the position vector in the reference configuration. In contrast, objects in the deformed configuration are denoted by small letters, e.g., $x = \Phi(X)$ for the position vector in the deformed configuration. The deformation gradient is then written as $\boldsymbol{F} = \frac{\partial x}{\partial X}$. Volume elements are related by the deformation determinant $dv = J\,dV$. A line element dx in deformed configuration can be expressed in reference configuration by $dx = \partial x/\partial X\, dX = \boldsymbol{F}\, dX$. So $dx^T dx = dX^T \boldsymbol{C} dX$ and we can define the Green strain tensor by relating the line elements $dx^T dx - dX^T dX = dX^T(\boldsymbol{C} - \boldsymbol{I})dX = 2dX^T\, \boldsymbol{E} dX$.*

1.2 Hyperelastic materials

We consider *hyperelastic constitutive relations*, i.e., the deformation energy is given by a potential $\Psi : \Omega \times \mathbb{R}^{d\times d} \to \mathbb{R}$

$$E_{\text{def}} = \int_\Omega \Psi(x, \boldsymbol{F}(u(x)))\, dx. \tag{1.2.1}$$

More general elastic materials and a derivation based on conservation laws can be found in the literature. Further, for ease of presentation, we assume that the potential is *homogeneous*, i.e.,

$$\Psi(x, \cdot) = \Psi(\cdot). \tag{1.2.2}$$

Given Dirichlet data u_D on Γ_D, a static body load f, and traction forces g on Γ_N we can define the following minimization problem

$$\mathcal{W}(u) := \int_\Omega \Psi(\boldsymbol{F}(u)) - f \cdot u\, dx - \int_{\Gamma_N} g \cdot u\, ds \to \min!. \tag{1.2.3}$$

Gravity is a classical body force, whereas a car driving over a bridge is an example of a traction force.

We seek a function u in the set of admissible displacements given by

$$U := \{u : \Omega \to \mathbb{R}^d \,|\, u = u_D \text{ on } \Gamma_D,\, \det(\boldsymbol{F}(u)) > 0\}. \tag{1.2.4}$$

Note that the constraint $\det(\boldsymbol{F}(u)) > 0$ is often given implicitly in the material law or is neglected in the small deformation case.

To compute the weak formulation of (1.2.3) we take the first variation in direction δu, well-known as the *principle of virtual works*, yielding

$$D_u\mathcal{W}(u)[\delta u] = \int_\Omega \frac{\partial \Psi}{\partial \boldsymbol{F}} : \nabla \delta u - f \cdot \delta u\, dx - \int_{\Gamma_N} g \cdot \delta u\, ds \stackrel{!}{=} 0 \tag{1.2.5}$$

for all admissible test functions δu, i.e., $\delta u \in U_{\Gamma_D}$, where

$$U_{\Gamma_D} := \{\delta u : \Omega \to \mathbb{R}^d \,|\, \delta u = 0 \text{ on } \Gamma_D\}. \tag{1.2.6}$$

In (1.2.5) we used the Frobenius scalar product of two matrices $\boldsymbol{A} : \boldsymbol{B} = \sum_{i,j=1}^d \boldsymbol{A}_{ij}\boldsymbol{B}_{ij}$ and the chain rule $D_u\Psi(\boldsymbol{F}(u))[\delta v] = \frac{\partial \Psi}{\partial \boldsymbol{F}}(\boldsymbol{F}(u)) : D_u(\boldsymbol{F}(u))[\delta u]$.

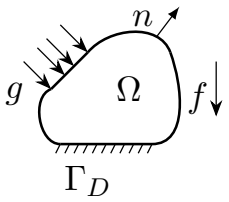

Figure 1.1: Initial configuration of a body Ω with Dirichlet boundary Γ_D, external forces f and g, and outer unit normal vector n.

By defining the *first Piola–Kirchhoff stress tensor*

$$\boldsymbol{P} := \frac{\partial \Psi}{\partial \boldsymbol{F}} \tag{1.2.7}$$

and integration by parts in (1.2.5), we obtain the Euler–Lagrange equation of (1.2.3)

$$\begin{cases} -\operatorname{div}(\boldsymbol{P}) = f & \text{in } \Omega, \\ u = u_D & \text{on } \Gamma_D, \\ \boldsymbol{P}n = g & \text{on } \Gamma_N, \end{cases} \tag{1.2.8}$$

where n denotes the outer normal vector of Ω, cf. Figure 1.1.

Definition 1.2.1 *We call a hyperelastic potential*

- objective *(*frame-indifferent*), if for all positive definite* $\boldsymbol{F} \in \mathbb{M}_+(d) := \{\boldsymbol{A} \in \mathbb{R}^{d\times d} \,|\, x^\top \boldsymbol{A} x > 0 \text{ for all } 0 \neq x \in \mathbb{R}^d\}$ *and* $\boldsymbol{Q} \in \mathrm{SO}(d)$

$$\Psi(\boldsymbol{Q}\boldsymbol{F}) = \Psi(\boldsymbol{F}). \tag{1.2.9}$$

- isotropic*, if for all* $\boldsymbol{F} \in \mathbb{M}_+(d)$ *and* $\boldsymbol{Q} \in \mathrm{SO}(d)$

$$\Psi(\boldsymbol{F}\boldsymbol{Q}) = \Psi(\boldsymbol{F}). \tag{1.2.10}$$

For objective materials, its response does not depend on the observer's frame of reference. In other words, the material depends only on stretches, not rotations (all real-life materials are objective). There are no preferred directions for an isotropic material, such as steel. Wood is a classical example of a strongly anisotropic material.

Example 1.2.2 *The potential* $\Psi(\boldsymbol{F}) := \frac{\mu}{4}\left(\boldsymbol{F}^\top\boldsymbol{F} - \boldsymbol{I}\right) : \left(\boldsymbol{F}^\top\boldsymbol{F} - \boldsymbol{I}\right) + \frac{\lambda}{8}\operatorname{tr}(\boldsymbol{F}^\top\boldsymbol{F} - \boldsymbol{I})^2$*, with* $\mu > 0$*,* $\lambda \geq 0$ *is objective and isotropic (Exercise!).*

A crucial consequence of objectivity is that the energy potential only depends on the Cauchy–Green strain tensor.

Theorem 1.2.3 *A potential* $\Psi : \mathbb{R}^{d\times d} \to \mathbb{R}$ *is frame-indifferent if and only if it is a function of the Cauchy–Green strain tensor* $\boldsymbol{C} = \boldsymbol{F}^\top\boldsymbol{F}$*, i.e.,*

$$\Psi(\boldsymbol{F}) = \hat{\Psi}(\boldsymbol{C}). \tag{1.2.11}$$

Proof: See e.g., [5, Chapter VI, Theorem 1.6] or [9, Theorem 3.3-1]. □

We will consider frame-indifferent potentials and write Ψ independently of arguments $\boldsymbol{F}$, $\boldsymbol{C}$, and $\boldsymbol{E}$. Using Theorem 1.2.3, the weak form (1.2.5) can be rewritten as: Find $u \in U$ such that for all $v \in U_{\Gamma_D}$

$$\int_\Omega 2\frac{\partial \Psi}{\partial \boldsymbol{C}}(\boldsymbol{C}(u)) : \operatorname{sym}(\boldsymbol{F}^\top(u)\nabla v)\, dx = \int_\Omega f \cdot v\, dx + \int_{\Gamma_N} g \cdot v\, ds, \tag{1.2.12}$$

where we utilized that $D_u\boldsymbol{C}(u)[v] = D_u\big(\boldsymbol{F}(u)^\top\big)[v]\boldsymbol{F}(u) + \boldsymbol{F}(u)^\top D_u\big(\boldsymbol{F}(u)\big)[v] = 2\,\mathrm{sym}(\boldsymbol{F}^\top(u)\nabla v)$.

Defining the *second Piola–Kirchhoff stress tensor*

$$\boldsymbol{\Sigma} := 2\frac{\partial \Psi}{\partial \boldsymbol{C}} \tag{1.2.13}$$

and exploiting the symmetry of $\boldsymbol{\Sigma}$ gives

$$\int_\Omega \boldsymbol{F}\boldsymbol{\Sigma} : \nabla v\, dx = \int_\Omega f \cdot v\, dx + \int_{\Gamma_N} g \cdot v\, ds. \tag{1.2.14}$$

Consequently, we obtain the relation

$$\boldsymbol{P} = \boldsymbol{F}\boldsymbol{\Sigma}. \tag{1.2.15}$$

Note that in contrast to $\boldsymbol{\Sigma}$, $\boldsymbol{P}$ is not symmetric. For the sake of completeness, the symmetric *Cauchy stress tensor* $\boldsymbol{\sigma}$ acting on the deformed configuration of the body is introduced by

$$\boldsymbol{\sigma} = \frac{1}{J}\boldsymbol{F}\boldsymbol{\Sigma}\boldsymbol{F}^\top = \frac{1}{J}\boldsymbol{P}\boldsymbol{F}^\top = \frac{1}{J}\frac{\partial \Psi}{\partial \boldsymbol{F}}\boldsymbol{F}^\top. \tag{1.2.16}$$

Then by applying the transformation theorem and the chain rule ($v \circ \Phi^{-1} = \tilde{v}$, $(\nabla_x v) \circ \Phi^{-1} = \nabla_{\tilde{x}}\tilde{v}\boldsymbol{F}$)

$$\int_{\tilde{\Omega}} \frac{1}{J}\boldsymbol{F}\boldsymbol{\Sigma} : (\nabla_{\tilde{x}}\tilde{v}\boldsymbol{F})\, d\tilde{x} = \int_{\tilde{\Omega}} \boldsymbol{\sigma} : \nabla_{\tilde{x}}\tilde{v}\, d\tilde{x}.$$

Assuming a frame-indifferent and isotropic potential yields that the energy potential Ψ is a function of the invariants of the Cauchy–Green strain tensor.

Theorem 1.2.4 (Rivlin–Ericksen) *Let $\mathbb{S}_>(d) := \{\boldsymbol{A} \in \mathbb{R}^{d\times d} \,|\, \boldsymbol{A}^\top = \boldsymbol{A}$ and $\det \boldsymbol{A} > 0\}$ denote the set of symmetric matrices with positive determinant. An energy potential $\Psi : \mathbb{R}^{d\times d} \to \mathbb{R}$ is frame-indifferent and isotropic if and only if there exists a function $\overline{\Psi} : \mathbb{S}_>(d) \to \mathbb{R}$ depending only on the invariants of the characteristic polynomial $\det(\lambda\boldsymbol{I} - \boldsymbol{C}) = \lambda^3 - I_1(\boldsymbol{C})\lambda^2 - I_2(\boldsymbol{C})\lambda - I_3(\boldsymbol{C})$ such that*

$$\Psi(\boldsymbol{F}) = \overline{\Psi}(I_1(\boldsymbol{C}), I_2(\boldsymbol{C}), I_3(\boldsymbol{C})) = \gamma_0(I_1, I_2, I_3)\boldsymbol{I} + \gamma_1(I_1, I_2, I_3)\boldsymbol{C} + \gamma_2(I_1, I_2, I_3)\boldsymbol{C}^2, \tag{1.2.17}$$

where, with $\mathrm{tr}(\boldsymbol{C})$ and $\det(\boldsymbol{C})$ denoting the trace and determinant of $\boldsymbol{C}$,

$$I_1(\boldsymbol{C}) = \mathrm{tr}(\boldsymbol{C}), \qquad I_2(\boldsymbol{C}) = \frac{1}{2}\left(\mathrm{tr}(\boldsymbol{C})^2 - \mathrm{tr}(\boldsymbol{C}^2)\right), \qquad I_3(\boldsymbol{C}) = \det(\boldsymbol{C}). \tag{1.2.18}$$

Proof: See e.g., [27] or [9, Theorem 3.6-1]. □

Exercise 1.2.5 *From the Rivlin–Ericksen theorem the potential in the Green strain tensor is of the form $\Psi(\boldsymbol{E}) = \Psi(\mathrm{tr}(\boldsymbol{E}), \mathrm{tr}(\boldsymbol{E}^2), \det \boldsymbol{E})$. Assume that Ψ has at $\boldsymbol{E} = 0$ a local minimum with value 0 and is smooth. Defining $\mu := \Psi_{,2}(\mathrm{tr}(\boldsymbol{E}), \mathrm{tr}(\boldsymbol{E}^2), \det \boldsymbol{E})|_{\boldsymbol{E}=0}$ and $\lambda := \Psi_{,11}(\mathrm{tr}(\boldsymbol{E}), \mathrm{tr}(\boldsymbol{E}^2), \det \boldsymbol{E})|_{\boldsymbol{E}=0}$, where $\Psi_{,2}(\cdot,\cdot,\cdot)$ denotes the partial derivative with respect to the second argument and $\Psi_{,11}(\cdot,\cdot,\cdot)$ two derivatives in the first one, there holds*

$$\Psi(\boldsymbol{E}) = \frac{\lambda}{2}\mathrm{tr}(\boldsymbol{E})^2 + \mu\,\boldsymbol{E} : \boldsymbol{E} + \mathcal{O}(\|\boldsymbol{E}\|^3).$$

Ignoring the higher-order terms we obtain the *St. Venant–Kirchhoff* material law

$$\Psi_{\mathrm{VK}}(\boldsymbol{E}) = \mu\|\boldsymbol{E}\|_F^2 + \frac{\lambda}{2}\mathrm{tr}(\boldsymbol{E})^2, \qquad \|\boldsymbol{A}\|_F^2 := \boldsymbol{A} : \boldsymbol{A}, \tag{1.2.19}$$

is widely used to model nonlinear behavior in a moderate deformation regime. However, it may happen for large deformations that elements get compressed heavily and are even pressed through others. The material law of *Neo–Hooke*

$$\Psi_{\mathrm{NH}}(\boldsymbol{C}) = \frac{\mu}{2}\left(\mathrm{tr}(\boldsymbol{C} - \boldsymbol{I}) - \log(\det(\boldsymbol{C}))\right) + \frac{\lambda}{8}(\log(\det(\boldsymbol{C})))^2 \tag{1.2.20}$$

Figure 1.2: Two solutions of rubber strip clamped on left and right boundary.

prevents the non-physical behavior of the St. Venant–Kirchhoff material law, as there holds

$$\Psi_{\mathrm{NH}}(\boldsymbol{C}) \to \infty \quad \text{for } \det(\boldsymbol{C}) = (\det(\boldsymbol{F}))^2 \to 0 \text{ or } \det(\boldsymbol{C}) \to \infty, \tag{1.2.21}$$

i.e., infinite energy is needed to completely compress or stretch the material. We remark that, especially in the (nearly) incompressible regime, a slightly different material law of Neo–Hooke is also used, namely

$$\tilde{\Psi}_{\mathrm{NH}}(\boldsymbol{C}) = \frac{\mu}{2}\left(\operatorname{tr}(\boldsymbol{C}-\boldsymbol{I}) - \log(\det(\boldsymbol{C}))\right) + \frac{\lambda}{2}(\underbrace{\sqrt{\det(\boldsymbol{C})}}_{=\det \boldsymbol{F}} - 1)^2. \tag{1.2.22}$$

The two material constants $\mu > 0$ and $\lambda > 0$ used above are the so-called Lamé parameters. Two more physically interpretable constants are the Young's modulus $E > 0$, representing the stiffness of a solid material, and the Poisson's ratio $0 \le \nu < 1/2$[1]. The latter describes the expansion or contraction in the perpendicular direction to the force compressing or stretching the material. Physical units are $[\mu] = [\lambda] = [E] = \frac{N}{m^2} = Pa$ Pascal, whereas the Poisson ratio is dimensionless. To convert these parameters, the following formulae are used

$$\nu = \frac{\lambda}{2(\lambda+\mu)}, \qquad E = \frac{\mu(3\lambda+2\mu)}{\lambda+\mu}, \tag{1.2.23a}$$

$$\lambda = \frac{E\nu}{(1+\nu)(1-2\nu)}, \qquad \mu = \frac{E}{2(1+\nu)}. \tag{1.2.23b}$$

Note that in the limit $\nu \to \frac{1}{2}$, or equivalently $\lambda \to \infty$, the material is called incompressible, necessitating special (numerical) treatment.

1.3 Theoretical results of nonlinear elasticity

The question of existence and uniqueness of this (highly nonlinear) equations is delicate. From physical examples, it is known that we cannot expect uniqueness. Considering e.g., a rubber strip with both ends fixed and neglecting gravity, the identity is a trivial solution for the displacement. When twisting one of the ends by 2π (360°), we obtain a different solution to the same boundary conditions, see Figure 1.2. In this manner, we can even produce infinitely many solutions by twisting. Other examples are given, e.g., by buckling (bifurcations) or snap-through problems, where two solutions exist for one external force (one before and one after the snap-through).

For existence, one approach exploits, if possible, the polyconvex structure of the energy potential Ψ in its invariants $I_i(\boldsymbol{C})$, compare (1.2.18), proving the existence of minimizers [3]. The material law of St. Venant–Kirchhoff is not polyconvex, but the Neo–Hooke material law falls in this category. A large class of Ogden-type materials fulfills this assumption. Another ansatz uses the implicit function theorem, obtaining a unique solution for small data. Therefore, relatively strong regularity assumptions must be made [9].

Only a little rigorous mathematical numerical analysis for finite elasticity has been accomplished so far. E.g., in [7] a priori error estimates for finite element discretizations in nonlinear elasticity are discussed for polyconvex materials under the assumption of sufficiently small right-hand sides.

1.4 Linearized elasticity

Under the assumption of small deformations all three stress tensors (1.2.7), (1.2.13), and (1.2.16) reduce to one, which we denote by $\boldsymbol{\sigma}$ (e.g., $\boldsymbol{P} = \boldsymbol{F}\boldsymbol{\Sigma} = (\boldsymbol{I} + \nabla u)\boldsymbol{\Sigma} = \boldsymbol{\Sigma} + \mathcal{O}(\varepsilon^2)$ as $\nabla u = \mathcal{O}(\varepsilon)$ by assumption).

[1] For meta-materials, the Poisson ratio can also take negative values.

Assuming a quadratic potential $\Psi(\cdot)$, we deduce a linear stress-strain relation by $\boldsymbol{\sigma} = \frac{\partial \Psi}{\partial \boldsymbol{\varepsilon}} = \mathcal{C}\boldsymbol{\varepsilon}$, where $\mathcal{C}$ denotes the fourth-order elasticity tensor. For an isotropic and frame-indifferent material, the stress-strain relation can be written in Voigt notation as

$$\begin{pmatrix} \boldsymbol{\sigma}_{11} \\ \boldsymbol{\sigma}_{22} \\ \boldsymbol{\sigma}_{33} \\ \boldsymbol{\sigma}_{23} \\ \boldsymbol{\sigma}_{13} \\ \boldsymbol{\sigma}_{12} \end{pmatrix} = \frac{E}{(1+\nu)(1-2\nu)} \begin{pmatrix} 1-\nu & \nu & \nu & & & 0 \\ \nu & 1-\nu & \nu & & & \\ \nu & \nu & 1-\nu & & & \\ & & & 1-2\nu & & \\ & & & & 1-2\nu & \\ & 0 & & & & 1-2\nu \end{pmatrix} \begin{pmatrix} \boldsymbol{\varepsilon}_{11} \\ \boldsymbol{\varepsilon}_{22} \\ \boldsymbol{\varepsilon}_{33} \\ \boldsymbol{\varepsilon}_{23} \\ \boldsymbol{\varepsilon}_{13} \\ \boldsymbol{\varepsilon}_{12} \end{pmatrix}, \tag{1.4.1}$$

or in matrix notation $\boldsymbol{\sigma} = \frac{E}{(1+\nu)(1-2\nu)}((1-2\nu)\boldsymbol{\varepsilon} + \nu \operatorname{tr}(\boldsymbol{\varepsilon})\boldsymbol{I}) = 2\mu\boldsymbol{\varepsilon} + \lambda \operatorname{tr}(\boldsymbol{\varepsilon})\boldsymbol{I}$. For $\nu \neq \frac{1}{2}$ relation (1.4.1) can be inverted, $\boldsymbol{\varepsilon} = \mathcal{C}^{-1}\boldsymbol{\sigma}$,

$$\begin{pmatrix} \boldsymbol{\varepsilon}_{11} \\ \boldsymbol{\varepsilon}_{22} \\ \boldsymbol{\varepsilon}_{33} \\ \boldsymbol{\varepsilon}_{23} \\ \boldsymbol{\varepsilon}_{13} \\ \boldsymbol{\varepsilon}_{12} \end{pmatrix} = \frac{1}{E} \begin{pmatrix} 1 & -\nu & -\nu & & & \\ -\nu & 1 & -\nu & & & \\ -\nu & -\nu & 1 & & & \\ & & & 1+\nu & & \\ & & & & 1+\nu & \\ & & & & & 1+\nu \end{pmatrix} \begin{pmatrix} \boldsymbol{\sigma}_{11} \\ \boldsymbol{\sigma}_{22} \\ \boldsymbol{\sigma}_{33} \\ \boldsymbol{\sigma}_{23} \\ \boldsymbol{\sigma}_{13} \\ \boldsymbol{\sigma}_{12} \end{pmatrix}, \tag{1.4.2}$$

and $\mathcal{C}^{-1}$ is called the *compliance tensor*. Relation (1.4.2) can be written compactly as

$$\boldsymbol{\varepsilon} = \frac{1}{E}\left((1+\nu)\boldsymbol{\sigma} - \nu \operatorname{tr}(\boldsymbol{\sigma})\boldsymbol{I}\right) = \frac{1}{E}\left((1+\nu)\operatorname{dev}(\boldsymbol{\sigma}) + \frac{1-2\nu}{2}\operatorname{tr}(\boldsymbol{\sigma})\boldsymbol{I}\right), \tag{1.4.3}$$

where $\operatorname{dev}(\boldsymbol{A}) = \boldsymbol{A} - \frac{1}{d}\operatorname{tr}(\boldsymbol{A})\boldsymbol{I}$ denotes the deviatoric (trace-free) part of a matrix. Here, the case $\nu = \frac{1}{2}$ is well-defined leading to the identity $\boldsymbol{\varepsilon} = \frac{1+\nu}{E}\operatorname{dev}(\boldsymbol{\sigma})$, which is unique up to the trace of $\boldsymbol{\sigma}$.

The strong form of (1.2.8) becomes in the linearized case

$$\begin{cases} -\operatorname{div}(\boldsymbol{\sigma}) = f & \text{in } \Omega, \\ u = u_D & \text{on } \Gamma_D, \\ \boldsymbol{\sigma} n = g & \text{on } \Gamma_N, \end{cases} \tag{1.4.4}$$

and the variational problem (inserting the stress-strain relation) reads: Find $u \in U$ such that for all $v \in U_{\Gamma_D}$

$$\int_\Omega \mathcal{C}\boldsymbol{\varepsilon}(u) : \boldsymbol{\varepsilon}(v)\, dx = \int_\Omega f \cdot v\, dx + \int_{\Gamma_N} g \cdot v\, ds. \tag{1.4.5}$$

The material laws of St. Venant–Kirchhoff and Neo–Hooke reduce to the linear material law of Hooke

$$\Psi_{\mathrm{H}}(\boldsymbol{\varepsilon}) := \mu\|\boldsymbol{\varepsilon}\|_F^2 + \frac{\lambda}{2}(\operatorname{tr}(\boldsymbol{\varepsilon}))^2 \tag{1.4.6}$$

and we obtain the problem: Find $u \in U$ such that for all test functions $v \in U_{\Gamma_D}$

$$\int_\Omega 2\mu\, \boldsymbol{\varepsilon}(u) : \boldsymbol{\varepsilon}(v) + \lambda \operatorname{div}(u)\operatorname{div}(v)\, dx = \int_\Omega f \cdot v\, dx + \int_{\Gamma_N} g \cdot v\, ds. \tag{1.4.7}$$

The unique solvability of (1.4.5) is proven in the next section. Note that (1.4.5) and (1.4.7) coincide for $\mathcal{C}$ defined as in (1.4.1).

1.5 Analysis of linear elasticity

We use the classical Lax–Milgram Lemma for elliptic problems to prove existence and uniqueness for the linear elasticity problem (1.4.7).

Lemma 1.5.1 (Lax–Milgram) *Let $a(\cdot,\cdot) : V \times V \to \mathbb{R}$ be a continuous and elliptic bilinear form with constants α and β, respectively. Then, for all $f \in V^*$ there exists a unique solution $u \in V$ of the problem*

$$a(u,v) = f(v), \qquad \text{for all } v \in V \tag{1.5.1}$$

and there holds the stability estimate

$$\|u\|_V \leq \frac{1}{\beta}\|f\|_{V^*}. \tag{1.5.2}$$

Surprisingly, the entire gradient of a vector-valued function can be bounded by its symmetric part, cf. [14], at the cost of possibly large constants for anisotropic domains.

Lemma 1.5.2 (Korn's inequality) *Let Ω be a connected and bounded Lipschitz domain (i.e., the boundary can locally be parameterized by a Lipschitz function). Then there exists a constant $\hat{c}_K > 0$ such that*

$$\hat{c}_K^2 \|u\|_{H^1}^2 \leq \|u\|_{L^2}^2 + \|\boldsymbol{\varepsilon}(u)\|_{L^2}^2 \tag{1.5.3}$$

for all $u \in H^1(\Omega,\mathbb{R}^d)$ and $\hat{c}_K$ depends only on Ω. Assume further that $\Gamma_D \subset \partial\Omega$ has positive measure. Then there exists a constant $c_K > 0$ such that

$$c_K^2 \|u\|_{H^1}^2 \leq \|\boldsymbol{\varepsilon}(u)\|_{L^2}^2 \tag{1.5.4}$$

for all $u \in H^1_{\Gamma_D}(\Omega,\mathbb{R}^d)$. The constants $\hat{c}_K$ and c_K tend to zero for deteriorating aspect ratio.

Korn's inequality relies on the fact that by setting Dirichlet boundary conditions at parts of the boundary, the kernel of the symmetric gradient operator consisting of linearized rigid body motions

$$\ker \boldsymbol{\varepsilon}(\cdot) = RB^{\text{lin}} := \{\Phi(x) = \boldsymbol{A}\,x + b \,|\, b \in \mathbb{R}^d,\, \boldsymbol{A} \in \mathbb{R}^{d\times d} \text{ with } \boldsymbol{A}^\top = -\boldsymbol{A}\} \tag{1.5.5}$$

is locked.

Corollary 1.5.3 *The bilinear form*

$$a(u,v) := \int_\Omega 2\mu\,\boldsymbol{\varepsilon}(u) : \boldsymbol{\varepsilon}(v) + \lambda\,\mathrm{div}u\,\mathrm{div}v\,dx \tag{1.5.6}$$

is continuous and coercive (elliptic) with

$$\begin{aligned} |a(u,v)| &\leq (2\mu+\lambda)\,\|u\|_{H^1}\,\|v\|_{H^1}\,, \\ a(u,u) &\geq 2\mu\,c_K^2\,\|u\|_{H^1}^2\,. \end{aligned}$$

Céa's lemma yields the following a-priori finite element error estimate for Lagrange elements $u_h \in U_h \subset U$

$$\|u-u_h\|_{H^1}^2 \leq \frac{2\mu+\lambda}{2\mu\,c_K^2} \inf_{v_h\in U_h} \|u-v_h\|_{H^1}^2\,, \tag{1.5.7}$$

from which we deduce that the problem is ill conditioned if the material is nearly incompressible, $\lambda \gg \mu$, or the geometry is anisotropic leading a small Korn constant, $c_K \ll 1$.

Exercise 1.5.4

1. *Proof Corollary 1.5.3 and that the right-hand sides* (1.4.7) *are continuous functionals in $H^1(\Omega,\mathbb{R}^d)$.*
2. *Show that Korn's inequality is sharp by constructing a specific displacement on $\Omega = (0,1)\times(-t/2,t/2)$ and $U = \{u \in H^1(\Omega,\mathbb{R}^2) \,|\, u(0,\cdot) = 0\}$ and showing that $c_K \leq ct$. Hint: Find u such that $\|\boldsymbol{\varepsilon}(u)\|^2/\|\nabla u\| \leq ct^2$.*
3. *Define the pressure-like variable $p = \lambda\,\mathrm{div}u$ as an additional field and rewrite the equations into a Stokes system (with penalty term). Argue that by using a Stokes stable pairing for (u,p), nearly incompressible elasticity can be simulated robustly.*

Chapter 2

Timoschenko and Bernoulli beam

We saw in the previous chapter that for strong anisotropic structures the elasticity problem is ill-posed (due to Korn's inequality) and numerical simulations showed so-called locking behavior. Discretizing thin-walled structures with isotropic (small) elements is inefficient due to the vast number of elements needed. Using elements reflecting the structure and aspect ratio would be more economical, but lead to (shear) locking behavior. For structures, where one dimension is of magnitudes smaller than the other directions, it is expected that the material's behaviour in this direction can be described with fewer parameters, such that a dimension reduction to the mid-surface is an attractive strategy. One has to mesh and discretize objects of one dimension less, leading to smaller matrices. In addition to the computational speed-up, it was hoped that the locking behavior of full elasticity would be cured. However, as we will see, the shear locking problem is shifted but not circumvented or replaced with the difficulties of solving a fourth-order (biharmonic) problem. Nevertheless, the resulting beam equations yield more insight into the issue, which will be helpful when going to plates and shells.

2.1 Dimension reduction to beams

If we have a structure $\Omega \subset \mathbb{R}^2$ where one dimension is significantly thinner than the other, a dimension reduction to a one-dimensional problem can be done. If the two-dimensional structure is of the form $\Omega = (0,1) \times (-t/2, t/2)$ we can perform a reduction to the mid-surface $\mathcal{S} = (0,1) \times \{0\}$. We assume for simplicity that Dirichlet boundary conditions are prescribed on the left and right boundary $\{0,1\} \times (-t/2, t/2)$ and homogeneous Neumann boundaries ("do-nothing condition") at the top and bottom.

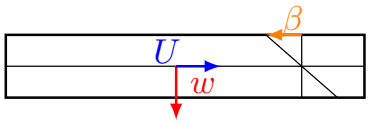

Figure 2.1: Horizontal deflection U, vertical deflection w, and rotation of normal β of a beam.

To derive the beam equation in the setting of linear elasticity, we can start with a Galerkin-semidiscretization by approximating an infinite sum in the thickness direction

$$u = (u^x, u^y) \approx \left(\sum_{i=0}^{N_x} u_i^x(x) y^i, \sum_{i=0}^{N_y} u_i^y(x) y^i \right). \tag{2.1.1}$$

We consider the lowest possible order, where the (linearized) rigid body motions, i.e. both translations and a rotation, are included, leading to $N_x = 1$, $N_y = 0$ and

$$u = (U(x) - y\,\beta(x), w(x)). \tag{2.1.2}$$

Here, $U(x)$ and $w(x)$ correspond to the horizontal and vertical deflection, respectively, and $\beta(x)$ is the linearized rotation of the normal vector on the initial configuration, cf. Figure 2.1. Analogously, test functions are given by $v = (V(x) - y\delta(x), v(x))$. Inserting into the equation of linear elasticity (1.4.7) we obtain

$$\varepsilon(u) = \begin{pmatrix} U' - y\beta' & \frac{1}{2}(w' - \beta) \\ \frac{1}{2}(w' - \beta) & 0 \end{pmatrix}, \qquad \varepsilon(v) = \begin{pmatrix} V' - y\delta' & \frac{1}{2}(v' - \delta) \\ \frac{1}{2}(v' - \delta) & 0 \end{pmatrix},$$

$$\varepsilon(u) : \varepsilon(v) = (U' - y\beta')(V' - y\delta') + \frac{1}{2}(w' - \beta)(v' - \delta), \qquad \operatorname{div}(u)\operatorname{div}(v) = (U' - y\beta')(V' - y\delta')$$

and further

$$\begin{aligned} a(u,v) &= \int_0^1 \int_{-t/2}^{t/2} 2\mu\, \varepsilon(u) : \varepsilon(v) + \lambda \operatorname{div}(u) \operatorname{div}(v)\, dy\, dx \\ &= \int_0^1 \int_{-t/2}^{t/2} (2\mu + \lambda)(U' - y\beta')(V' - y\delta') + \frac{\mu}{2}(w' - \beta)(v' - \delta)\, dy\, dx \\ &= \int_0^1 (2\mu + \lambda) t\, U'V' + (2\mu + \lambda)\frac{t^3}{12}\beta'\delta' + \frac{t\,\mu}{2}(w' - \beta)(v' - \delta)\, dx. \end{aligned}$$

Assuming that the force is independent of the thickness direction $f = (f^x(x), f^y(x))$ the elasticity problem decouples into a Poisson-like *membrane problem*: Find $U \in H_0^1((0,1))$ such that for all $V \in H_0^1((0,1))$

$$(2\mu + \lambda)t \int_0^1 U'V' \, dx = t \int_0^1 f^x V \, dx \tag{2.1.3}$$

and the *bending problem*: Find $(w, \beta) \in H_0^1((0,1)) \times H_0^1((0,1))$ such that for all $(v, \delta) \in H_0^1((0,1)) \times H_0^1((0,1))$

$$(2\mu + \lambda)\frac{t^3}{12} \int_0^1 \beta'\delta' \, dx + \frac{t\,\mu}{2} \int_0^1 (w' - \beta)(v' - \delta) \, dx = t \int_0^1 f^y v \, dx. \tag{2.1.4}$$

Neglecting the Lamé parameters and constants and rescaling the right-hand side $f := \frac{1}{t^2} f^y$ we obtain the *Timoshenko beam* (also called Timoshenko–Ehrenfest beam): Find $(w, \beta) \in H_0^1((0,1)) \times H_0^1((0,1))$ such that for all $(v, \delta) \in H_0^1((0,1)) \times H_0^1((0,1))$

$$\int_0^1 \beta'\delta' \, dx + \frac{1}{t^2} \int_0^1 (w' - \beta)(v' - \delta) \, dx = \int_0^1 f\, v \, dx, \tag{2.1.5}$$

which corresponds to the minimization problem

$$\mathcal{W}(w, \beta) := \frac{1}{2} \int_0^1 (\beta')^2 \, dx + \frac{1}{2t^2} \int_0^1 (w' - \beta)^2 \, dx - \int_0^1 f\, w \, dx \to \min!. \tag{2.1.6}$$

The first term is the beam's bending energy, which measures how strongly the beam curves. The second term is the shearing energy, which measures how much the initial configuration's deformed normal deviates from the deformed configuration's normal (given by w').

The Timoshenko beam involves a parameter, the thickness t, so the bending and shearing parts are scaled differently. Although the Timoshenko beam is $H_0^1 \times H_0^1$ elliptic, its constant depends on the thickness, which leads with Céa's Lemma to a parameter dependent a-priori error estimate

$$\|(w_h, \beta_h) - (w, \beta)\|_X \le c(t) \inf_{(v_h, \delta_h) \in X_h} \|(v_h, \delta_h) - (w, \beta)\|_X. \tag{2.1.7}$$

In the limit of vanishing thickness, $t \to 0$, it acts as a penalty enforcing the constraint $\beta = w'$. Therefore, in the limit, we can eliminate the rotation β leading to the fourth-order minimization problem

$$\mathcal{W}(w) = \frac{1}{2} \int_0^1 (w'')^2 \, dx - \int_0^1 f\, w \, dx \to \min!, \tag{2.1.8}$$

which corresponds to the variational formulation: Find $w \in H_0^2((0,1))$ such that for all $v \in H_0^2((0,1))$

$$\int_0^1 w''v'' \, dx = \int_0^1 f\, v \, dx. \tag{2.1.9}$$

This fourth-order ODE problem is called the *Euler–Bernoulli beam*.

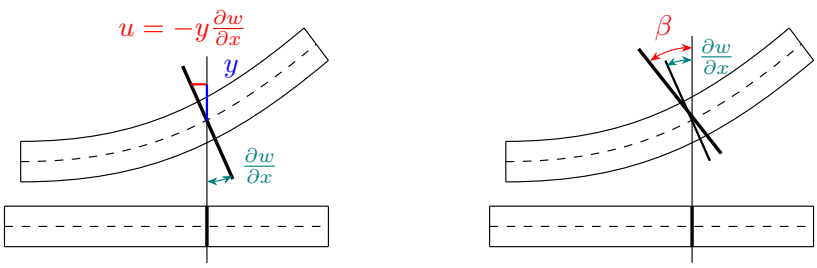

Figure 2.2: Rotation of Euler–Bernoulli beam and Timoshenko beam.

2.2 Discretization of Timoshenko beam

A straightforward discretization is to use Lagrangian finite elements of the same order for the displacement and rotation $(w_h, \beta_h) \in U_h^k \times U_h^k$, which we will see may induce locking for a small thickness parameter t. In the limit $t \to 0$, the shearing energy can be seen as a penalty enforcing $w_h' = \beta_h$. In the lowest order case, this identity forces the piece-wise constant w_h' to fit with the linear and continuous β_h, leading to the trivial solution, $w_h = \beta_h = 0$. From the theory of mixed methods, we will see that inserting an L^2-projection into the shearing term cures this problem by relaxing the constraint. In 1D, this is equivalent to a numerical under-integration using only the mid-point rule for the shearing term. Using for w_h one polynomial order higher than β_h improves the locking behavior. This, however, leads to sub-optimal (linear) convergence rates for β. In Section 2.4 we analyze and present a shear-locking-free (discretized) method for the Timoshenko beam.

We used clamped boundary conditions in the derivation, $u, \beta \in H_0^1((0,1))$. Other boundary conditions like free, simply supported or constrained rotation are possible, define $Q := \frac{1}{t^2}(w' - \beta)$ and $M := \beta'$:

boundary condition	w	β	
clamped	D	D	$w = 0,\ \beta = 0$
simply supported	D	N	$w = 0,\ M = 0$
free	N	N	$Q = 0,\ M = 0$
constraint rotation	N	D	$Q = 0,\ \beta = 0$

Exercise 2.2.1 *Derive, implement, and test the different boundary conditions for the Timoshenko beam. Motivate the physical quantities Q and M.*

In the limit $t \to 0$, the equality $w' = \beta$ holds. Therefore, the rotation β has to coincide with the linearized normal vector of the deformed beam and can be eliminated from the equation, leading to the Euler–Bernoulli beam.

2.3 Discretization of Euler–Bernoulli beam

In contrast to the Timoshenko beam, the thickness parameter t does not enter the Euler–Bernoulli beam equation anymore. Therefore, it does not suffer from locking, but C^1-conforming finite elements are required, as we now face a fourth-order problem. In 1D, constructing C^1-elements is easy by e.g. Hermite polynomials. This task is much more involved for higher dimensions, especially if unstructured (triangular) grids are required. As pre-work for plates and shells, we focus on formulations enabling Lagrangian elements for the vertical deflection w.

Let us rewrite the Euler–Bernoulli beam as a mixed saddle-point problem by introducing the linearized moment $\sigma = w''$ as an additional unknown

$$\int_0^1 \sigma\tau\,dx \qquad - \int_0^1 w''\tau\,dx = 0 \qquad \text{for all } \tau, \tag{2.3.1a}$$

$$-\int_0^1 \sigma\, v''\,dx \qquad\qquad = -\int_0^1 f\,v\,dx \quad \text{for all } v, \tag{2.3.1b}$$

and use integration by parts such that all terms are well defined for $(w, \sigma) \in H_0^1((0,1)) \times H^1((0,1))$

$$\int_0^1 \sigma\tau\,dx \;+ \int_0^1 w'\tau'\,dx = 0 \qquad \text{for all } \tau \in H^1((0,1)), \tag{2.3.2a}$$

$$\int_0^1 \sigma' v'\,dx \qquad\qquad = -\int_0^1 f\,v\,dx \quad \text{for all } v \in H_0^1((0,1)). \tag{2.3.2b}$$

We can use Lagrange finite elements for discretization. The following section shows that this leads to a stable formulation and method.

Exercise 2.3.1 *Show that $\sigma \in H^1((0,1))$ together with $w \in H_0^1((0,1))$ leads to clamped boundary conditions, $w = w' = 0$. What changes if $\sigma \in H_0^1((0,1))$? How can we incorporate free boundary conditions at $x = 1$ and clamped boundary conditions at $x = 0$?*

2.4 Analysis of Timoshenko and Euler–Bernoulli beam

For analyzing mixed saddle-point problems, the Lax–Milgram Lemma cannot be applied due to the missing coercivity on the whole product space. Brezzi's Theorem [5, 4.3 Theorem, 4.11 Theorem] gives sufficient conditions to prove well-posedness for this kind of problem.

2.4.1 Brezzi's Theorem for saddle point problems

Indefinite saddle-point problems, arising e.g., for minimization problems under constraints, are of the following general form: Find $(u,p) \in V \times Q$ such that for all $(v,q) \in V \times Q$

$$a(u,v) + b(v,p) = f(v), \tag{2.4.1a}$$
$$b(u,q) \qquad\quad = g(q). \tag{2.4.1b}$$

Equation (2.4.1b) enforces a constraint on u, which can be incorporated as a penalty formulation yielding the structure ($t > 0$ small)

$$a(u,v) + b(v,p) \;= f(v), \tag{2.4.2a}$$
$$b(u,q) - t\,c(p,q) = g(q). \tag{2.4.2b}$$

Theorem 2.4.1 (Brezzi) *Assume that $a(\cdot,\cdot) : V \times V \to \mathbb{R}$ and $b(\cdot,\cdot) : V \times Q \to \mathbb{R}$ are continuous bilinear forms, i.e.,*

$$|a(u,v)| \le \alpha_2 \|u\|_V \|v\|_V \quad \text{for all } u,v \in V, \tag{2.4.3}$$
$$|b(u,q)| \le \beta_2 \|u\|_V \|q\|_Q \quad \text{for all } u \in V, \text{ for all } q \in Q. \tag{2.4.4}$$

Assume there holds coercivity of $a(\cdot,\cdot)$ on the kernel, i.e.,

$$a(u,u) \ge \alpha_1 \|u\|_V^2 \quad \text{for all } u \in V_0, \tag{2.4.5}$$
$$V_0 := \{u \in V \mid b(u,q) = 0 \quad \text{for all } q \in Q\} \tag{2.4.6}$$

and there holds the Ladyzhenskaya–Babuška–Brezzi (LBB) condition

$$\sup_{u \in V} \frac{b(u,q)}{\|u\|_V} \ge \beta_1 \|q\|_Q \quad \text{for all } q \in Q. \tag{2.4.7}$$

Then, the mixed problem (2.4.1) *is uniquely solvable. The solution fulfills the stability estimate*

$$\|u\|_V + \|p\|_Q \le c\,(\|f\|_{V^*} + \|g\|_{Q^*}) \tag{2.4.8}$$

with the constant c depending on $\alpha_1, \alpha_2, \beta_1$, and β_2.

Theorem 2.4.2 (extended Brezzi) *Assume all requirements of Theorem 2.4.1 are fulfilled. Further, let $c(\cdot,\cdot)$ be a continuous and non-negative bilinear form and $a(\cdot,\cdot)$ be non-negative. Then, for $t \le 1$, the mixed problem* (2.4.2) *has a unique solution, fulfilling the following stability estimate independent of t*

$$\|u\|_V + \|p\|_Q \le c\,(\|f\|_{V^*} + \|g\|_{Q^*})\,, \qquad c \ne c(t). \tag{2.4.9}$$

2.4.2 Analysis of Timoshenko beam

We analyze the Timoshenko beam as mixed formulation by defining the shear $\gamma = \frac{1}{t^2}(w' - \beta)$ as additional unknown: Find $(w,\beta,\gamma) \in H_0^1((0,1)) \times H_0^1((0,1)) \times L^2((0,1))$ such that for all $(v,\delta,\xi) \in H_0^1((0,1)) \times H_0^1((0,1)) \times L^2((0,1))$

$$\int_0^1 \beta'\delta'\,dx \qquad + \int_0^1 (v' - \delta)\gamma\,dx = \int_0^1 f\,v\,dx, \tag{2.4.10a}$$
$$\int_0^1 (w' - \beta)\xi\,dx - t^2 \int_0^1 \gamma\,\xi\,dx \qquad = 0. \tag{2.4.10b}$$

Note that we multiplied (2.4.10b) with t^2 such that the thickness appears in the numerator. The limit case $t = 0$ is therefore well-defined.

Proposition 2.4.3 *The mixed formulation of the Timoshenko beam* (2.4.10) *is uniquely solvable and stable.*

Proof: Continuity of the bilinear forms and non-negativity of $a(\cdot,\cdot)$ and $c(\cdot,\cdot)$ are apparent.

On the kernel

$$\begin{aligned} B_0 &= \Big\{(w,\beta) \in H_0^1((0,1)) \times H_0^1((0,1)) \,\Big|\, \int_0^1 (w'-\beta)\gamma \, dx = 0 \text{ for all } \gamma \in L^2((0,1))\Big\} \\ &= \{(w,\beta) \in H_0^1((0,1)) \times H_0^1((0,1)) \,|\, w' = \beta\} \end{aligned}$$

there holds with Friedrichs's inequality[1]

$$\|\beta'\|_{L^2}^2 = \frac{1}{2}|\beta|_{H^1}^2 + \frac{1}{2}|\beta|_{H^1}^2 \geq c\left(\|\beta\|_{H^1}^2 + \|\beta\|_{L^2}^2\right) \geq c\left(\|\beta\|_{H^1}^2 + \|w\|_{H^1}^2\right). \tag{2.4.11}$$

Further, following [5], for given $\gamma \in L^2((0,1))$ define $\rho(x) := x(1-x)$ and

$$A := \int_0^1 \gamma(s)\, ds \,/ \int_0^1 \rho(s)\, ds, \quad w(x) := \int_0^x \gamma(s)\, ds - A\int_0^x \rho(s)\, ds, \quad \beta(x) := -A\rho(x).$$

Then $\rho, w, \beta \in H_0^1((0,1))$ and there holds with a constant $c > 0$, $\|w'\|_{L^2} \leq c\|\gamma\|_{L^2}$, $\|\beta'\|_{L^2} \leq c\|\gamma\|_{L^2}$, and $w' - \beta = \gamma$. Thus, the LBB condition is fulfilled

$$\sup_{(w,\beta)\in H^1\times H^1} \frac{\int_0^1 (w'-\beta)\gamma \, dx}{\|w\|_{H^1} + \|\beta\|_{H^1}} \geq \frac{\|\gamma\|_{L^2}^2}{\|w'\|_{L^2} + \|\beta'\|_{L^2}} \geq \frac{1}{2c}\|\gamma\|_{L^2}. \tag{2.4.12}$$

Brezzi's Theorem 2.4.2 now finishes the proof, giving the robust estimate

$$\|\beta\|_{H^1} + \|w\|_{H^1} + \frac{1}{t^2}\|w' - \beta\|_{L^2} \leq c\|f\|_{H^{-1}}, \quad c \neq c(t). \tag{2.4.13}$$

□

Using Lagrange elements for w and β and one polynomial order less L^2-conforming discontinuous (i.e. piece-wise polynomials) elements for γ gives a stable discretization for the Timoshenko beam, which can easily be shown (Exercise!). We obtain the optimal t-independent convergence rates:

Corollary 2.4.4 *Let (w,β,γ) be the solution of the continuous problem* (2.4.10) *and $(w_h,\beta_h,\gamma_h) \in U_{h,0}^k \times U_{h,0}^k \times Q_h^{k-1}$ (the space of continuous piece-wise polynomials of order k and discontinuous piece-wise polynomials of order $k-1$) the corresponding discrete one for a positive integer k. If the exact solution is smooth enough, there holds*

$$\|w - w_h\|_{H^1} + \|\beta - \beta_h\|_{H^1} + \|\gamma - \gamma_h\|_{L^2} \leq ch^k(\|w\|_{H^{k+1}} + \|\beta\|_{H^{k+1}} + \|\gamma\|_{H^k}), \qquad c \neq c(t). \tag{2.4.14}$$

The second equality (2.4.10b) states in the discrete case that the shearing can be expressed as $\gamma_h = \frac{1}{t^2}\Pi^{L^2,k-1}(w_h' - \beta_h)$. Inserting this into the first equation (2.4.10a) yields the problem: Find $(w_h,\beta_h) \in U_{h,0}^k \times U_{h,0}^k$ such that for all $(v_h,\delta_h) \in U_{h,0}^k \times U_{h,0}^k$

$$\int_0^1 \beta_h'\delta_h' \, dx + \frac{1}{t^2}\int_0^1 \Pi^{L^2,k-1}(w_h' - \beta_h)\Pi^{L^2,k-1}(v_h' - \delta_h)\, dx = \int_0^1 f\, v_h \, dx, \tag{2.4.15}$$

which corresponds to a numerical under-integration of the shear term. For example, in the lowest-order case, the projection into piece-wise constants can be realized using the mid-point rule for numerical integration.

This (non-standard) primal method is equivalent to the mixed formulation, so we obtain the same stability and convergence results. Its advantage is obtaining a positive definite stiffness matrix, whereas the mixed system leads to an indefinite matrix.

[1] Friedrich: $\|u\|_{H^1} \leq c_F|u|_{H^1}$, for all $u \in H_0^1(\Omega)$

Remark 2.4.5 *When using at least quadratic polynomials for the vertical deflection and rotation no shear locking occurs for the Timoshenko beam anymore, however, convergence rates with a sub-optimal rate are obtained for β in a pre-asymptotic regime depending on t. As we will see later for the Reissner–Mindlin plate (the 2D analog to the Timoshenko beam), its analysis and numerical treatment to avoid shear locking is more involved.*

Remark 2.4.6 *Setting $t = 0$ in* (2.4.10b) *leads to a stable discretization for the Euler–Bernoulli beam.*

Exercise 2.4.7 *Show with Remark 2.4.6, that the solution of the Timoshenko beam $(w, \beta, \gamma)^{\mathrm{TB}}$ converges to the Euler–Bernoulli beam solution $(w, \beta, \gamma)^{\mathrm{EBB}}$*

$$\|(w, \beta, \gamma)^{\mathrm{TB}} - (w, \beta, \gamma)^{\mathrm{EBB}}\| \leq c\, t^2, \qquad c \neq c(t). \tag{2.4.16}$$

Hint: Take the difference of the solutions as a new unknown for the difference of the corresponding equations and use Brezzi's Theorem.

2.4.3 Analysis of Bernoulli beam

From the Lax–Milgram Lemma, we directly deduce that the Euler–Bernoulli beam is well-posed on $H_0^2((0,1))$ and Céa's Lemma yields a standard a-priori error estimate. The big drawback is that we need C^1 finite elements for a conforming discretization. In 1D, Hermite polynomials are directly applicable; however, extensions to 2D Kirchhoff–Love plates are complicated. Therefore, we analyze the mixed method (2.3.2) with Brezzi enabling the usage of Lagrange finite elements.

Proposition 2.4.8 *The mixed formulation* (2.3.2) *of the Euler–Bernoulli beam yields a unique solution.*

Proof: By choosing $\sigma = w$, the LBB condition is fulfilled. The kernel

$$V_0 = \Big\{ \sigma \in H^1((0,1)) \,\Big|\, \int_0^1 \sigma' w' = 0, \quad \text{for all } w \in H_0^1((0,1)) \Big\} = \{ \sigma = ax + b \,|\, a, b \in \mathbb{R} \}$$

consists only of linear functions. As all norms are equivalent in finite-dimensional spaces, the kernel coercivity is also fulfilled. All bilinear forms are continuous for the H^1-norm such that the conditions for Brezzi's theorem 2.4.1 are fulfilled. □

Chapter 3

Reissner–Mindlin and Kirchhoff–Love plates

After deriving the beam equations, we focus on the 2D extension to plates.

3.1 Reissner–Mindlin plate equation

Assuming a thin three-dimensional plate $\Omega = (0,1)^2 \times (-t/2, t/2)$, we can perform a dimension reduction to the mid-surface $\mathcal{S} = (0,1)^2 \times \{0\}$ by a semi-discretization approach, which ansatz would read

$$u = (U_1(x,y) - z\beta_1(x,y), U_2(x,y) - z\beta_2(x,y), w(x,y)). \tag{3.1.1}$$

Note, that the horizontal displacement $U = (U_1, U_2)$ and the rotation $\beta = (\beta_1, \beta_2)$ are now two-dimensional quantities, whereas the vertical deflection w is again a scalar.

Again, we assume the structure to be clamped on all boundaries except the top and bottom ones, where homogeneous Neumann boundary conditions are prescribed. We consider a second approach of derivation in this section. To this end, we postulate kinematic assumptions, which are named after Reissner and Mindlin:

H1. Lines normal to the mid-surface get deformed linearly, and they remain lines.

H2. The displacements in z-direction are independent of the z-coordinate.

H3. Points on the mid-surface can only be deformed in the z-direction.

H4. Stresses $\boldsymbol{\sigma}_{33}$ in normal direction vanish (called plane-stress assumption).

With H1–H3 the displacements are of the form

$$u_1(x,y,z) = -z\beta_1(x,y), \qquad u_2(x,y,z) = -z\beta_2(x,y), \qquad u_3(x,y,z) = w(x,y). \tag{3.1.2}$$

Hypothesis H3 directly enforces that the horizontal displacements of the membrane problem are eliminated and yields together with H1 the form of the shearing-related horizontal displacements u_1 and u_2. H2 in combination with H1 gives the form of the vertical displacement. Assumption H4 is needed as from $u_3 = w(x,y)$ there follows $\boldsymbol{\varepsilon}_{33}(u) = 0$, i.e., no strains in thickness direction. Using (1.4.1) to compute $\boldsymbol{\sigma}_{33}$ yields $\boldsymbol{\sigma}_{33} = \frac{E}{(1+\nu)(1-2\nu)}\left((1-\nu)\boldsymbol{\varepsilon}_{33} + \nu(\boldsymbol{\varepsilon}_{11} + \boldsymbol{\varepsilon}_{22})\right) = \lambda(\boldsymbol{\varepsilon}_{11} + \boldsymbol{\varepsilon}_{22}) \neq 0$ in general. This is non-physical and leads to a not asymptotically correct model. It induces a too stiff behavior, yielding artificial stiffness. Thus, $\boldsymbol{\sigma}_{33} = 0$ is postulated to re-obtain an asymptotically correct model, which converges to the 3D solution in the limit of vanishing thickness. Setting $\boldsymbol{\sigma}_{33} = 0$ implies that the material can stretch in the thickness direction without inducing stresses. The 3D elasticity strain tensor reads with (3.1.2)

$$\boldsymbol{\varepsilon}(u) = \begin{pmatrix} -z\partial_1\beta_1 & -z\frac{1}{2}(\partial_2\beta_1 + \partial_1\beta_2) & \frac{1}{2}(\partial_1 w - \beta_1) \\ & -z\partial_2\beta_2 & \frac{1}{2}(\partial_2 w - \beta_2) \\ \text{sym} & & 0 \end{pmatrix} \tag{3.1.3}$$

From H4, $\boldsymbol{\sigma}_{33} = 0$, we can express $\boldsymbol{\varepsilon}_{33} = -\frac{\nu}{1-\nu}(\boldsymbol{\varepsilon}_{11} + \boldsymbol{\varepsilon}_{22})$ by using (1.4.1) and reinserting yields

$$\begin{pmatrix} \boldsymbol{\sigma}_{11} \\ \boldsymbol{\sigma}_{22} \\ \boldsymbol{\sigma}_{12} \\ \boldsymbol{\sigma}_{13} \\ \boldsymbol{\sigma}_{23} \end{pmatrix} = \frac{E}{1-\nu^2} \begin{pmatrix} 1 & \nu & & & \\ \nu & 1 & & & \\ & & 1-\nu & & \\ & & & 1-\nu & \\ & & & & 1-\nu \end{pmatrix} \begin{pmatrix} \boldsymbol{\varepsilon}_{11} \\ \boldsymbol{\varepsilon}_{22} \\ \boldsymbol{\varepsilon}_{12} \\ \boldsymbol{\varepsilon}_{13} \\ \boldsymbol{\varepsilon}_{23} \end{pmatrix}. \tag{3.1.4}$$

E.g., there holds

$$\begin{aligned} \boldsymbol{\sigma}_{11} &= \frac{E}{(1+\nu)(1-2\nu)}\left((1-\nu)\boldsymbol{\varepsilon}_{11} + \nu\boldsymbol{\varepsilon}_{22} + \nu\boldsymbol{\varepsilon}_{33}\right) \\ &= \frac{E}{(1+\nu)(1-2\nu)}\left((1-\nu-\frac{\nu^2}{1-\nu})\boldsymbol{\varepsilon}_{11} + (\nu - \frac{\nu^2}{1-\nu})\boldsymbol{\varepsilon}_{22}\right) \\ &= \frac{E}{(1-\nu^2)(1-2\nu)}\left((1-2\nu+\nu^2-\nu^2)\boldsymbol{\varepsilon}_{11} + (\nu-2\nu^2)\boldsymbol{\varepsilon}_{22}\right) = \frac{E}{1-\nu^2}(\boldsymbol{\varepsilon}_{11} + \nu\boldsymbol{\varepsilon}_{22}). \end{aligned}$$

The energy $\|\boldsymbol{\varepsilon}\|_{\mathcal{C}}^2 = \mathcal{C}\boldsymbol{\varepsilon} : \boldsymbol{\varepsilon} = \boldsymbol{\sigma} : \boldsymbol{\varepsilon}$ reads

$$\boldsymbol{\sigma} : \boldsymbol{\varepsilon} = \sum_{i,j=1}^{2} \boldsymbol{\sigma}_{ij}\boldsymbol{\varepsilon}_{ij} + 2\sum_{j=1}^{2} \boldsymbol{\varepsilon}_{3j}\boldsymbol{\sigma}_{3j} = \frac{E}{1+\nu}\Big(\sum_{i,j=1}^{2} \boldsymbol{\varepsilon}_{ij}^2 + \frac{\nu}{1-\nu}(\boldsymbol{\varepsilon}_{11} + \boldsymbol{\varepsilon}_{22})^2 + 2\sum_{j=1}^{2} \boldsymbol{\varepsilon}_{3j}^2\Big).$$

Next, we integrate the arising terms over the thickness and insert the strain definition (3.1.3)

$$\begin{aligned}
\int_{-t/2}^{t/2} \sum_{i,j=1}^{2} \boldsymbol{\varepsilon}_{ij}^2 \, dz &= \int_{-t/2}^{t/2} z^2 \underline{\boldsymbol{\varepsilon}}(\beta) : \underline{\boldsymbol{\varepsilon}}(\beta) \, dz = \frac{t^3}{12} \underline{\boldsymbol{\varepsilon}}(\beta) : \underline{\boldsymbol{\varepsilon}}(\beta), \\
\int_{-t/2}^{t/2} (\boldsymbol{\varepsilon}_{11} + \boldsymbol{\varepsilon}_{22})^2 \, dz &= \frac{t^3}{12} \underline{\operatorname{div}}(\beta)^2, \\
\int_{-t/2}^{t/2} 2\sum_{j=1}^{2} \boldsymbol{\varepsilon}_{3j}^2 \, dz &= \int_{-t/2}^{t/2} \frac{2}{4} (\underline{\nabla} w - \beta) \cdot (\underline{\nabla} w - \beta) \, dz = \frac{t}{2} \|\underline{\nabla} w - \beta\|^2,
\end{aligned}$$

where $\underline{\nabla}$, $\underline{\boldsymbol{\varepsilon}}$, and $\underline{\operatorname{div}}$ denote the differential operators acting only on the first two indices $i, j = 1, 2$. Thus, the total energy $\mathcal{W}(w, \beta) = \frac{1}{2}\int_\Omega \boldsymbol{\sigma} : \boldsymbol{\varepsilon} \, d(x, y, z)$ becomes with the notation $ds = d(x, y)$

$$\mathcal{W}(w, \beta) = \frac{1}{2}\int_{\mathcal{S}} \boldsymbol{\sigma} : \boldsymbol{\varepsilon} \, d(s, z) = \frac{t^3 E}{24(1-\nu^2)} \int_{\mathcal{S}} (1-\nu)\|\underline{\boldsymbol{\varepsilon}}(\beta)\|^2 + \nu \, \underline{\operatorname{div}}(\beta)^2 \, ds + \frac{Gt}{2}\int_{\mathcal{S}} \|\underline{\nabla} w - \beta\|^2 \, ds, \tag{3.1.5}$$

where $G = \frac{E}{2(1+\nu)}$ denotes the shearing modulus. Classically, the shear correction factor $\kappa = \frac{5}{6}$ is additionally inserted into the shearing energy term to compensate for high-order effects of the shear stresses, which are not constant through the thickness.

The right-hand side f is assumed to act only vertically on the plate and is independent of the thickness $f = (0, 0, f^z(x, y))$. Integrating over the thickness and rescaling $f := t^{-2} f^z$ leads to the term $t^3 \int_{\mathcal{S}} f \, v \, ds$. To simplify notation, we set $\Omega = \mathcal{S}$, use dx for integration over the mid-surface, neglect the underline for the differential operators, and define the plate elasticity tensor

$$\mathcal{C}\boldsymbol{A} := \frac{E}{1-\nu^2}((1-\nu)\boldsymbol{A} + \nu \operatorname{tr}(\boldsymbol{A})\boldsymbol{I}). \tag{3.1.6}$$

Note, that after the elimination of $\boldsymbol{\varepsilon}_{33}$ the Poisson ratio $\nu \in (0, 1)$ is allowed instead of $(0, \frac{1}{2})$. All together, taking the variations of energy (3.1.5) and dividing by t^3 yields the clamped *Reissner–Mindlin plate equation*: Find $(w, \beta) \in H_0^1(\Omega) \times H_0^1(\Omega, \mathbb{R}^2)$ such that for all $(v, \delta) \in H_0^1(\Omega) \times H_0^1(\Omega, \mathbb{R}^2)$

$$\frac{1}{12}\int_\Omega \mathcal{C}\boldsymbol{\varepsilon}(\beta) : \boldsymbol{\varepsilon}(\delta) \, dx + \frac{\kappa G}{t^2}\int_\Omega (\nabla w - \beta) \cdot (\nabla v - \delta) \, dx = \int_\Omega f \, v \, dx. \tag{3.1.7}$$

We distinguish between the following plate boundary conditions depending on the different combination of Dirichlet and Neumann boundary conditions for the vertical deflection w and the rotations β. Let $\boldsymbol{M} := \frac{1}{12}\mathcal{C}\boldsymbol{\varepsilon}(\beta)$ be the bending moment tensor and $Q := \frac{\kappa G}{t^2}(\nabla w - \beta)$ the shear force.

boundary condition	w	β_n	β_t	
clamped	D	D	D	$w = 0$, $\beta = 0$
free	N	N	N	$Q \cdot n = 0$, $\boldsymbol{M}n = 0$
hard simply supported	D	N	D	$w = 0$, $n^\top \boldsymbol{M} n = 0$, $\beta_t = 0$
soft simply supported	D	N	N	$w = 0$, $\boldsymbol{M}n = 0$

Table 3.1: Reissner–Mindlin plate boundary conditions split into the rotations' vertical deflection and normal/tangential components. D denotes Dirichlet and N Neumann boundary.

The Reissner–Mindlin plate equations entail, in addition to shear locking, possible boundary layers, where the (stress) solutions rapidly change. To generate accurate solutions, these boundary layers need to be resolved. The scaling of the layer is of order $\mathcal{O}(t)$ and the strength differ on the prescribed boundary

conditions. For clamped and hard simply supported plates the boundary layer is less intensive than for free and soft simply supported. An asymptotic boundary layer analysis can be found, e.g. in [1]. An explanation of the appearance of boundary layers is that on the one hand, we have prescribed the rotations at the boundary, and on the other hand, for $t \to 0$, the equality $\nabla w = \beta$ is enforced by the shearing term. This might lead to discrepancies such that inside the boundary layer the rotations change from fitting the boundary conditions to minimizing the difference to ∇w. For Kirchhoff–Love plates, described in the next section, these boundary layers do not occur, as the rotations β, which cause them, are eliminated from the equation.

Remark 3.1.1 *The analysis cannot be performed directly with Brezzi's Theorem 2.4.1 following the analysis of the Timoshenko beam. Instead, a Helmholtz decomposition is used to decompose the equation into two Poisson problems and one Stokes problem, which can then be solved separately (see e.g. [5]).*

3.2 Kirchhoff–Love plate equation

For thin plates like metal sheets, the Kirchhoff–Love hypothesis is assumed additionally to H1–H4.

H5. Lines normal to the mid-surface are, after deformation, again normal to the deformed mid-surface.

It states that normal vectors of the original plate stay perpendicular to the mid-surface of the deformed plate. This means that no shearing occurs, i.e., the rotations β from the Reissner–Mindlin plate equation can be eliminated by the gradient of the vertical deflection w of the mid-surface. Note that ∇w is the linearization of the rotated normal vector of the plate, cf. Figure 2.2 (the linearization of the deformed normal vector is given by $\nu = \hat{\nu} - \nabla w + \mathcal{O}(\|\nabla w\|^2)$). Eliminating β from (3.1.7) leads to the Kirchhoff–Love plate equation, which is of the form of a biharmonic problem. Assuming clamped boundary conditions it reads: Find $w \in H_0^2(\Omega)$ such that for all $v \in H_0^2(\Omega)$

$$\int_\Omega \mathcal{C}\nabla^2 w : \nabla^2 v \, dx = \int_\Omega f\, v \, dx. \tag{3.2.1}$$

Like for the Euler–Bernoulli beam, the thickness parameter t does not enter the equation. The problem is well-posed for $w \in H_0^2(\Omega)$ and reads in strong form

$$\begin{cases} \operatorname{div}(\operatorname{div}(\mathcal{C}\nabla^2 w)) = f & \text{in } \Omega, \\ w = \frac{\partial w}{\partial n} = 0 & \text{on } \partial\Omega. \end{cases} \tag{3.2.2}$$

In addition to clamped boundary conditions, free and simply supported boundary conditions can also be prescribed. The general case in strong form reads:

$$\operatorname{div}(\operatorname{div}(\boldsymbol{\sigma})) = f, \qquad \boldsymbol{\sigma} := \mathcal{C}\nabla^2 w \qquad \text{in } \Omega, \tag{3.2.3a}$$

$$w = 0, \quad \frac{\partial w}{\partial n} = 0 \qquad \text{on } \Gamma_c, \tag{3.2.3b}$$

$$w = 0, \quad \boldsymbol{\sigma}_{nn} = 0 \qquad \text{on } \Gamma_s, \tag{3.2.3c}$$

$$\boldsymbol{\sigma}_{nn} = 0, \ \frac{\partial \boldsymbol{\sigma}_{nt}}{\partial t} + \operatorname{div}(\boldsymbol{\sigma}) \cdot n = 0 \qquad \text{on } \Gamma_f, \tag{3.2.3d}$$

$$[\![\boldsymbol{\sigma}_{nt}]\!]_x = \boldsymbol{\sigma}_{n_1 t_1}(x) - \boldsymbol{\sigma}_{n_2 t_2}(x) = 0 \qquad \text{for all } x \in \mathcal{V}_{\Gamma_f}, \tag{3.2.3e}$$

where the boundary $\Gamma = \partial\Omega$ splits into clamped, simply supported, and free boundaries Γ_c, Γ_s, and Γ_f, respectively. $\mathcal{V}_{\Gamma_f}$ denotes the set of corner points where the two adjacent edges belong to Γ_f. Here, n and t denote the plate boundary's outer normal and tangential vector. Physically, $\boldsymbol{\sigma}_{nn} := n^\top \boldsymbol{\sigma} n$ is the normal bending moment, $\partial_t(t^\top \boldsymbol{\sigma} n) + n^\top \operatorname{div}(\boldsymbol{\sigma})$ the effective transverse shear force, and $\boldsymbol{\sigma}_{nt} := t^\top \boldsymbol{\sigma} n$ the torsion moment. Further, the shear force Q is given by $Q = -\operatorname{div}(\boldsymbol{\sigma})$.

Due to the increased regularity of w, point forces f are well-defined for dimensions 2 and 3 as then $H^2(\Omega) \hookrightarrow C^0(\Omega)$ by Sobolev inequalities. In 2D $H^1(\Omega) \not\hookrightarrow C^0(\Omega)$, the Dirac delta is a distribution in $H^{-1-\varepsilon}(\Omega)$, such that for Reissner–Mindlin plates, we cannot prescribe a point force. In 1D this is valid as then $H^1(\Omega) \hookrightarrow C^0(\Omega)$. Another advantage is that the problem of shear locking is circumvented,

and no boundary layers occur. However, to solve the Kirchhoff–Love plate equation with a conforming Galerkin method in the elliptic setting, however, would require H^2-conforming finite elements, where the derivatives have to be also continuous over elements, i.e. elements which are globally in $C^1(\Omega)$.

Remark 3.2.1 (Convergence to 3D elasticity) *Although it makes sense that the plate equations approximate the 3D elasticity problem for small thickness, the question of convergence arises. In [6] a rigorous proof was given that there holds under sufficient regularity assumptions on the domain Ω that*

$$\|u^{3\mathrm{d}} - u_{\mathrm{RM}}^{(1,1,2)}\| = \mathcal{O}(t^{\frac{1}{2}}), \qquad \|u^{3\mathrm{d}} - u_{\mathrm{KL}}^{(1,1,2)}\| = \mathcal{O}(t^{\frac{1}{2}}), \tag{3.2.4}$$

where $u^{3\mathrm{d}}$ denotes the full 3D computation and $u_{\mathrm{RM}}^{(1,1,2)}$, $u_{\mathrm{KL}}^{(1,1,2)}$ the Reissner–Mindlin and Kirchhoff–Love plate solutions where a quadratic instead of a constant ansatz for the vertical deflection has been made, $u_3 = w(x,y) + z^2 W(x,y)$, cf. (3.1.2)*.*

3.3 Hellan–Herrmann–Johnson (HHJ) method for Kirchhoff–Love plates

For ease of presentation, we assume clamped boundary conditions, such that the plate equation reads

$$\begin{cases} \operatorname{div}(\operatorname{div}(\mathcal{C}\nabla^2 w)) = f, & \text{in } \Omega, \\ w = \frac{\partial w}{\partial n} = 0 & \text{on } \partial\Omega. \end{cases} \tag{3.3.1}$$

The construction of general H^2-conforming finite elements is a difficult task as they have to be globally C^1 instead of being "just" continuous over interfaces. Such elements include the Argyris and Bell triangles or the Bogner–Fox–Schmit quadrilateral. The Hsieh–Clough–Tocher element falls in the category of so-called macro-elements, where one triangle is divided into three smaller ones. The famous Morley triangle [22] is a nonconforming H^2 finite element, where the normal derivative is used as a degree of freedom at the edges.

The HHJ method overcomes the issue of C^1-conformity by introducing the linearized moment tensor

$$\boldsymbol{\sigma} := \mathcal{C}\nabla^2 w \tag{3.3.2}$$

as an additional tensor field leading to a mixed saddle point problem: Find $(w, \boldsymbol{\sigma}) \in H_0^1(\Omega) \times H(\operatorname{divdiv}, \Omega)$ such that for all $(v, \boldsymbol{\tau}) \in H_0^1(\Omega) \times H(\operatorname{divdiv}, \Omega)$

$$\int_\Omega \mathcal{C}^{-1}\boldsymbol{\sigma} : \boldsymbol{\tau}\, dx + \langle \operatorname{div}(\boldsymbol{\tau}), \nabla w \rangle_{H(\operatorname{curl})^* \times H(\operatorname{curl})} = 0, \tag{3.3.3a}$$

$$\langle \operatorname{div}(\boldsymbol{\sigma}), \nabla v \rangle_{H(\operatorname{curl})^* \times H(\operatorname{curl})} = -\int_\Omega f v, \tag{3.3.3b}$$

where $\mathcal{C}^{-1}\boldsymbol{\sigma} = \frac{1+\nu}{E}(\boldsymbol{\sigma} - \frac{\nu}{1+\nu}\operatorname{tr}(\boldsymbol{\sigma})\boldsymbol{I}) = \frac{1}{E}((1+\nu)\boldsymbol{\sigma} - \nu \operatorname{tr}(\boldsymbol{\sigma})\boldsymbol{I})$ is the inverted plate material (3.1.6).

Due to the relation $\nabla H^1 \subset H(\operatorname{curl})$, the duality pairing above is well defined. With the Hellan–Herrmann–Johnson stress finite elements (A.1.21) for $\boldsymbol{\sigma}$ and Lagrange finite elements for the vertical deflection the discrete problem reads: Find $(w_h, \boldsymbol{\sigma}_h) \in U_{h,0}^{k+1} \times M_h^k$ such that for all $(v_h, \boldsymbol{\tau}_h) \in U_{h,0}^{k+1} \times M_h^k$

$$\int_\Omega \mathcal{C}^{-1}\boldsymbol{\sigma}_h : \boldsymbol{\tau}_h\, dx + \langle \operatorname{div}(\boldsymbol{\tau}_h), \nabla w_h \rangle_{H(\operatorname{curl})^* \times H(\operatorname{curl})} = 0, \tag{3.3.4a}$$

$$\langle \operatorname{div}(\boldsymbol{\sigma}_h), \nabla v_h \rangle_{H(\operatorname{curl})^* \times H(\operatorname{curl})} = -\int_\Omega f v_h, \tag{3.3.4b}$$

with the duality pairing defined as in (A.1.20).

Theorem 3.3.1 *Problems* (3.3.3) *and* (3.3.4) *are uniquely solvable.*

Theorem 3.3.2 (Comodi [11]) *Let* $(\boldsymbol{\sigma}, w)$ *be the solution of* (3.3.3), $(\boldsymbol{\sigma}_h, w_h) \in M_h^k \times U_{h,\Gamma_D}^{k+1}$, *with* k *a non-negative integer, the solution of* (3.3.4) *and* $\tilde{w} \in H^{k+3}(\Omega) \cap H_0^2(\Omega)$ *the solution of* (3.3.1). *Then*

$$\|\boldsymbol{\sigma} - \boldsymbol{\sigma}_h\|_{L^2} + \|w - w_h\|_{H^1} \leq c h^{k+1} \left(|\tilde{w}|_{H^{k+2}} + |\tilde{w}|_{H^{k+3}}\right), \tag{3.3.5}$$

$$\|w - w_h\|_{L^2} \leq c h^{k+2} \left(|\tilde{w}|_{H^{k+2}} + |\tilde{w}|_{H^{k+3}}\right). \tag{3.3.6}$$

Exercise 3.3.3 *The Ciarlet–Raviart method for Kirchhoff–Love plates uses that* $\mathrm{divdiv}\nabla^2 w = \Delta^2 w$ *is the bi-Laplace and defines* $\sigma = \Delta u$ *as an additional scalar field. Derive the weak formulation for clamped plates and solve the biharmonic plate equation.*

Exercise 3.3.4 *How can the other boundary conditions be incorporated for the HHJ method? What changes are needed to incorporate different boundary conditions for the Ciarlet–Raviart method?*

3.4 TDNNS Tangential-displacement normal-normal stress elements for Reissner–Mindlin plates

As we have observed in Section 2.2 and Section 3.1, the appearance of the rotation field β yields possible shear locking. Discretizing w and β both with Lagrange finite elements does not mimic the continuous property that the gradient of H^1-functions is in $H(\mathrm{curl})$ (or in L^2 in 1D), $\nabla H^1 \subset H(\mathrm{curl})$, but $\nabla w_h \nsubseteq U_h^k$. If we discretize the rotations β with $H(\mathrm{curl})$-conforming Nédélec elements, we obtain the relation $\nabla w_h \subset \mathcal{N}$ such that the constraint $\nabla w_h = \beta_h$ can be fulfilled in the discrete case. The gradient of an $H(\mathrm{curl})$ function needed for the bending energy, however, is not square-integrable and thus the linearized moment stress tensor $\boldsymbol{\sigma}$ is introduced, leading to the clamped Reissner–Mindlin problem: Find $(w, \boldsymbol{\sigma}, \beta) \in H_0^1(\Omega) \times H(\mathrm{divdiv}, \Omega) \times H_0(\mathrm{curl}, \Omega)$ such that for all $(v, \boldsymbol{\tau}, \delta) \in H_0^1(\Omega) \times H(\mathrm{divdiv}, \Omega) \times H_0(\mathrm{curl}, \Omega)$

$$\int_\Omega \mathcal{C}^{-1}\boldsymbol{\sigma} : \boldsymbol{\tau}\, dx + \langle \mathrm{div}(\boldsymbol{\tau}), \beta \rangle_{H(\mathrm{curl})^* \times H(\mathrm{curl})} = 0, \tag{3.4.1a}$$

$$\langle \mathrm{div}(\boldsymbol{\sigma}), \delta \rangle_{H(\mathrm{curl})^* \times H(\mathrm{curl})} - \frac{\kappa G}{t^2} \int_\Omega (\nabla w - \beta) \cdot (\nabla v - \delta)\, dx = -\int_\Omega f v. \tag{3.4.1b}$$

The first equation states that $\boldsymbol{\sigma} = \mathcal{C}\boldsymbol{\varepsilon}(\beta)$ and the second is the Reissner–Mindlin plate equation.

With (A.1.1), (A.1.21), and (A.1.6) the discretized problem reads: Find $(w_h, \boldsymbol{\sigma}_h, \beta_h) \in U_{h,0}^{k+1} \times M_h^k \times \mathcal{N}_{II,0}^k$ such that for all $(v_h, \boldsymbol{\tau}_h, \delta_h) \in U_{h,0}^{k+1} \times M_h^k \times \mathcal{N}_{II,0}^k$

$$\int_\Omega \mathcal{C}^{-1}\boldsymbol{\sigma}_h : \boldsymbol{\tau}_h\, dx + \langle \mathrm{div}(\boldsymbol{\tau}_h), \beta_h \rangle_{H(\mathrm{curl})^* \times H(\mathrm{curl})} = 0, \tag{3.4.2a}$$

$$\langle \mathrm{div}(\boldsymbol{\sigma}_h), \delta_h \rangle_{H(\mathrm{curl})^* \times H(\mathrm{curl})} - \frac{\kappa G}{t^2} \int_\Omega (\nabla w_h - \beta_h) \cdot (\nabla v_h - \delta_h)\, dx = -\int_\Omega f v_h. \tag{3.4.2b}$$

Formulation (3.4.2) is called the TDNNS method for Reissner–Mindlin plates [26].

Note that the same duality pairings in (3.3.3) and (3.4.1) (respectively (3.3.4) and (3.4.2)) are used as $\nabla H^1 \subset H(\mathrm{curl})$. Due to the De'Rham complex, this relation is inherited by the discrete counterparts.

Using by a change of variables the shear $\gamma = \nabla w - \beta \in H(\mathrm{curl})$ instead of the rotation β as unknown, (3.4.1) changes to the equivalent form: Find $(w, \boldsymbol{\sigma}, \gamma) \in H_0^1(\Omega) \times H(\mathrm{divdiv}, \Omega) \times H_0(\mathrm{curl}, \Omega)$ such that for all $(v, \boldsymbol{\tau}, \xi) \in H_0^1(\Omega) \times H(\mathrm{divdiv}, \Omega) \times H_0(\mathrm{curl}, \Omega)$

$$\int_\Omega \mathcal{C}^{-1}\boldsymbol{\sigma} : \boldsymbol{\tau}\, dx + \langle \mathrm{div}(\boldsymbol{\tau}), \nabla w - \gamma \rangle_{H(\mathrm{curl})^* \times H(\mathrm{curl})} = 0, \tag{3.4.3a}$$

$$\langle \mathrm{div}(\boldsymbol{\sigma}), \nabla v - \xi \rangle_{H(\mathrm{curl})^* \times H(\mathrm{curl})} - \frac{\kappa G}{t^2} \int_\Omega \gamma \cdot \xi\, dx = -\int_\Omega f v. \tag{3.4.3b}$$

Here we can see the close relation to the HHJ formulation for the Kirchhoff–Love plate: We obtain that in the limit $t \to 0$ there holds $|\gamma| \to 0$ (or equivalently $|\nabla w - \beta| \to 0$) and thus, (3.3.3) is (formally) recovered. In [26] the auxiliary variable $\tilde{\gamma} := \frac{\kappa G}{t^2}(\nabla w - \beta)$, which can be seen as a kind of normalized shear stress, is introduced as additional unknown and equation to prove convergence independently of the thickness parameter t, i.e., shear locking is circumvented.

Theorem 3.4.1 *[26, Theorem 4] Let* $(w, \boldsymbol{\sigma}, \beta) \in H_0^1(\Omega) \times H(\mathrm{divdiv}, \Omega) \times H_0(\mathrm{curl}, \Omega)$ *the exact solution of* (3.4.1)*,* $(w_h, \boldsymbol{\sigma}_h, \beta_h) \in U_{h,0}^{k+1} \times M_h^k \times \mathcal{N}_{II,0}^k$ *the corresponding finite element solution, and* $\tilde{\gamma} := \frac{\kappa G}{t^2}(\nabla w - \beta)$*,* $\tilde{\gamma}_h := \frac{\kappa G}{t^2}(\nabla w_h - \beta_h)$*. Then there holds the a priori estimate for* $1 \leq m \leq k$ *with a constant* $c \neq c(t)$

$$\|w - w_h\|_{H^1} + \|\beta - \beta_h\|_{H(\mathrm{curl})} + \|\boldsymbol{\sigma} - \boldsymbol{\sigma}_h\|_{M_h} + t\|\tilde{\gamma} - \tilde{\gamma}_h\|_{L^2} \leq c h^m \left(\|\beta\|_{H^{m+1}} + \|\boldsymbol{\sigma}\|_{H^m} + t\|\tilde{\gamma}\|_{H^m}\right).$$

3.5 Hybridization of HHJ and TDNNS method

One possible disadvantage of the HHJ and TDNNS method presented above is their saddle-point structure, leading to an indefinite matrix after assembling. For the HHJ method for Kirchhoff–Love plates (3.3.4), the system matrix is of the form

$$\begin{pmatrix} A & B^\top \\ B & 0 \end{pmatrix} \begin{pmatrix} \underline{\boldsymbol{\sigma}} \\ \underline{w} \end{pmatrix} = \underline{f}, \tag{3.5.1}$$

where $\underline{\boldsymbol{\sigma}}$, $\underline{w}$, and $\underline{f}$ represent the coefficient vectors of the finite elements $\boldsymbol{\sigma}_h$ and w_h and the right-hand side f, respectively. The displacement w can be interpreted as a Lagrange multiplier enforcing the force balance equation $-\mathrm{div}(\boldsymbol{\sigma}) = f$. With the usage of hybridization techniques, however, a positive definite matrix can be recovered.

For hybridization, the continuity condition of finite elements is broken and reinforced in a weak sense. Therefore, so-called hybridization or facet spaces have to be used. Define the facet space

$$\Gamma_h^k := \mathcal{P}^k(\mathcal{F}), \qquad \Gamma_{h,0}^k := \{\alpha \in \Gamma_h^k \,|\, \alpha = 0 \text{ on } \partial\Omega\}, \tag{3.5.2}$$

i.e., piece-wise polynomials on the skeleton $\mathcal{F}$. We equip it with the normal vector n_F, such that its functions are facet-wise two-valued, differing only in the sign. More precisely, by defining this space as the normal-facet space

$$\Lambda_h^k := \{\alpha_h n_F \,|\, \alpha_h \in \Gamma_h^k\} \tag{3.5.3}$$

we have for $\alpha_h \in \Lambda_h^k$ that $\alpha_{h,n_{T_1}} = -\alpha_{h,n_{T_2}}$. Thus, a normal-normal continuous function with zero normal-normal trace on $\partial\Omega$ of a function $\boldsymbol{\sigma}_h \in M_h^{dc,k}$ can be achieved by the equation

$$0 = \sum_{T \in \mathcal{T}} \int_{\partial T} \boldsymbol{\sigma}_{h,nn}\, \alpha_{h,n}\, ds = \sum_{F \in \mathcal{F}} \int_F [\![\boldsymbol{\sigma}_{h,nn}]\!]\, \alpha_h\, ds \text{ for all } \alpha_h \in \Lambda_h^k. \tag{3.5.4}$$

For the HHJ method, we break the normal-normal-continuity and denote the discontinuous stress space by M_h^{dc}. More precisely, let $\alpha_h \in \Lambda_h$ from the hybridization space (3.5.3). Further, α_h has to satisfy the essential boundary conditions on Γ_D. Then the hybridized HHJ problem reads: Find stress, displacement, and hybridization fields $(\boldsymbol{\sigma}_h, w_h, \alpha_h) \in M_h^{\mathrm{dc},k} \times U_{h,0}^{k+1} \times \Lambda_{h,0}^k$ for all $(\boldsymbol{\tau}_h, v_h, \xi_h) \in M_h^{\mathrm{dc},k} \times U_{h,0}^{k+1} \times \Lambda_{h,0}^k$

$$\int_\Omega \mathcal{C}^{-1}\boldsymbol{\sigma}_h : \boldsymbol{\tau}_h\, dx + \langle \mathrm{div}(\boldsymbol{\tau}_h), \nabla w_h \rangle_{H(\mathrm{curl})^* \times H(\mathrm{curl})} - \sum_{T \in \mathcal{T}} \int_{\partial T} \alpha_{h,n} \boldsymbol{\tau}_{h,nn}\, ds = 0, \tag{3.5.5a}$$

$$\langle \mathrm{div}(\boldsymbol{\sigma}_h), \nabla v_h \rangle_{H(\mathrm{curl})^* \times H(\mathrm{curl})} = \int_\Omega f\, v_h\, dx, \tag{3.5.5b}$$

$$-\sum_{T \in \mathcal{T}} \int_{\partial T} \xi_{h,n} \boldsymbol{\sigma}_{h,nn}\, ds = 0, \tag{3.5.5c}$$

The Lagrange multiplier α_h enforces in equation (3.5.5c) the normal-normal continuity of $\boldsymbol{\sigma}_h$ and the boundary condition. Combining the surface terms in (3.5.5a), one observes that α_h has the physical meaning of the normal derivative of the displacement $\frac{\partial w_h}{\partial n} \approx \alpha_{h,n}$.

Exercise 3.5.1 *Incorporate and test the different boundary conditions for the mixed and hybrid mixed HHJ method for Kirchhoff–Love plates.*

As for $\boldsymbol{\sigma}_h$ and α_h the same polynomial order is used, the hybridized system (3.5.5) is equivalent to the original one (3.3.4). However, the discontinuous stress $\boldsymbol{\sigma}_h \in M_h^{k,dc}$ does not have any coupling dofs and thus, one can use static condensation to eliminate it at the element level, reducing the number of total dofs drastically for the final system, and making it therefore symmetric and positive definite again

$$\begin{aligned} \begin{pmatrix} A & B^\top \\ B & 0 \end{pmatrix} \begin{pmatrix} \underline{\boldsymbol{\sigma}} \\ \begin{pmatrix} \underline{w} \\ \underline{\alpha} \end{pmatrix} \end{pmatrix} &= \begin{pmatrix} 0 \\ \underline{f} \end{pmatrix}, \\ \underline{\boldsymbol{\sigma}} = -A^{-1}B^\top \begin{pmatrix} \underline{w} \\ \underline{\alpha} \end{pmatrix}, \qquad -BA^{-1}B^\top \begin{pmatrix} \underline{w} \\ \underline{\alpha} \end{pmatrix} &= \underline{f}. \end{aligned} \tag{3.5.6}$$

From the first equation, $\underline{\boldsymbol{\sigma}}$ can be explicitly expressed in terms of $\underline{w}$ and $\underline{\alpha}$. This identity is inserted into the second equation, leading to the Schur-complement matrix $-BA^{-1}B^\top$. Note that A is a block diagonal matrix and thus cheap to invert. Regarding the TDNNS method, α_h corresponds to the normal component of the rotations, $\alpha_{h,n} \approx \beta_{h,n}$.

Exercise 3.5.2 *The Föppl–von Kármán equations reading*

$$\begin{aligned} \frac{Et^3}{12(1-\nu^2)}\Delta^2 w - t\sum_{i,j=1}^{2} \frac{\partial}{\partial x_j}\Big(\boldsymbol{\sigma}_{ij}\frac{\partial w}{\partial x_i}\Big) &= P, \\ \operatorname{div}\boldsymbol{\sigma} &= 0, \end{aligned}$$

are used to simulate large deformations for thin plates. Here $\Delta^2 w$ denotes the bi-Laplace and P a volume force. In the derivation, the initial stress-strain relation also contains the quadratic terms of the vertical deflection $\sigma = \mathcal{C}\boldsymbol{\varepsilon} = \mathcal{C}\big(\varepsilon(u) + 0.5\nabla w \otimes \nabla w\big)$, $u = (u_x, u_y, w)$ with u_x, u_y the horizontal displacements. Show that with the Airy stress function φ with $\boldsymbol{\sigma}_{11} = \frac{\partial^2\varphi}{\partial x_2^2}$, $\boldsymbol{\sigma}_{22} = \frac{\partial^2\varphi}{\partial x_1^2}$, and $\boldsymbol{\sigma}_{12} = -\frac{\partial^2\varphi}{\partial x_1 \partial x_2}$ the equations become

$$\frac{Et^3}{12(1-\nu^2)}\Delta^2 w - t\,[\varphi, w] = P, \qquad\qquad \Delta^2\varphi + \frac{E}{2}\,[w, w] = 0,$$

with $[u, v] := \operatorname{cof}(\nabla^2 u) : \nabla^2 v = \frac{\partial^2 u}{\partial x_2^2}\frac{\partial^2 v}{\partial x_1^2} + \frac{\partial^2 u}{\partial x_1^2}\frac{\partial^2 v}{\partial x_2^2} - 2\frac{\partial^2 u}{\partial x_1 \partial x_2}\frac{\partial^2 v}{\partial x_1 \partial x_2}$. Derive the weak formulation for clamped boundary conditions $w = \frac{\partial w}{\partial n} = \varphi = \frac{\partial \varphi}{\partial n} = 0$.

Exercise 3.5.3 *Reformulate the Föppl–von Kármán equations in terms of the Hellan–Herrmann–Johnson method such that Lagrangian finite elements can be used for w and φ.*

Chapter 4

Differential geometry and curvature

One fundamental difference between plates and general shell structures is that plates are non-curved (in the initial configuration). This entails the usage of standard (Euclidean) derivatives and components based on the Euclidean basis, which does not change spatially. For example, the normal vector of a plate $\mathcal{S} \subset \mathbb{R}^2 \times \{0\}$ is $\nu = \begin{pmatrix} 0 & 0 & 1 \end{pmatrix}^\top$ and thus $\nabla\nu = 0$. To define tangential and normal components of curved surfaces, however, the basis vectors depend on the position on the surface. To define and treat objects like surface derivatives, we need tools from differential geometry. If the surface is not smooth, e.g., if we use an affine triangulation consisting of piece-wise flat triangles to approximate a curved surface, additional questions arise in discrete differential geometry (DDG). Literature including classical, modern, and discrete differential geometry are e.g. [13, 16, 29, 4, 31, 20, 23].

Remark 4.0.1 *Different approaches/dialects are used in differential geometry. For example, defining more or less all objects in terms of coordinates, or using more coordinate-free notation. We will use a notation comparable to tangential differential calculus (TDC), where differential operators are defined in a more compact notation. The notation of curvilinear coordinates is widely used. Another language used in differential geometry is exterior calculus, which is more "abstract" than the others.*

As shells are two-dimensional objects embedded in the three-dimensional Euclidean space, we will use in this section the concept of sub-manifolds embedded in $\mathbb{R}^n$, leading to extrinsic differential geometry.

4.1 (Sub-) Manifolds

For completeness, we recap the definition of a smooth submanifold.

Definition 4.1.1 *Let $0 \leq k < n$ be an integer. A differentiable function $\varphi : \omega \to \mathbb{R}^n$ with $\omega \subset \mathbb{R}^k$ open is called an* embedding *if $\nabla\varphi \in \mathbb{R}^{n\times k}$ has full rank, i.e., $\nabla\varphi$ is injective. $\mathcal{S} \subset \mathbb{R}^n$ is a k-dimensional* submanifold *of $\mathbb{R}^n$ if for every $x \in \mathcal{S}$ there exists an embedding $\varphi : V \to U$ from $V \subset \mathbb{R}^k$ open to an open neighborhood $U \subset \mathbb{R}^n$ of x such that $\mathcal{S} \cap U = \varphi(V)$. For $n = 3$ and $k = 2$ we call $\mathcal{S}$ a* surface *and for $k = 1$ a* curve.

In the following, we assume w.l.o.g. that the manifold $\mathcal{S}$ can be parameterized with a single embedding and note that the results can easily be extended by using an atlas, i.e., a set of embeddings covering the whole manifold. Several ways exist to define the tangent space of $\mathcal{S}$ at a point $p \in \mathcal{S}$. We use the embedding (the definition is, in fact, independent of the chosen embedding).

Definition 4.1.2 *Let $\varphi : \mathbb{R}^k \to \mathcal{S}$ be an embedding such that $p \in \mathcal{S}$ is an interior point of the range of φ. Then the* tangent space *at $p \in \mathcal{S}$ is defined by*

$$T_p\mathcal{S} := \nabla\varphi(q)\mathbb{R}^k := \{\nabla\varphi(q)\eta \in \mathbb{R}^n \,|\, \eta \in \mathbb{R}^k\}, \qquad p = \varphi(q) \tag{4.1.1}$$

and the tangent bundle *by $T\mathcal{S} := \bigsqcup_{p\in\mathcal{S}} T_p\mathcal{S} := \bigcup_{p\in\mathcal{S}} \{p\} \times T_p\mathcal{S}$.*

We focus on $n-1$ dimensional submanifolds such that a unique normal vector (up to orientation) exists.

Definition 4.1.3 *Let $\mathcal{S}$ be an $n-1$ dimensional submanifold of $\mathbb{R}^n$. A function $\nu : \mathcal{S} \to \mathbb{S}^{n-1}$ is a* normal vector *field of $\mathcal{S}$ if for all $p \in \mathcal{S}$ there holds $\nu(p) \perp T_p\mathcal{S}$. A surface $\mathcal{S}$ is called* orientable *if a globally continuous normal vector field exists $\nu : \mathcal{S} \to \mathbb{S}^{n-1}$. The* projection operator *onto the tangent bundle $\boldsymbol{P}_\mathcal{S} : \mathbb{R}^n \to T\mathcal{S}$ is defined by $\boldsymbol{P}_\mathcal{S} := \boldsymbol{I} - \nu \otimes \nu$.*

There are two, equivalent, ways to define derivatives of functions $f : \mathcal{S} \to \mathbb{R}$ on the surface: Using the embedding going back to $\mathbb{R}^k$, where we know how to differentiate, or to use the surrounding space $\mathbb{R}^n$ computing the classical derivative and projecting the result back onto the surface.

Definition 4.1.4 *Let $\mathcal{S} \subset \mathbb{R}^n$ be a smooth k-dimensional sub-manifold, $p \in \mathcal{S}$, $f : \mathcal{S} \to \mathbb{R}$ and $\varphi : \mathbb{R}^k \to \mathcal{S}$ an embedding. Then we call the function f* differentiable, *$f \in C^1(\mathcal{S})$, at $p \in \mathcal{S}$, w.l.o.g. $\varphi(0) = p$, if*

$$\nabla_\mathcal{S} f(p) := \nabla((f \circ \varphi)(0))(\nabla\varphi(0))^\dagger \tag{4.1.2}$$

is differentiable in classical sense and call $\nabla_\mathcal{S} f$ the tangential *or* surface gradient *of f. Here, $(\nabla\varphi)^\dagger \in \mathbb{R}^{k\times n}$ denotes the* Moore–Penrose pseudo-inverse *of $\nabla\varphi \in \mathbb{R}^{n\times k}$.*

The Moore–Penrose pseudo-inverse $\boldsymbol{A}^\dagger$ of a rank k matrix $\boldsymbol{A} \in \mathbb{R}^{n\times k}$ is given by $\boldsymbol{A}^\dagger = (\boldsymbol{A}^\top\boldsymbol{A})^{-1}\boldsymbol{A}^\top$.

The definition is independent of the particular embedding φ and can be extended easily to vector-valued functions $f : \mathcal{S} \to \mathbb{R}^n$.

For smooth manifolds we can define an ε-tube around it, where we can then extend functions. We focus on surfaces in 3D.

Theorem 4.1.5 *Let $\omega \subset \mathbb{R}^2$ be a domain and let $\varphi \in C^3(\overline{\omega}, \mathbb{R}^3)$ be an embedding. Then there exists $\varepsilon > 0$ such that the mapping $\Theta : \overline{\Omega} \to \mathbb{R}^3$, $\Omega := \omega \times (-\varepsilon/2, \varepsilon/2)$ defined by*

$$\Theta(x, z) := \varphi(x) + z\nu(x) \qquad \text{for all } (x, z) \in \overline{\Omega} \tag{4.1.3}$$

is a C^2-diffeomorphism from $\overline{\Omega}$ onto $\Theta(\overline{\Omega})$ and $\det(\tau_1, \tau_2, \nu) > 0$ in $\overline{\Omega}$, where $\tau_i = \frac{\partial \Theta}{\partial x_i}$ and $\nu = \frac{\tau_1 \times \tau_2}{\|\tau_1 \times \tau_2\|_2}$.

Proof: See e.g., [10, Theorem 4.1-1]. □

The requirement on the thickness ε depends on the curvature of the surface.

With Theorem 4.1.5 and the projection $\boldsymbol{P}_{\mathcal{S}}$ for given $f : \mathcal{S} \to \mathbb{R}$ an extension $F : \mathbb{R}^3 \to \mathbb{R}$ can be defined such that $F|_{\mathcal{S}} = f$, e.g., by extending it constantly in ν direction. With this at hand, we define the tangential derivative as

$$\nabla_{\mathcal{S}} f = \boldsymbol{P}_{\mathcal{S}} \nabla F, \tag{4.1.4}$$

which is independent of the choice of the extension F. Note that (4.1.4) is an equivalent definition to (4.1.2). For vector valued functions $f : \mathcal{S} \to \mathbb{R}^3$ the surface gradient via extension is given by $\nabla_{\mathcal{S}} f = \nabla F \boldsymbol{P}_{\mathcal{S}}$.

Definition 4.1.6 *The* surface divergence *of a vector-valued function $u \in C^1(\mathcal{S}, \mathbb{R}^n)$ is defined by* $\operatorname{div}_{\mathcal{S}}(u) := \operatorname{tr}(\nabla_{\mathcal{S}} u)$.

With the projection operator $\boldsymbol{P}_{\mathcal{S}}$ onto the tangent space at hand we can define the covariant surface derivative.

Definition 4.1.7 *Let $\mathcal{S} \subset \mathbb{R}^n$ be a smooth $n-1$-dimensional sub-manifold, $\boldsymbol{P}_{\mathcal{S}}$ the projection onto the tangent space, and $f : \mathcal{S} \to \mathbb{R}^n$ a differentiable vector field. The* covariant surface gradient *of f is defined by*

$$\nabla_{\mathcal{S}}^{\mathrm{cov}} f := \boldsymbol{P}_{\mathcal{S}} \nabla_{\mathcal{S}} f \tag{4.1.5}$$

or via extension $F : \mathbb{R}^n \to \mathbb{R}^n$ as $\nabla_{\mathcal{S}}^{\mathrm{cov}} f := \boldsymbol{P}_{\mathcal{S}} \nabla_{\mathcal{S}} F \boldsymbol{P}_{\mathcal{S}}$. The Riemannian Hesse *of $f \in C^2(\mathcal{S})$ is given by $\nabla_{\mathcal{S}}^2 f := \nabla_{\mathcal{S}}^{\mathrm{cov}} \nabla_{\mathcal{S}} f$.*

Note, that for a vector field f on $\mathcal{S}$ there holds $\nu^\top \nabla_{\mathcal{S}}^{\mathrm{cov}} f = 0$ and $\nabla_{\mathcal{S}}^{\mathrm{cov}} f \, \nu = 0$, but in general $\nu^\top \nabla_{\mathcal{S}} f \neq 0$ (only $\nabla_{\mathcal{S}} f \, \nu = 0$).

4.1.1 Shape operator and fundamental forms

The following fundamental forms are introduced to measure distances and curvatures on manifolds.

Definition 4.1.8 *Let $\mathcal{S}$ be a surface with normal vector ν and $v, w \in T\mathcal{S}$. Then the first, second, and third fundamental forms are given by*

$$I(v, w) := \langle v, w \rangle, \tag{4.1.6a}$$

$$II(v, w) := \langle \nabla_{\mathcal{S}} \nu \, v, w \rangle, \tag{4.1.6b}$$

$$III(v, w) := \langle \nabla_{\mathcal{S}} \nu \, v, \nabla_{\mathcal{S}} \nu \, w \rangle, \tag{4.1.6c}$$

where $\langle \cdot, \cdot \rangle$ denotes the Euclidean scalar product in $\mathbb{R}^3$ restricted on the tangent space.

$\nabla_{\mathcal{S}} \nu$ is the Weingarten tensor, which is symmetric and acts on tangent vectors. It induces the shape operator $\mathfrak{S} : T\mathcal{S} \to T\mathcal{S} : X \mapsto \nabla_{\mathcal{S}} \nu X$. It is further referred to as the curvature tensor because the second derivatives of the underlying embedding of the shell contain all the curvature information. The sign convention is not unique, it is also possible to define $-\nabla_{\mathcal{S}} \nu$ as the Weingarten tensor.

4.2 Mapping between surfaces

Next, we consider two surfaces $\hat{\mathcal{S}}$ and $\mathcal{S}$ connected diffeomorphically by $\Phi : \hat{\mathcal{S}} \to \mathcal{S}$. In the context of shells, $\hat{\mathcal{S}}$ and $\mathcal{S}$ correspond to the initial and deformed mid-surface of the shell, respectively, and Φ will be the deformation of the mid-surface. We are interested in how the tangential and normal vectors and the fundamental forms can be expressed (pulled-back) in terms of vectors living on $\hat{\mathcal{S}}$ and the deformation Φ.

4.2.1 Pull back of vectors

We start with a tangent vector $v \in T_p\mathcal{S}$. By definition and the chain rule we obtain that $\exists q, \eta \in \mathbb{R}^2 : \Phi\circ\varphi(q) = p, \varphi(q) = \hat{p}$, $v = \nabla(\Phi\circ\varphi)(q)\eta = (\nabla_{\hat{\mathcal{S}}}\Phi)(\hat{p})(\nabla\varphi)(q)\eta = (\nabla_{\hat{\mathcal{S}}}\Phi)(\hat{p})\hat{v}$, where $\hat{v} = (\nabla\varphi)(q)\eta \in T_{\hat{p}}\hat{\mathcal{S}}$. Thus $v = (\nabla_{\hat{\mathcal{S}}}\Phi)(\hat{p})\hat{v}$, or in terms of vector fields $v : \mathcal{S} \to T\mathcal{S}$, $v = (\nabla_{\hat{\mathcal{S}}}\Phi)\hat{v}$, $\hat{v} : \hat{\mathcal{S}} \to T\hat{\mathcal{S}}$.

We observe that the tangent vectors of $\hat{\mathcal{S}}$ get explicitly mapped to $\mathcal{S}$ by the push forward $\nabla_{\hat{\mathcal{S}}}\Phi =: \boldsymbol{F}_{\hat{\mathcal{S}}}$, which we will denote in the following by $\boldsymbol{F}_{\hat{\mathcal{S}}}$, having the physical meaning of the surface deformation gradient later in the context of shells.

The cofactor matrix $\operatorname{cof}(\boldsymbol{A})$ is well-defined for all matrices $\boldsymbol{A} \in \mathbb{R}^{n\times n}$. If $\boldsymbol{A}$ is regular there holds the identity $\operatorname{cof}(\boldsymbol{A}) = \det\boldsymbol{A}\,\boldsymbol{A}^{-\top}$. As $\boldsymbol{F}_{\hat{\mathcal{S}}}$ interpreted as 3×3 matrix has only rank 2, we will make use of the following results.

Lemma 4.2.1 *Let $\boldsymbol{A} \in \mathbb{R}^{3\times 3}$ with $\operatorname{rank}(\boldsymbol{A}) = 2$. Then there holds*

$$\boldsymbol{A}^\top \operatorname{cof}(\boldsymbol{A}) = 0.$$

Proof: As the set of regular matrices GL(3) is dense in the set of all matrices there exists for all $\boldsymbol{A} \in \mathbb{R}^{3\times 3}$ and $\varepsilon > 0$ some $\boldsymbol{A}_\varepsilon \in \mathrm{GL}(3)$ such that $\|\boldsymbol{A}_\varepsilon - \boldsymbol{A}\|_F < \varepsilon$. Therefore, with continuity of the determinant, there holds

$$\boldsymbol{A}^\top \operatorname{cof}(\boldsymbol{A}) = \lim_{\varepsilon\to 0} \boldsymbol{A}_\varepsilon^\top \operatorname{cof}(\boldsymbol{A}_\varepsilon) = \lim_{\varepsilon\to 0} \det(\boldsymbol{A}_\varepsilon) = 0.$$

□

Lemma 4.2.1 states that the range of $\operatorname{cof}(\boldsymbol{A})$ is exactly the kernel of $\boldsymbol{A}$ for a rank two matrix, such that we can describe the transformation of normal vectors.

Lemma 4.2.2 *Let $\hat{\mathcal{S}}$ be a surface with normal vector field $\hat{\nu}$. For the mapped surface $\mathcal{S} := \phi(\hat{\mathcal{S}})$, $\phi : \hat{\mathcal{S}} \to \mathbb{R}^3$ a diffeomorphism, let ν be the corresponding normal vector. Then, with $\boldsymbol{F}_{\hat{\mathcal{S}}} := \nabla_{\hat{\mathcal{S}}}\phi$*

$$\nu \circ \phi = \frac{\operatorname{cof}(\boldsymbol{F}_{\hat{\mathcal{S}}})\hat{\nu}}{\|\operatorname{cof}(\boldsymbol{F}_{\hat{\mathcal{S}}})\hat{\nu}\|_2} = \frac{\operatorname{cof}(\boldsymbol{F}_{\hat{\mathcal{S}}})\hat{\nu}}{\|\operatorname{cof}(\boldsymbol{F}_{\hat{\mathcal{S}}})\|_F}. \tag{4.2.1}$$

Proof: Let $p \in \mathcal{S}$ and $\eta \in T_p\mathcal{S}$ be arbitrary. Then with $\eta \circ \phi = \boldsymbol{F}_{\hat{\mathcal{S}}}\hat{\eta}$ for some $\hat{\eta} \in T\hat{\mathcal{S}}$

$$\eta \circ \phi \cdot \nu \circ \phi = \frac{1}{\|\operatorname{cof}(\boldsymbol{F}_{\hat{\mathcal{S}}})\hat{\nu}\|_2}\hat{\eta}^\top \boldsymbol{F}_{\hat{\mathcal{S}}}^\top \operatorname{cof}(\boldsymbol{F}_{\hat{\mathcal{S}}})\hat{\nu} \overset{\text{Lemma 4.2.1}}{=} 0.$$

□

4.2.2 Pull back of fundamental forms

The fundamental forms on the mapped surface $\mathcal{S} = \Phi(\hat{\mathcal{S}})$ can directly be pulled-back, with $\hat{v}, \hat{w} \in T\hat{\mathcal{S}}$ via

$$\Phi^* I(\hat{v}, \hat{w}) = \langle \nabla_{\hat{\mathcal{S}}}\Phi\,\hat{v}, \nabla_{\hat{\mathcal{S}}}\Phi\,\hat{w}\rangle, \tag{4.2.2a}$$
$$\Phi^* II(\hat{v}, \hat{w}) = \langle (\nabla_{\mathcal{S}}\nu)\circ\Phi\,\nabla_{\hat{\mathcal{S}}}\Phi\,\hat{v}, \nabla_{\hat{\mathcal{S}}}\Phi\,\hat{w}\rangle, \tag{4.2.2b}$$
$$\Phi^* III(\hat{v}, \hat{w}) = \langle (\nabla_{\mathcal{S}}\nu)\circ\Phi\,\nabla_{\hat{\mathcal{S}}}\Phi\,\hat{v}, (\nabla_{\mathcal{S}}\nu)\circ\Phi\,\nabla_{\hat{\mathcal{S}}}\Phi\,\hat{w}\rangle. \tag{4.2.2c}$$

We will neglect the Φ^* for ease of presentation.

4.3 Curvature

Let $\mathcal{S}$ be a surface in $\mathbb{R}^3$ throughout this section. We discuss the types and computation of different curvatures of the surface.

Definition 4.3.1 *Let κ_1, κ_2 be the two eigenvalues of the Weingarten tensor $\nabla_{\mathcal{S}}\nu$ not corresponding to the eigenvector ν. They are called the* principal curvatures *and the corresponding eigenvectors the* principal curvature directions*. The* mean *and* Gauss *curvature, respectively, are given by the mean and product of the eigenvalues, $H = \frac{1}{2}(\kappa_1 + \kappa_2)$ and $K = \kappa_1\kappa_2$.*

The mean curvature can directly be obtained from the trace of the Weingarten tensor, $H = \frac{1}{2}\operatorname{tr}(\nabla_{\mathcal{S}}\nu)$, for the Gauss curvature, however, we cannot take the determinant, which is zero. The cofactor matrix is used instead.

Lemma 4.3.2 *Let $\boldsymbol{A} \in \mathbb{R}^{3\times 3}_{\text{sym}}$ be a rank 2 matrix with kernel $v \in \mathbb{R}^3$, $\boldsymbol{A}v = 0$, such that $\|v\|_2 = 1$. Then the product of the two non-zero eigenvalues is given by $\operatorname{cof}(\boldsymbol{A})_{vv}$. Especially, there holds for the Gauss curvature $K = \operatorname{cof}(\nabla_{\mathcal{S}}\nu)_{\nu\nu}$.*

Proof: Entry $\operatorname{cof}(\boldsymbol{A})_{ij}$ is the determinant of the 2×2 sub-matrix where the i*th* row and j*th* column is neglected. Thus, $\operatorname{cof}(\boldsymbol{A})_{vv}$ is the determinant of the 2×2 matrix when deleting the zero row and column. □

Remark 4.3.3 *Another possibility the compute the Gauss curvature is to regularize the Weingarten tensor, $K = \det(\nabla_{\mathcal{S}}\nu + \nu \otimes \nu)$.*

Depending on the Gauss curvature, four types of surfaces can (locally) be identified. We call a surface at point $p \in \mathcal{S}$

- elliptic, if $K(p) > 0$,
- hyperbolic, if $K(p) < 0$,
- parabolic, if $K(p) = 0$ and $\kappa_1 \neq 0$ or $\kappa_2 \neq 0$.
- flat (planar), if $K(p) = \kappa_1(p) = \kappa_2(p) = 0$

4.4 Approximated surfaces and discrete curvature

We discuss the computation of the curvature if only an approximation of the surface is given. For a quick introduction to finite elements on surfaces, see Appendix A.2.

For a triangulation $\mathcal{T}$ approximating $\mathcal{S}$ we assume that it is densely inscribed, i.e., the vertices of $\mathcal{T}$ lie on $\mathcal{S}$. If the triangulation is not affine, but polynomial, it will be curved for better approximation. We say a triangulation is curved of order k if for all $T \in \mathcal{T}$ there exists a function $\Phi_T \in \mathcal{P}^k(\hat{T}, \mathbb{R}^3)$ mapping the reference triangle to T, $T = \Phi_T(\hat{T})$. There are several ways to curve the triangulation appropriately. The projection-based interpolation uses the dofs of Lagrangian elements, first determining the edge dofs and then the inner dofs to obtain an L^2- (or H^1-) best approximation of $\mathcal{S}$. Note that $\mathcal{T}$ is globally continuous but in general not differentiable.

For an affine triangulation $\mathcal{T}$ the discrete outer normal vector ν is piece-wise constant and thus, $\nabla_{\mathcal{T}}\nu|_T = 0$ for all $T \in \mathcal{T}$, where we used the notation $\nabla_{\mathcal{T}}$ to emphasize that we are on a triangulated surface. Moreover, the normal vector may jump over the interfaces, see Figure 4.1. Hence, the discrete Weingarten tensor can at best be a distribution.

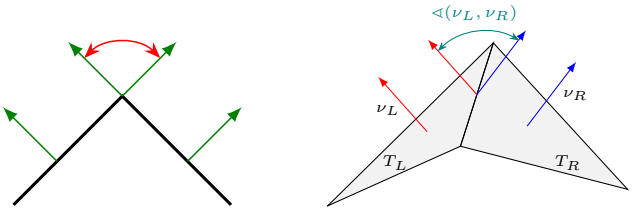

Figure 4.1: Jump of normal vector over two affine elements in 2D and 3D.

Definition 4.4.1 *Let $\mathcal{T}$ be a triangulation of order k of a surface $\mathcal{S}$ and $\mathcal{E}$ the corresponding skeleton. We define the distributional Weingarten tensor acting on co-normal–co-normal continuous HHJ functions, $\boldsymbol{\sigma} \in M^k_{h,0}$ by*

$$\langle \nabla_{\mathcal{T}} \nu, \boldsymbol{\sigma} \rangle = \sum_{T \in \mathcal{T}} \int_T \nabla_{\mathcal{T}} \nu|_T : \boldsymbol{\sigma} \, ds + \sum_{E \in \mathcal{E}} \int_E \sphericalangle(\nu_L, \nu_R) \boldsymbol{\sigma}_{\mu\mu} \, dl, \tag{4.4.1}$$

where $\sphericalangle(a, b) := \arccos\left(\frac{a \cdot b}{\|a\|_2 \|b\|_2}\right)$ denotes the angle of two vectors and ν_L, ν_R the normal vectors on the two triangles T_L, T_R sharing the same edge E.

Remark 4.4.2 *In the case of a polygon (affine) triangulation $\mathcal{T}$, only the edge terms in* (4.4.1) *remain, where the angle of the normal vector jump is computed. This is in common with discrete differential geometry, where the dihedral angle is also used as part of the curvature computation.*

Note that for a high-order surface approximation, the jump term becomes less important regarding curvature information; however, it is crucial for numerical stability and obtaining optimal convergence rates. We also define the lifted Weingarten tensor for visualisation purposes, where a discrete L^2-Riesz representative is computed.

Definition 4.4.3 *Let $\mathcal{T}$ be a triangulation of order k of the surface $\mathcal{S}$. Then the lifted curvature $\boldsymbol{\kappa}_h \in M^k_{h,0}$ is given as the solution of*

$$\int_{\mathcal{T}} \boldsymbol{\kappa}_h : \boldsymbol{\sigma}_h \, ds = \langle \nabla_{\mathcal{T}} \nu, \boldsymbol{\sigma}_h \rangle, \qquad \text{for all } \boldsymbol{\sigma}_h \in M^k_{h,0}. \tag{4.4.2}$$

Chapter 5

Shells

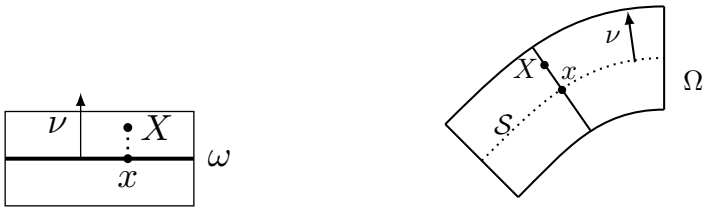

Figure 5.1: Description of shell structures by its mid-surface $\mathcal{S}$ and normal vector ν. Every point X can be represented in the form $X = x + z\nu$. (left) Flat structure. (right) Curved structure.

The appearance of shell structures, where one direction is significantly smaller than the others, is common in nature and technology. The scaling ranges from small, like cell membranes, to large, such as parts of cars and aeroplanes. Like for beams and plates, models were developed where only the mid-surface of the structure gets discretized and assumptions are made to "neglect" the thin direction, i.e., a dimension reduction. Koiter [17] derived consistent equations for shells from continuum mechanics, and Naghdi [24] proposed shell models of arbitrary order. Another idea from Cosserat [12] directly starts with a 2D model and postulates the balance equations. Therein, the shell is described by its mid-surface and an additional independent director field on it, called geometrically exact shell models.

The behavior of shell models should coincide with the full model, especially in the limit $t \to 0$, when the thickness tends to zero. Besides asymptotic analysis in the thickness parameter t the derivation of beam, plate, and shell models from 3D elasticity has also been discussed via Γ-convergence (see e.g. [18]).

5.1 Shell description

Looking at a plate structure as depicted in Figure 5.1 (left), one can describe every point X in it by its mid-surface ω and going along the normal vector, $X = x + z\nu$. Therefore, the question arises whether we can describe every thin-walled structure in this form. The answer is positive if the structure is smooth and "thin" enough. If the thickness t is smaller than ε of Theorem 4.1.5, it justifies to split a shell Ω into its mid-surface $\mathcal{S}$ and the corresponding normal vector ν

$$\Omega = \{X = x + z\,\nu(x) \,|\, x \in \mathcal{S},\, z \in [-t/2, t/2]\}\,, \tag{5.1.1}$$

as depicted in Figure 5.1 (right).

Definition 5.1.1 *We call a surface $\mathcal{S}$ with its normal vector field $\nu : \mathcal{S} \to \mathbb{S}^2$ the* initial configuration *of a shell and $(\mathcal{S}, \tilde{\nu})$ with a unit vector field $\tilde{\nu} : \mathcal{S} \to \mathbb{S}^2$, also called* director*, a* configuration of a shell.

The director $\tilde{\nu}$, which does not have to be perpendicular to the shell surface, is used to model shearing.

Definition 5.1.2 *Let $\tilde{\nu} : \mathcal{S} \to \mathbb{S}^2$ a director field. The shear form $\sigma_{\tilde{\nu}} : T\mathcal{S} \to \mathbb{R}$ is given for all $p \in \mathcal{S}$ by*

$$(\sigma_{\tilde{\nu}})_p : T_p\mathcal{S} \to \mathbb{R}, \quad v \mapsto \langle \tilde{\nu}(p), v\rangle. \tag{5.1.2}$$

Definition 5.1.3 *Let $(\hat{\mathcal{S}},\, \hat{\nu})$ be the initial configuration of a shell. A deformation $\Phi = (\phi, \overline{\nu})$ of $\hat{\mathcal{S}}$ is*

$$\Phi : \hat{\mathcal{S}} \times [-t/2, t/2] \to \mathbb{R}^3, \qquad (x, z) \mapsto \phi(x) + z\overline{\nu}(x), \tag{5.1.3}$$

where ϕ is the deformation of the mid-surface and $\overline{\nu} : \hat{\mathcal{S}} \to \mathbb{S}^2$ a differentiable unit vector field. We call $\mathcal{S} := \phi(\hat{\mathcal{S}})$ together with $\tilde{\nu} := \overline{\nu} \circ \phi^{-1}$ a deformed configuration *of the shell.*

Analogously to (4.2.2) we can pull back the generalized fundamental and shear forms from the deformed shell configuration to the initial shell mid-surface, $\hat{v}, \hat{w} \in T\hat{\mathcal{S}}$,

$$\Phi^* II_{\tilde{\nu}}(\hat{v}, \hat{w}) := \frac{1}{2}\left(\langle (\nabla_{\mathcal{S}}\tilde{\nu}) \circ \Phi\, \nabla_{\hat{\mathcal{S}}}\Phi\, \hat{v}, \nabla_{\hat{\mathcal{S}}}\Phi\, \hat{w}\rangle + \langle \nabla_{\hat{\mathcal{S}}}\Phi\, \hat{v}, (\nabla_{\mathcal{S}}\tilde{\nu}) \circ \Phi\, \nabla_{\hat{\mathcal{S}}}\Phi\, \hat{w}\rangle\right), \tag{5.1.4a}$$

$$\Phi^* III_{\tilde{\nu}}(\hat{v}, \hat{w}) := \langle (\nabla_{\mathcal{S}}\tilde{\nu}) \circ \Phi\, \nabla_{\hat{\mathcal{S}}}\Phi\, \hat{v}, (\nabla_{\mathcal{S}}\tilde{\nu}) \circ \Phi\, \nabla_{\hat{\mathcal{S}}}\Phi\, \hat{w}\rangle, \tag{5.1.4b}$$

$$\Phi^* \sigma_{\tilde{\nu}}(\cdot) := \sigma_{\tilde{\nu}}(\nabla_{\hat{\mathcal{S}}}\Phi\, \cdot). \tag{5.1.4c}$$

We denote by $\hat{I}$, $\hat{II}$, and $\hat{III}$ the fundamental forms of the initial shell configuration. The matrix representations of the (pull-backed) forms are given, $\boldsymbol{F}_{\hat{\mathcal{S}}} := \nabla_{\hat{\mathcal{S}}}\Phi$, by

$$\begin{aligned} &\hat{I} \mathrel{\hat{=}} \boldsymbol{P}_{\hat{\mathcal{S}}}^\top \boldsymbol{P}_{\hat{\mathcal{S}}} = \boldsymbol{P}_{\hat{\mathcal{S}}}, \qquad \hat{II}_{\hat{\nu}} \mathrel{\hat{=}} \nabla_{\hat{\mathcal{S}}}\hat{\nu}, \qquad \hat{III}_{\hat{\nu}} \mathrel{\hat{=}} \nabla_{\hat{\mathcal{S}}}\hat{\nu}\nabla_{\hat{\mathcal{S}}}\hat{\nu}, \qquad \sigma_{\hat{\nu}} \equiv 0, \qquad \Phi^* I \mathrel{\hat{=}} \boldsymbol{F}_{\hat{\mathcal{S}}}^\top \boldsymbol{F}_{\hat{\mathcal{S}}}, \\ &\Phi^* II_{\tilde{\nu}} \mathrel{\hat{=}} \operatorname{sym}(\boldsymbol{F}_{\hat{\mathcal{S}}}^\top (\nabla_{\mathcal{S}}\tilde{\nu}) \circ \Phi\, \boldsymbol{F}_{\hat{\mathcal{S}}}), \quad \Phi^* III_{\tilde{\nu}} \mathrel{\hat{=}} \boldsymbol{F}_{\hat{\mathcal{S}}}^\top (\nabla_{\mathcal{S}}\tilde{\nu}) \circ \Phi^\top (\nabla_{\mathcal{S}}\tilde{\nu}) \circ \Phi\, \boldsymbol{F}_{\hat{\mathcal{S}}}, \quad \Phi^*\sigma_{\tilde{\nu}} \mathrel{\hat{=}} \boldsymbol{F}_{\hat{\mathcal{S}}}^\top \tilde{\nu} \circ \Phi. \end{aligned} \tag{5.1.5}$$

5.2 Shell models

We assume that the deformation in Definition 5.1.3 is of the following form

$$\Phi : \hat{\mathcal{S}} \times [-t/2, t/2] \to \mathbb{R}^3, \qquad (x, z) \mapsto \phi(x) + z\boldsymbol{R}(\hat{\nu}(x), \phi(x)), \tag{5.2.1}$$

where ϕ is the deformation of the mid-surface and $\boldsymbol{R} : \mathbb{S}^2 \times \mathcal{S} \to \mathbb{S}^2$ can be understood as a nonlinear rotation of the normal vector. To simplify notation, we neglect the x and ϕ dependency of $\boldsymbol{R}$. We denote the projection onto the normal direction by $\boldsymbol{P}_z := \boldsymbol{P}_{\hat{\mathcal{S}}}^\perp = \hat{\nu} \otimes \hat{\nu}$.

Lemma 5.2.1 *There holds for the Cauchy–Green strain tensor of full 3D elasticity, $\boldsymbol{C} = \nabla\Phi^\top\nabla\Phi$,*

$$\boldsymbol{C} = I + 2zII_{\boldsymbol{R}(\hat{\nu})} + z^2 III_{\boldsymbol{R}(\hat{\nu})} + \left(\sigma_{\boldsymbol{R}(\hat{\nu})} \otimes \hat{\nu} + \hat{\nu} \otimes \sigma_{\boldsymbol{R}(\hat{\nu})}\right) + \boldsymbol{P}_z \tag{5.2.2}$$

and for the undeformed Cauchy–Green tensor $\hat{\boldsymbol{C}} = \hat{I} + 2z\hat{II}_{\hat{\nu}} + z^2\hat{III}_{\hat{\nu}} + \boldsymbol{P}_z$.

5.2.1 Nonlinear Naghdi shell

The Green strain tensor of the full 3D structure is given by $\boldsymbol{E} = \frac{1}{2}\left(\boldsymbol{C} - \hat{\boldsymbol{C}}\right)$ and together with the material law of St. Venant–Kirchhoff the whole energy of the deformed shell reads

$$\mathcal{W} := \frac{1}{2}\int_{-\frac{t}{2}}^{\frac{t}{2}} \int_{\hat{\mathcal{S}}} \|\boldsymbol{E}\|_{\mathcal{C}}^2 \, ds_z \, dz, \tag{5.2.3}$$

where, under the assumptions of Reissner–Mindlin, the material norm is of the form

$$\|\cdot\|_{\mathcal{C}}^2 := \frac{E}{1-\nu^2}\left(\nu\,\operatorname{tr}(\cdot)^2 + (1-\nu)\operatorname{tr}(\cdot^2)\right). \tag{5.2.4}$$

Steiner's formula [30] $ds_z = \left(1 - 2zH + z^2K\right) ds$ with the mean and Gauß curvature H and K yields

$$\mathcal{W} = \frac{1}{2}\int_{\hat{\mathcal{S}}} \left(\int_{-\frac{t}{2}}^{\frac{t}{2}} \|\boldsymbol{E}\|_{\mathcal{C}}^2 \, dz - 2H \int_{-\frac{t}{2}}^{\frac{t}{2}} z\|\boldsymbol{E}\|_{\mathcal{C}}^2 \, dz + K \int_{-\frac{t}{2}}^{\frac{t}{2}} z^2 \|\boldsymbol{E}\|_{\mathcal{C}}^2 \, dz \right) ds. \tag{5.2.5}$$

Theorem 5.2.2 (Shell energy) *Assume that $t/L \ll 1$ (L denoting the characteristic length), $\|I - \hat{I}\|_{\mathcal{C}} \leq t$, and $K \leq t$, i.e., that the membrane energy and Gauß curvature are small. Then neglecting all terms of order $\mathcal{O}(t^4)$ yields the shell energy*

$$\mathcal{W} = \frac{1}{2}\int_{\hat{\mathcal{S}}} \left(\frac{t}{4}\|I - \hat{I}\|_{\mathcal{C}}^2 + \frac{t^3}{12}\|II_{\boldsymbol{R}(\hat{\nu})} - \hat{II}\|_{\mathcal{C}}^2 + t\kappa G|\sigma_{\boldsymbol{R}(\hat{\nu})}|^2 \right) ds, \tag{5.2.6}$$

where $G = \frac{E}{2(1+\nu)}$ and $\kappa = 5/6$ denote the shearing modulus and shear correction factor, respectively. With the matrix representations (5.1.5) together with $\boldsymbol{E}_{\hat{\mathcal{S}}} := 0.5(\boldsymbol{F}_{\hat{\mathcal{S}}}^\top \boldsymbol{F}_{\hat{\mathcal{S}}} - \boldsymbol{P}_{\hat{\mathcal{S}}})$ the energy reads

$$\mathcal{W} = \int_{\hat{\mathcal{S}}} \left(\frac{t}{2}\|\boldsymbol{E}_{\hat{\mathcal{S}}}\|_{\mathcal{C}}^2 + \frac{t^3}{24}\|\operatorname{sym}(\boldsymbol{F}_{\hat{\mathcal{S}}}^\top \nabla_{\hat{\mathcal{S}}}\boldsymbol{R}(\hat{\nu})) - \nabla_{\hat{\mathcal{S}}}\hat{\nu}\|_{\mathcal{C}}^2 + \frac{t\kappa G}{2}|\boldsymbol{F}_{\hat{\mathcal{S}}}^\top \boldsymbol{R}(\hat{\nu})|^2 \right) ds. \tag{5.2.7}$$

The three terms in (5.2.6) correspond to the membrane, bending, and shearing energy, cf. Figure 5.2. Using β to parameterize the rotation, we arrived at the nonlinear Reissner–Mindlin/Naghdi shell model.

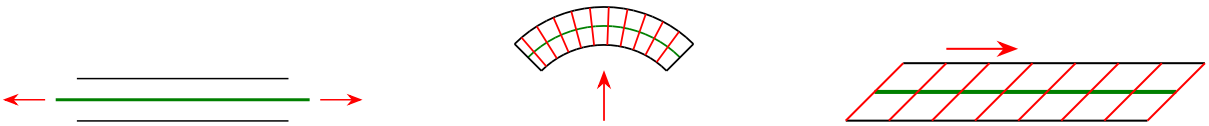

Figure 5.2: Sketched membrane, bending, and shearing energy of a shell.

5.2.2 Linear Naghdi shell

In the following, we denote with $u : \hat{\mathcal{S}} \to \mathbb{R}^3$ the displacement of the mid-surface such that $\phi = \mathrm{id} + u$. Under the small strain assumption (e.g. $\nabla_{\hat{\mathcal{S}}} u = \mathcal{O}(\varepsilon)$), we can linearize the nonlinear shell model (5.2.7). We start with the linearization of the normal and tangential vectors.

Lemma 5.2.3 *Let $\hat{\mathcal{S}}$ be a shell with normal vector field $\hat{\nu}$ and $\phi : \hat{\mathcal{S}} \to \mathbb{R}^3$ a diffeomorphism of the form $\phi = \mathrm{id} + u$. For the resulting deformed shell $\mathcal{S} := \phi(\hat{\mathcal{S}})$ let ν, τ, and μ by the normal, tangent, and co-normal vectors. Assume that $\nabla_{\hat{\mathcal{S}}} u = \mathcal{O}(\varepsilon)$. Then the linearization of these vectors is given by*

$$\nu \circ \phi = \hat{\nu} - \nabla_{\hat{\mathcal{S}}} u^\top \hat{\nu} + \mathcal{O}(\varepsilon^2), \tag{5.2.8a}$$

$$\tau \circ \phi = \hat{\tau} + (\boldsymbol{I} - \hat{\tau} \otimes \hat{\tau}) \nabla_{\hat{\mathcal{S}}} u \, \hat{\tau} + \mathcal{O}(\varepsilon^2), \tag{5.2.8b}$$

$$\mu \circ \phi = \hat{\mu} + ((\boldsymbol{I} - \hat{\tau} \otimes \hat{\tau}) \nabla_{\hat{\mathcal{S}}} u - \nabla_{\hat{\mathcal{S}}} u^\top) \hat{\mu} + \mathcal{O}(\varepsilon^2). \tag{5.2.8c}$$

Lemma 5.2.4 *There holds for the director $\tilde{\nu}$ under the small strain assumption*

$$\tilde{\nu} \circ \phi = \hat{\nu} + \beta + \mathcal{O}(\varepsilon^2) \tag{5.2.9}$$

where $\beta \in T\hat{\mathcal{S}}$ denotes the (linearized) rotation vector.

Theorem 5.2.5 (Linearized Naghdi/Reissner–Mindlin shell) *Under the small strain assumption $u = \beta = \nabla_{\hat{\mathcal{S}}} u = \nabla_{\hat{\mathcal{S}}} \beta = \mathcal{O}(\varepsilon)$ (5.2.7) simplifies to the linearized Naghdi shell energy*

$$\mathcal{W}_{\mathrm{RM}}^{\mathrm{lin}} = \int_{\hat{\mathcal{S}}} \left(\frac{t}{2} \| \operatorname{sym}(\nabla_{\hat{\mathcal{S}}}^{\mathrm{cov}} u) \|_{\mathcal{C}}^2 + \frac{t^3}{24} \| \operatorname{sym}(\nabla_{\hat{\mathcal{S}}}^{\mathrm{cov}} \beta + \nabla_{\hat{\mathcal{S}}} u^\top \nabla_{\hat{\mathcal{S}}} \hat{\nu}) \|_{\mathcal{C}}^2 + \frac{t \kappa G}{2} | \nabla_{\hat{\mathcal{S}}} u^\top \hat{\nu} + \beta |^2 \right) ds. \tag{5.2.10}$$

5.2.3 Nonlinear Koiter shell

With hypothesis (H5) and Lemma 4.2.2 the director $\tilde{\nu} \circ \phi$ coincides with the normal vector on the deformed configuration. Thus, the shearing energy is zero, and the nonlinear Koiter shell energy reads

$$\mathcal{W}_{\mathrm{KL}} = \int_{\hat{\mathcal{S}}} \left(\frac{t}{2} \| \boldsymbol{E}_{\hat{\mathcal{S}}} \|_{\mathcal{C}}^2 + \frac{t^3}{24} \| \boldsymbol{F}_{\hat{\mathcal{S}}}^\top \nabla_{\hat{\mathcal{S}}} \left(\frac{\operatorname{cof}(\boldsymbol{F}_{\hat{\mathcal{S}}}) \hat{\nu}}{\| \operatorname{cof}(\boldsymbol{F}_{\hat{\mathcal{S}}}) \|_F} \right) - \nabla_{\hat{\mathcal{S}}} \hat{\nu} \|_{\mathcal{C}}^2 \right) ds. \tag{5.2.11}$$

5.2.4 Linear Koiter shell

Lemma 5.2.6 *Under the small strain assumption, the linearization of (5.2.11) is given by*

$$\mathcal{W}_{\mathrm{KL}}^{\mathrm{lin}} = \int_{\hat{\mathcal{S}}} \left(\frac{t}{2} \| \operatorname{sym}(\nabla_{\hat{\mathcal{S}}}^{\mathrm{cov}} u) \|_{\mathcal{C}}^2 + \frac{t^3}{24} \| \mathcal{H}_{\hat{\nu}} \|_{\mathcal{C}}^2 \right) ds, \tag{5.2.12}$$

where $\mathcal{H}_{\hat{\nu}} := \sum_{i=1}^3 (\nabla_{\hat{\mathcal{S}}}^2 u_i) \hat{\nu}_i$ with $\nabla_{\hat{\mathcal{S}}}^2$ denoting the surface Hessian, cf. Definition 4.1.7.

Remark 5.2.7 *In the limit $t \to 0$ in (5.2.10) we obtain $\beta = -\nabla_{\hat{\mathcal{S}}} u^\top \hat{\nu}$ recovering (5.2.12) as then $\nabla_{\hat{\mathcal{S}}}^{\mathrm{cov}} \beta + \nabla_{\hat{\mathcal{S}}} u^\top \nabla_{\hat{\mathcal{S}}} \hat{\nu} = -\mathcal{H}_{\hat{\nu}}$.*

5.3 Discretization of Koiter/Kirchhoff–Love shells

This seminar considers only the Koiter shell model, where no shearing appears. To overcome the necessity of C^1-finite elements, the mixed HHJ method is applied. Further, as the underlying shell geometry of the initial or deformed configuration is in general not C^1 (only continuous), we use the distributional Weingarten tensor from Definition 4.4.1.

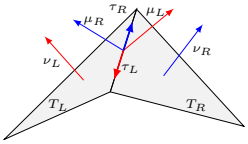

Figure 5.3: Normal, edge tangential and co-normal vectors.

5.3.1 HHJ for nonlinear Koiter shells

We start with shell energy (5.2.11), the notation $\nu \circ \phi = \frac{\operatorname{cof}(\boldsymbol{F}_{\hat{\mathcal{S}}})\hat{\nu}}{\|\operatorname{cof}(\boldsymbol{F}_{\hat{\mathcal{S}}})\|_F}$, and material law (5.2.4)

$$\mathcal{W}_{\mathrm{KL}}(u_h) = \int_{\hat{\mathcal{S}}} \left(\frac{t}{2} \|\boldsymbol{E}_{\hat{\mathcal{S}}}\|_{\mathcal{C}}^2 + \frac{t^3}{24} \|\operatorname{sym}(\boldsymbol{F}_{\hat{\mathcal{S}}}^\top \nabla_{\hat{\mathcal{S}}}(\nu \circ \phi)) - \nabla_{\hat{\mathcal{S}}} \hat{\nu}\|_{\mathcal{C}}^2 \right) ds. \tag{5.3.1}$$

We neglect the subscript h for the finite element functions for ease of presentation. Further, we use e.g. $\nabla_{\hat{\mathcal{S}}}$ instead of $\nabla_{\mathcal{T}}$. For a possibly curved but not C^1 triangulation $\mathcal{T}$ of $\hat{\mathcal{S}}$ consisting of triangles and quadrilaterals, we cannot use the bending energy term in (5.3.1). Instead, we use the distributional curvature (4.4.1) for the initial and deformed configuration and define a lifting to a new unknown, the curvature difference $\boldsymbol{\kappa}^{\mathrm{diff}}$, according to Definition 4.4.3. The resulting three-field formulation reads

$$\begin{aligned} \mathcal{L}(u, \boldsymbol{\kappa}^{\mathrm{diff}}, \boldsymbol{\sigma}) = \int_{\mathcal{T}} \frac{t}{2} \|\boldsymbol{E}_{\hat{\mathcal{S}}}\|_{\mathcal{C}}^2 + \frac{t^3}{24} \|\boldsymbol{\kappa}^{\mathrm{diff}}\|_{\mathcal{C}}^2 \, ds + \sum_{T \in \mathcal{T}} \int_T \left((\boldsymbol{F}_{\hat{\mathcal{S}}}^\top \nabla_{\hat{\mathcal{S}}} \nu \circ \phi - \nabla_{\hat{\mathcal{S}}} \hat{\nu}) - \boldsymbol{\kappa}^{\mathrm{diff}} \right) : \boldsymbol{\sigma} \, ds \\ + \sum_{E \in \mathcal{E}} \int_E (\sphericalangle(\nu_L, \nu_R) \circ \phi - \sphericalangle(\hat{\nu}_L, \hat{\nu}_R)) \boldsymbol{\sigma}_{\hat{\mu}\hat{\mu}} \, dl, \end{aligned} \tag{5.3.2}$$

compare Figure 5.3 for the normal vector ν_L and ν_R on neighbored elements. The Lagrange parameter $\boldsymbol{\sigma}$ has the physical meaning of the moment tensor, which is the energetic conjugate of the difference of the curvatures of the deformed and initial configuration. We can eliminate $\boldsymbol{\kappa}^{\mathrm{diff}}$ if $\mathcal{C}$ is invertible.

Lemma 5.3.1 *Three-field formulation* (5.3.2) *is equivalent to the two-field formulation*

$$\begin{aligned} \mathcal{L}(u, \boldsymbol{\sigma}) = \frac{t}{2} \int_{\mathcal{T}} \|\boldsymbol{E}_{\hat{\mathcal{S}}}\|_{\mathcal{C}}^2 \, ds - \int_{\mathcal{T}} \frac{6}{t^3} \|\boldsymbol{\sigma}\|_{\mathcal{C}^{-1}}^2 \, ds + \sum_{T \in \mathcal{T}} \int_T (\boldsymbol{F}_{\hat{\mathcal{S}}}^\top \nabla_{\hat{\mathcal{S}}} (\nu \circ \phi) - \nabla_{\hat{\mathcal{S}}} \hat{\nu}) : \boldsymbol{\sigma} \, ds \\ + \sum_{E \in \mathcal{E}} \int_E (\sphericalangle(\nu_L, \nu_R) \circ \phi - \sphericalangle(\hat{\nu}_L, \hat{\nu}_R)) \, \boldsymbol{\sigma}_{\hat{\mu}\hat{\mu}} \, dl, \end{aligned} \tag{5.3.3}$$

where the inverse material is given by $\|\cdot\|_{\mathcal{C}^{-1}}^2 := \frac{1+\nu}{E}(\operatorname{tr}(\cdot^2) - \frac{\nu}{\nu+1} \operatorname{tr}(\cdot)^2)$.

Note that the thickness parameter t also appears in the denominator. We reduced the fourth-order minimization problem (5.3.1) to a second-order mixed saddle point problem. With some computations, we arrive at the following Lagrange functional.

Lemma 5.3.2 *For Lagrange functional* (5.3.3) *there holds*

$$\begin{aligned} \mathcal{L}(u, \boldsymbol{\sigma}) = \frac{t}{2} \int_{\mathcal{T}} \|\boldsymbol{E}_{\hat{\mathcal{S}}}\|_{\mathcal{C}}^2 \, ds - \frac{6}{t^3} \int_{\mathcal{T}} \|\boldsymbol{\sigma}\|_{\mathcal{C}^{-1}}^2 \, ds - \int_{\mathcal{T}} (\mathcal{H}_{\nu \circ \phi} + (1 - \hat{\nu} \cdot \nu \circ \phi) \nabla_{\hat{\mathcal{S}}} \hat{\nu}) : \boldsymbol{\sigma} \, ds \\ + \sum_{E \in \mathcal{E}} \int_E (\sphericalangle(\nu_L, \nu_R) \circ \phi - \sphericalangle(\hat{\nu}_L, \hat{\nu}_R)) \boldsymbol{\sigma}_{\hat{\mu}\hat{\mu}} \, dl, \end{aligned} \tag{5.3.4}$$

where $\mathcal{H}_{\nu \circ \phi} := \sum_{i=1}^3 (\nabla_{\hat{\mathcal{S}}}^2 u_i) \nu_i \circ \phi$.

Remark 5.3.3 *In case of a flat plane as initial configuration* (5.3.4) *simplifies to*

$$\mathcal{L}(u, \boldsymbol{\sigma}) = \frac{t}{2} \int_{\mathcal{T}} \|\boldsymbol{E}_{\hat{\mathcal{S}}}\|_{\mathcal{C}}^2 \, ds - \frac{6}{t^3} \int_{\mathcal{T}} \|\boldsymbol{\sigma}\|_{\mathcal{C}^{-1}}^2 \, ds - \int_{\mathcal{T}} \mathcal{H}_{\nu \circ \phi} : \boldsymbol{\sigma} \, ds + \sum_{E \in \mathcal{E}} \int_E \sphericalangle(\nu_L, \nu_R) \circ \phi \, \boldsymbol{\sigma}_{\hat{\mu}\hat{\mu}} \, dl. \tag{5.3.5}$$

The resulting system is a saddle point problem, which would lead to an indefinite matrix after assembling. To overcome this problem, we can use completely discontinuous elements for the moment tensor $\boldsymbol{\sigma} \in M_h^{\mathrm{dc}}$ and introduce a hybridization variable $\alpha \in \Lambda_h^{k-1}$ to reinforce the normal-normal continuity of $\boldsymbol{\sigma}$.

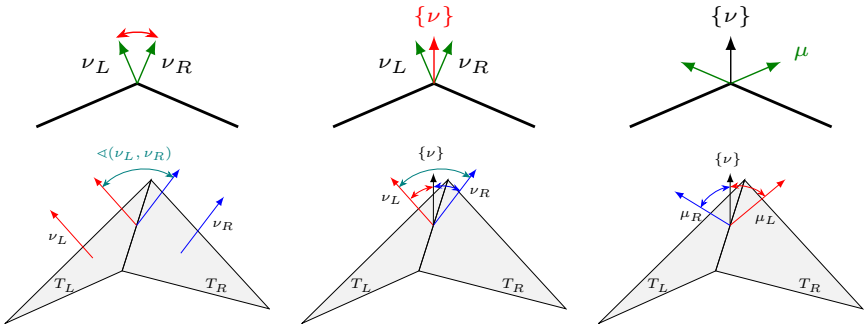

Figure 5.4: Angle computation in 2D and 3D: (left) Angle between ν_L and ν_R. (middle) Averaged normal vector with normal vector ν. (right) Averaged normal vector with element normal vector μ.

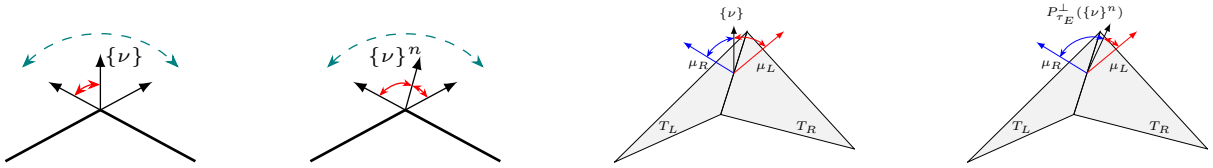

Figure 5.5: Angle computation with the current averaged normal vector $\{\nu\}$ and the averaged normal vector $\{\nu\}^n$ from the previous step in 2D and 3D.

5.3.2 Computational aspects

Using the angle $\sphericalangle(\nu_L,\nu_R)$ is numerically unstable if $\nu_L \approx \nu_R$. Thus, we rewrite it in an equivalent form

$$\sum_{E\in\mathcal{E}}\int_E \sphericalangle(\nu_L,\nu_R)\circ\phi - \sphericalangle(\hat{\nu}_L,\hat{\nu}_R)\,dl = \sum_{T\in\mathcal{T}}\int_{\partial T} \sphericalangle(\{\nu\},\nu)\circ\phi - \sphericalangle(\{\hat{\nu}\},\hat{\nu})\,dl \tag{5.3.6}$$

$$= \sum_{T\in\mathcal{T}}\int_{\partial T} \sphericalangle(\{\hat{\nu}\},\hat{\mu}) - \sphericalangle(\{\nu\},\mu)\circ\phi\,dl, \tag{5.3.7}$$

as $\sphericalangle(\{\nu\},\nu) = \frac{\pi}{2} - \sphericalangle(\{\nu\},\mu)$, see Figure 5.4. Here, $\{\nu\} := \frac{1}{\|\nu_L+\nu_R\|_2}(\nu_L+\nu_R)$ denotes the averaged normal vector. This algebraic equivalent reformulation is numerically much more stable as the derivative of $\arccos(x)$, $\arccos'(x) = -\frac{1}{\sqrt{1-x^2}}$, has singularities at $x=\pm1$ and we expect (for the triangulation of a smooth surface) $\{\nu\}\cdot\nu \approx 1$, whereas for $\{\nu\}\cdot\mu \approx 0$ the derivatives of arccos are well-defined.

To compute the deformed averaged normal vector $\{\nu\}\circ\phi$ on an edge, information of the two neighbouring elements is needed at once, which would require, e.g., Discontinuous Galerkin techniques, leading to a denser stiffness matrix. Instead, one can use the information of the last (loadstep or Newton iteration) solution $\{\nu\}^n$, cf. Figure 5.5. This, and also (5.3.6), is based on the following simple observation.

Lemma 5.3.4 *Let $a,b\in\mathbb{R}^3$ with $\|a\|_2 = \|b\|_2 = 1$. Further let $c\in\mathbb{R}^3$ with $\|c\|_2 = 1$ and c "lies between" a and b, i.e., $\exists t\in(0,1)$ such that $c\in\operatorname{span}\{t\,a+(1-t)b\}$. Then* $\arccos(a\cdot b) = \arccos(a\cdot c)+\arccos(c\cdot b)$.

In three spatial dimensions, to fulfill the requirement of Lemma 5.3.4 that $\{\nu\}^n$ "lies between" μ_R and μ_L, i.e., to measure the correct angle, we have to project $\{\nu\}^n$ to the plane orthogonal to the tangent vector τ by using the orthogonal projection $\boldsymbol{P}^\perp_{\tau_E} = \boldsymbol{I} - \tau\circ\phi\otimes\tau\circ\phi$, and then re-normalize it yielding

$$P^\perp_{\tau_E}(\{\nu\}^n) := \frac{1}{\|\boldsymbol{P}^\perp_{\tau_E}\{\nu\}^n\|_2}\boldsymbol{P}^\perp_{\tau_E}\{\nu\}^n. \tag{5.3.8}$$

5.3.3 HHJ for linear Koiter shells

In the small deformation regime, we have the following (hybridized) HHJ method of the linear Koiter shell formulation (5.2.12). Find $(u, \boldsymbol{\sigma}, \alpha) \in \boldsymbol{U}_h^k \times M_h^{\mathrm{dc},k-1} \times \Lambda_h^{k-1}$ for the saddle point problem

$$\mathcal{L}_{\mathrm{lin}}^{\mathrm{hyb}}(u, \boldsymbol{\sigma}, \alpha) = \int_{\mathcal{T}} \frac{t}{2} \| \operatorname{sym}(\nabla_{\hat{\mathcal{S}}}^{\mathrm{cov}} u)\|_{\mathcal{C}}^2 - \frac{6}{t^3} \|\boldsymbol{\sigma}\|_{\mathcal{C}^{-1}}^2 \, ds + \sum_{T \in \mathcal{T}} \Big(- \int_T \mathcal{H}_{\hat{\nu}} : \boldsymbol{\sigma} \, ds + \int_{\partial T} ((\nabla_{\hat{\mathcal{S}}} u^\top \hat{\nu})_{\hat{\mu}} + \alpha_{\hat{\mu}}) \boldsymbol{\sigma}_{\hat{\mu}\hat{\mu}} \, dl \Big).$$

5.4 Membrane locking

As the thickness t becomes small, the shell falls in one of two different categories: the membrane-dominated (inhibited pure bending) or bending-dominated (non-inhibited pure bending) case [8]. It relies on the specific geometry type (elliptic, hyperbolic, parabolic), prescribed boundary conditions, and given right-hand side. For complex problems, it is therefore difficult to predict the behavior a-priori.

Membrane dominated: In the membrane-dominated regime, the loading f must be of order $\mathcal{O}(t)$ to obtain a well-defined limit solution for $t \to 0$. Dividing the shell energy (5.2.7) by t with $f = t\tilde{f}$ gives

$$\int_{\mathcal{S}} \frac{1}{2} \|\boldsymbol{E}_{\hat{\mathcal{S}}}\|_{\mathcal{C}}^2 + \frac{t^2}{24} \| \operatorname{sym}(\boldsymbol{F}_{\hat{\mathcal{S}}}^\top \nabla_{\hat{\mathcal{S}}} \boldsymbol{R}(\hat{\nu})) - \nabla_{\hat{\mathcal{S}}} \hat{\nu}\|_{\mathcal{C}}^2 + \frac{\kappa G}{2} |\boldsymbol{F}_{\hat{\mathcal{S}}}^\top \boldsymbol{R}(\hat{\nu})|^2 \, ds - \int_{\hat{\mathcal{S}}} \tilde{f} \cdot u \, ds$$

and we see that the bending energy becomes less important for $t \to 0$, the shell energy is of the form of a perturbed problem. In this setting, no locking occurs.

Bending dominated: In the case of a bending dominated regime, the right-hand side has to be of order $\mathcal{O}(t^3)$ and thus after dividing through t^3

$$\int_{\mathcal{S}} \frac{1}{2t^2} \|\boldsymbol{E}_{\hat{\mathcal{S}}}\|_{\mathcal{C}}^2 + \frac{1}{24} \| \operatorname{sym}(\boldsymbol{F}_{\hat{\mathcal{S}}}^\top \nabla_{\hat{\mathcal{S}}} \boldsymbol{R}(\hat{\nu})) - \nabla_{\hat{\mathcal{S}}} \hat{\nu}\|_{\mathcal{C}}^2 + \frac{\kappa G}{2t^2} |\boldsymbol{F}_{\hat{\mathcal{S}}}^\top \boldsymbol{R}(\hat{\nu})|^2 \, ds - \int_{\hat{\mathcal{S}}} \tilde{f} \cdot u \, ds$$

we observe that the membrane and shear energies are penalized to be zero in the limit $t \to 0$. When working with finite elements, these pure bending modes can generally only be approximated and thus will induce non-zero parasitic membrane and/or shear modes. As a result of the penalty, the discrete solution tends to be much smaller than expected. This is then called membrane and shear locking.

Motivated by the procedures to avoid shear locking, we will use Regge finite elements to relax the kernel constraints by inserting the corresponding interpolation operator in the membrane energy part

$$\|\mathcal{I}_h^{\mathcal{R},k-1} \operatorname{sym}(\nabla_{\hat{\mathcal{S}}}^{\mathrm{cov}} u_h)\|_{\mathcal{C}}^2, \qquad u_h \in \boldsymbol{U}_h^k \tag{5.4.1}$$

reducing the number of constraints to the dimension of the Regge space.

5.5 Boundary layer in shells

If shear dofs are included, all plate and shell examples where transversal deflection appears, i.e., except a pure membrane problem, boundary layers of order of the thickness $\mathcal{O}(t)$ may occur. These layers are called short-range or "plate layer modes", which are independent of the curvature and thus 1-dimensional.

For shells, additional boundary layers of magnitude $\mathcal{O}(\sqrt{t})$ might appear, called simple edge effects. In the case of hyperbolic and parabolic geometries layers of order $\mathcal{O}(\sqrt[3]{t})$ and $\mathcal{O}(\sqrt[4]{t})$, respectively, can be induced by a singularity due to the loading, reentering corners, or change of boundary conditions. These layers, sometimes named generalized edge effects, spread along the characteristic lines of the geometry and might be "reflected" at boundaries. Further, they also depend on the curvature of the shell. As a result, at most two different boundary layers must be resolved per edge to obtain reliable numerical results.

Appendix A

Appendix

A.1 Function spaces and finite elements

We define different function and finite element spaces such as the classical Lagrange finite elements, vector-valued spaces like Nédélec and Raviart–Thomas/Brezzi–Douglas–Marini, and less common matrix-valued finite elements.

A.1.1 H^1 and Lagrange elements

The Sobolev space $H^1(\Omega) := \{u \in L^2(\Omega) \,|\, \nabla u \in L^2(\Omega, \mathbb{R}^d)\}$, with its norm $\|u\|_{H^1}^2 = \|u\|_{L^2}^2 + \|\nabla u\|_{L^2}^2$ and semi-norm $|u|_{H^1} = \|\nabla u\|_{L^2}$, is defined as the set of square-integrable functions, which have a weak derivative. Functions in $H^1(\Omega)$ have a well defined continuous trace operator $\mathrm{tr} : H^1(\Omega) \to H^{\frac{1}{2}}(\partial\Omega)$, which coincides with point evaluation for continuous fields, $\mathrm{tr} u = u|_{\partial\Omega}$ for $u \in C^0(\overline{\Omega})$. Therefore, we can prescribe Dirichlet boundary data. $H^{\frac{1}{2}}(\partial\Omega)$ denotes the trace space of $H^1(\Omega)$. It can be defined either as the set of traces of all $H^1(\Omega)$-functions or, equivalently, as Hilbert interpolation space between $L^2(\partial\Omega)$ and $H^1(\partial\Omega)$. Sobolev spaces $H^k(\Omega)$ can be defined, e.g. by induction.

To define a conforming finite element subspace, we consider a regular (shape regular or quasi-uniform) triangulation[1] $\mathcal{T}$ of Ω. Further, the set of piece-wise polynomials up to order k on the triangulation is denoted by $\mathcal{P}^k(\mathcal{T})$. Further, the set of edges and vertices of the triangulation are denoted by $\mathcal{E}$ and $\mathcal{V}$, respectively. The set of facets, which coincide with edges in 2D and faces in 3D, is given by $\mathcal{F}$. Analogously, we define e.g. $\mathcal{P}^k(\mathcal{F})$ as the set of polynomials living on the skeleton $\mathcal{F}$.

The Lagrangian finite element space of order k defined by

$$U_h^k := \mathcal{P}^k(\mathcal{T}) \cap C^0(\Omega) \qquad\qquad U_{h,0}^k := \{u_h \in U_h^k \,|\, \mathrm{tr}\, u_h = 0 \text{ on } \partial\Omega\} \tag{A.1.1}$$

consists of piece-wise (smooth) polynomials and is globally continuous, such that $U_h^k \subset H^1(\Omega)$. If only parts of the boundary are used for defining zero boundary conditions, we use the notation U_{h,Γ_D}^k.

Example A.1.1 *Consider $\Omega \subset \mathbb{R}^2$ and linear elements U_h^1. A basis of U_h^1 is given by the set of hat-functions φ_i, fulfilling $\varphi_i(V_j) = \delta_{ij}$, where V_j denotes a vertex of $\mathcal{T}$. Thus $u_h = \sum_{i=1}^N \alpha_i \varphi_i \in U_h^1$. The α_i are the coefficients with respect to the basis $\{\varphi_i\}$. The corresponding functionals are given by $\Psi_i : u \mapsto u(V_i)$ such that $\Psi_i(\varphi_j) = \delta_{ij}$. The canonical interpolation operator $\mathcal{I}_h^1 : C^0(\Omega) \to U_h^1$ is given by $u_h = \mathcal{I}_h^1 u = \sum_{i=0}^N \Psi_i(u)\varphi_i$ (Note that point-evaluation is not well-defined for $H^1(\Omega)$ in dimensions 2 or higher).*

To extend the hat-function basis to higher orders, several constructions exist, e.g. a hierarchical basis, where only new basis functions are added. We define the canonical interpolation operator $\mathcal{I}_h^k : C^0(\Omega) \to U_h^k$ by the following equations in two dimensions

$$\mathcal{I}_h^k u(V) = u(V) \qquad \text{for all } v \in \mathcal{V}, \tag{A.1.2a}$$

$$\int_E \mathcal{I}_h^k u q \, ds = \int_E u q \, ds \qquad \text{for all } q \in \mathcal{P}^{k-2}(E),\ E \in \mathcal{E}, \tag{A.1.2b}$$

$$\int_T \mathcal{I}_h^k u q \, dx = \int_T u q \, dx \qquad \text{for all } q \in \mathcal{P}^{k-3}(T),\ T \in \mathcal{T}, \tag{A.1.2c}$$

and analogously in 3D for tetrahedra.

Mostly, the shape functions are defined on a reference triangle/tetrahedron $\hat{T}$ and then mapped to the physical elements $T = \Phi(\hat{T})$. For Lagrange elements, this is done by simple composition $u_h \circ \Phi = \hat{u}_h$. E.g., the barycentric coordinates $\hat{\lambda}$ on the reference triangle are directly mapped to the barycentric coordinates on the physical element by $\lambda \circ \phi = \hat{\lambda}$. Therefore, one can define the Lagrange elements by

$$U_h^k = \{u_h \in H^1(\Omega) \,|\, \text{ for all } T \in \mathcal{T}\ \exists \hat{u} \in \mathcal{P}^k(\hat{T}) :\ u|_T \circ \Phi = \hat{u}\}.$$

[1] For simplicity, we will solely consider non-curved elements.

A.1.2 $H(\mathrm{curl})$ and Nédélec elements

The $H(\mathrm{curl})$ space in two and three dimensions is defined as the set of all L^2-functions, where the curl is also in L^2, $H(\mathrm{curl},\Omega) := \{u \in L^2(\Omega,\mathbb{R}^d) \,|\, \mathrm{curl}\, u \in L^2(\Omega,\mathbb{R}^{2d-3})\}$, with the norm $\|u\|^2_{H(\mathrm{curl})} := \|u\|^2_{L^2} + \|\mathrm{curl}\, u\|^2_{L^2}$. In contrast to H^1 only the tangential trace is available $\mathrm{tr}_t : H(\mathrm{curl},\Omega) \to H^{-\frac{1}{2}}(\partial\Omega,\mathbb{R}^{2d-3})$ such that $\mathrm{tr}_t u = u|_{\partial\Omega} \cdot t$ in 2D and $\mathrm{tr}_t u = u|_{\partial\Omega} \times n$ in 3D, respectively, for $u \in C^0(\overline{\Omega},\mathbb{R}^d)$. $H^{-\frac{1}{2}}(\partial\Omega)$ denotes the dual space of $H^{\frac{1}{2}}(\partial\Omega)$ such that e.g. $\int_{\partial\Omega} \mathrm{tr}_t u \,\mathrm{tr}\, v\, ds$ is well defined for $u \in H(\mathrm{curl},\Omega)$ and $v \in H^1(\Omega,\mathbb{R}^{2d-3})$. The trace theorem hints that for a conforming discretization, the finite element space should be tangential continuous, and the normal component might jump over elements. The lowest-order Nédélec elements of first kind in three dimensions are element-wise of the form

$$\mathcal{N}^0_I(T) = \{a + x \times b \,|\, a,b \in \mathbb{R}^3\} \quad T \in \mathcal{T} \tag{A.1.3}$$

and the global finite element space is given by

$$\mathcal{N}^0_I = \{v_h \in \Pi_{T\in\mathcal{T}} \mathcal{N}^0_I(T) \,|\, v_h \text{ is tangential continuous}\} \subset H(\mathrm{curl},\Omega). \tag{A.1.4}$$

The functionals Ψ_i enforcing the tangential continuity are given by the edge moment of the tangential component, $\Psi_i(u) = \int_{E_i} u \cdot t_{E_i}\, ds$, enforcing the tangential continuity. The space has 6 degrees of freedom fitting to the six edges of a tetrahedron. The shape function corresponding to edge E_i is given by

$$\varphi_{E_i} = \lambda_{E_i^1} \nabla \lambda_{E_i^2} - \lambda_{E_i^2} \nabla \lambda_{E_i^1}, \tag{A.1.5}$$

where e.g., $\lambda_{E_i^1}$ denotes the barycentric coordinate of the first vertex of edge E_i.

By increasing to full polynomial space $\mathcal{P}^1(\mathcal{T},\mathbb{R}^d)$ and adding the first tangential moments as functionals, $\Psi_i(u) = \int_{E_i} (\lambda_{E_i^2} - \lambda_{E_i^1})\, u \cdot t_{E_i}\, ds$, the second type Nédélec elements are obtained. The arbitrary order k definitions are

$$\mathcal{N}^k_I := \{v_h \in \Pi_{T\in\mathcal{T}} \mathcal{N}^k_I(T) \,|\, v_h \text{ is t-continuous}\}, \qquad \mathcal{N}^k_I(T) := \{a + x \times b \,|\, a,b \in \mathcal{P}^k(T,\mathbb{R}^3)\}, \tag{A.1.6}$$

$$\mathcal{N}^k_{II} := \{v_h \in \mathcal{P}^k(\mathcal{T},\mathbb{R}^3) \,|\, v_h \text{ is t-continuous}\} \qquad \mathcal{N}^k_{II,0} := \{v_h \in \mathcal{N}^k_{II} \,|\, \mathrm{tr}_t v_h = 0 \text{ on } \partial\Omega\}. \tag{A.1.7}$$

There holds the relation

$$\mathcal{N}^0_I \subsetneq \mathcal{N}^1_{II} = \mathcal{P}^1(\mathcal{T},\mathbb{R}^d) \subsetneq \mathcal{N}^1_I \subsetneq \mathcal{N}^2_{II} = \mathcal{P}^2(\mathcal{T},\mathbb{R}^d) \subsetneq \dots$$

and we will use the notation $\mathcal{N}$ if we do not specify the kind of Nédélec elements. The canonical Nédélec interpolant will be denoted by $\mathcal{I}^{\mathcal{N}}_h : C^0(\Omega,\mathbb{R}^d) \to \mathcal{N}^k$ by the following equations for

- $\mathcal{N}_I$ elements by

$$\int_E \mathcal{I}^{\mathcal{N},k}_h u \cdot t_E\, q\, dl = \int_E u \cdot t_E\, q\, dl \qquad \text{for all } q \in \mathcal{P}^k(E), E \in \mathcal{E}, \tag{A.1.8a}$$

$$\int_F \mathcal{I}^{\mathcal{N},k}_h u_t \cdot q\, ds = \int_F u_t \cdot q\, ds \qquad \text{for all } q \in \mathcal{P}^{k-1}(F,\mathbb{R}^3) \cap n_F^\perp, F \in \mathcal{F}, \tag{A.1.8b}$$

$$\int_T \mathcal{I}^{\mathcal{N},k}_h u \cdot q\, dx = \int_T u \cdot q\, dx \qquad \text{for all } q \in \mathcal{P}^{k-2}(T,\mathbb{R}^3), T \in \mathcal{T}, \tag{A.1.8c}$$

  where $\mathcal{P}^{k-1}(F,\mathbb{R}^3) \cap n_F^\perp$ denote vector-valued polynomials living in the tangent plane of F.

- $\mathcal{N}_{II}$ elements by

$$\int_E \mathcal{I}^{\mathcal{N},k}_h u \cdot t_E\, q\, dl = \int_E u \cdot t_E\, q\, dl \qquad \text{for all } q \in \mathcal{P}^k(E), E \in \mathcal{E}, \tag{A.1.9a}$$

$$\int_F \mathcal{I}^{\mathcal{N},k}_h u_t \cdot q\, ds = \int_F u_t \cdot q\, ds \qquad \text{for all } q \in RT^{k-2}(F), F \in \mathcal{F}, \tag{A.1.9b}$$

$$\int_T \mathcal{I}^{\mathcal{N},k}_h u \cdot q\, dx = \int_T u \cdot q\, dx \qquad \text{for all } q \in RT^{k-3}(T), T \in \mathcal{T}, \tag{A.1.9c}$$

  where $RT^{k-2}(F)$ and $RT^{k-3}(T)$ are Raviart–Thomas spaces defined in (A.1.11).

When mapping Nédélec elements from the reference to the physical element, we must preserve the tangential continuity. Therefore the so-called covariant transformation is used, $u \circ \Phi = \boldsymbol{F}^{-\top}\hat{u}$ with $\boldsymbol{F} = \nabla\Phi$, as then with $E = \Phi(\hat{E})$

$$\int_E u \cdot t \, ds = \int_{\hat{E}} \hat{u} \cdot \hat{t} \, d\hat{s} \quad \text{and} \quad (\operatorname{curl} u) \circ \Phi = \begin{cases} \frac{1}{J} \operatorname{curl}_{\hat{x}} \hat{u} & \text{in 2D} , \\ \frac{1}{J} \boldsymbol{F} \operatorname{curl}_{\hat{x}} \hat{u} & \text{in 3D} . \end{cases} \tag{A.1.10}$$

A.1.3 $H(\mathrm{div})$ and Raviart–Thomas/Brezzi–Douglas–Marini elements

In a similar manner to the previous section we define $H(\mathrm{div}, \Omega) := \{u \in L^2(\Omega, \mathbb{R}^d) \,|\, \mathrm{div} u \in L^2(\Omega)\}$, $\|u\|^2_{H(\mathrm{div})} = \|u\|^2_{L^2} + \|\mathrm{div} u\|^2_{L^2}$. Now, the normal trace is well-defined, $\mathrm{tr}_n : H(\mathrm{div}, \Omega) \to H^{-\frac{1}{2}}(\partial\Omega)$, such that $\mathrm{tr}_n u = u|_{\partial\Omega} \cdot n$ for $u \in C^0(\overline{\Omega}, \mathbb{R}^d)$. The Raviart–Thomas (RT) elements consist of polynomials of order k where homogeneous polynomials $\mathcal{P}^{k,*}(T) := \{p \in \mathcal{P}^k(T) \,|\, p = \sum_{i=1}^m \alpha_i x_1^{k_{i1}} \cdots x_d^{k_{id}}, \sum_{l=1}^d k_{il} = k, \text{ for all } i \in \{1, \ldots, m\}\}$ are added and are normal continuous

$$RT^k(T) := \{a + cx \,|\, a \in \mathcal{P}^k(T, \mathbb{R}^d),\, c \in \mathcal{P}^{k,*}(T)\}, \tag{A.1.11}$$

$$RT^k := \{v_h \in \Pi_{T\in\mathcal{T}} RT^k(T) \,|\, [\![v_h \cdot n]\!]_F = 0 \text{ for all } F \in \mathcal{F}^{\mathrm{int}}\} \subset H(\mathrm{div}, \Omega). \tag{A.1.12}$$

Here, we defined $\mathcal{F}^{\mathrm{int}} := \mathcal{F} \backslash \partial\Omega$ as the set of all interior facets and used the notation of the normal jump across element facets $[\![v_h \cdot n]\!]_F = (v_h \cdot n)|_{T_1} + (v_h \cdot n)|_{T_2} = (v_h|_{T_1} - v_h|_{T_2}) \cdot n|_{T_1}$. In the lowest-order case $k = 0$ in 2D, the three dofs correspond to the three edges of the triangle, whereas in 3D there are four dofs for the four faces of the tetrahedron.

Using the full polynomial spaces leads to Brezzi–Douglas–Marini (BDM) elements

$$\begin{aligned} BDM^k &:= \{v_h \in \mathcal{P}^k(\mathcal{T}, \mathbb{R}^d) \,|\, [\![v_h \cdot n]\!]_F = 0 \text{ for all } F \in \mathcal{F}^{\mathrm{int}}\} \subset H(\mathrm{div}, \Omega), \\ BDM_0^k &:= \{u_h \in BDM^k \,|\, \mathrm{tr}_n u_h = 0 \text{ on } \partial\Omega\}. \end{aligned} \tag{A.1.13}$$

If we do not distinguish between RT and BDM, we use the notation V_h.

The functionals are the moments of the normal component on edges/faces and inner moments. The canonical interpolant $\mathcal{I}_h^{V_h,k} : C^0(\Omega, \mathbb{R}^d) \to V_h^k$ is defined for

- RT elements by

$$\Psi_F(v) = \int_F v \cdot n \, q \, ds \qquad \text{for all } q \in \mathcal{P}^k(F),\, F \in \mathcal{F}, \tag{A.1.14a}$$

$$\Psi_T(v) = \int_T v \cdot q \, dx \qquad \text{for all } q \in \mathcal{P}^{k-1}(T, \mathbb{R}^d),\, T \in \mathcal{T}. \tag{A.1.14b}$$

- BDM elements by

$$\Psi_F(v) = \int_F v \cdot n \, q \, ds \qquad \text{for all } q \in \mathcal{P}^k(F),\, F \in \mathcal{F}, \tag{A.1.15a}$$

$$\Psi_T(v) = \int_T v \cdot q \, dx \qquad \text{for all } q \in \mathcal{N}_I^{k-2}(T),\, T \in \mathcal{T}. \tag{A.1.15b}$$

By using the Piola transformation, $u \circ \Phi = \frac{1}{J}\boldsymbol{F}\hat{u}$ the normal continuity is preserved during transformation $T = \Phi(\hat{T})$ and there holds with $F = \Phi(\hat{F})$

$$\int_F u \cdot n \, ds = \int_{\hat{F}} \hat{u} \cdot \hat{n} \, d\hat{s}, \quad \text{and} \quad (\mathrm{div} u) \circ \Phi = \frac{1}{J} \mathrm{div}_{\hat{x}} \hat{u}. \tag{A.1.16}$$

A.1.4 L^2 elements and De'Rham complex

For completeness, we define the set of piece-wise polynomials of order k as $L^2(\Omega)$-conforming finite elements

$$Q_h^k = \mathcal{P}^k(\mathcal{T}) \subset L^2(\Omega). \tag{A.1.17}$$

There holds on the continuous level in three dimensions $\nabla H^1 \subset H(\mathrm{curl})$, $\mathrm{curl}(H(\mathrm{curl})) \subset H(\mathrm{div})$, and $\mathrm{div}(H(\mathrm{div})) \subset L^2$. Further, on simply connected domains, the following sequence is exact. If the domain is not simply connected, the range of one operator is still inside the kernel of the next, but in general, the reverse does not hold.

$$\{1\} \xrightarrow{\mathrm{id}} H^1 \xrightarrow{\nabla} H(\mathrm{curl}) \xrightarrow{\mathrm{curl}} H(\mathrm{div}) \xrightarrow{\mathrm{div}} L^2 \xrightarrow{0} 0.$$

The following diagram, called De'Rham complex, commutes

$$\begin{array}{ccccccc} H^1 \cap C^0 & \xrightarrow{\nabla} & H(\mathrm{curl}) \cap C^0 & \xrightarrow{\mathrm{curl}} & H(\mathrm{div}) \cap C^0 & \xrightarrow{\mathrm{div}} & L^2 \\ \downarrow{\scriptstyle \mathcal{I}_h} & & \downarrow{\scriptstyle \mathcal{I}_h^{\mathcal{N}}} & & \downarrow{\scriptstyle \mathcal{I}_h^{V_h}} & & \downarrow{\scriptstyle \Pi^{L^2}} \\ U_h & \xrightarrow{\nabla} & \mathcal{N} & \xrightarrow{\mathrm{curl}} & V_h & \xrightarrow{\mathrm{div}} & Q_h \end{array}.$$

Remark A.1.2 *We need to increase the regularity of spaces to use the canonical interpolation operators, as e.g. point evaluation is not well-defined for H^1 functions. Recently, local L^2-bounded and commuting projection operators have been constructed without the requirement of increased regularity [2].*

A.1.5 $H(\mathrm{divdiv})$, TDNNS, and Hellan–Herrmann–Johnson elements

In several applications, we consider stress fields of the form $\boldsymbol{\sigma} = \mathcal{C}\boldsymbol{\varepsilon}$ as an additional unknown. These fields are symmetric, $\boldsymbol{\sigma}^\top = \boldsymbol{\sigma}$, and need to have a divergence operator defined due to the force balance equation

$$-\mathrm{div}(\boldsymbol{\sigma}) = f.$$

When considering linear elasticity (1.4.5) the mixed formulation reads

$$\int_\Omega \mathcal{C}^{-1}\boldsymbol{\sigma} : \boldsymbol{\tau}\, dx + \langle \mathrm{div}\boldsymbol{\tau}, u\rangle = 0 \qquad \text{for all } \boldsymbol{\tau}, \tag{A.1.18a}$$

$$\langle \mathrm{div}\boldsymbol{\sigma}, v\rangle = -\int_\Omega f\, v\, dx \qquad \text{for all } v. \tag{A.1.18b}$$

The first equation forces $\boldsymbol{\sigma} = \mathcal{C}\boldsymbol{\varepsilon}(u)$, the second one the force balance equation, where $\mathcal{C}^{-1}$ is the compliance tensor (1.4.3). Note that we did not specify any spaces, regularity assumptions, or the pairings $\langle\cdot,\cdot\rangle$ so far.

If we keep $u \in H^1(\Omega, \mathbb{R}^d)$ like in the standard primal setting we can define $\langle \mathrm{div}\boldsymbol{\sigma}, u\rangle_{H^{-1}\times H^1} = -\int_\Omega \boldsymbol{\sigma} : \varepsilon(u)\, dx$ such that $\boldsymbol{\sigma} \in L^2(\Omega, \mathbb{R}^{d\times d}_{\mathrm{sym}})$ is sufficient. However, this formulation is equivalent to the primal version and thus less interesting.

Shifting the regularity from the displacement u to the stress $\boldsymbol{\sigma}$ yields the requirement $\mathrm{div}\boldsymbol{\sigma} \in L^2(\Omega, \mathbb{R}^d)$ and $u \in L^2(\Omega, \mathbb{R}^d)$. The stress has therefore to be in the space $H^{\,\mathrm{sym}}(\mathrm{div}, \Omega) := \{\boldsymbol{\sigma} \in L^2(\Omega, \mathbb{R}^{d\times d}_{\mathrm{sym}}) \,|\, \mathrm{div}\boldsymbol{\sigma} \in L^2(\Omega, \mathbb{R}^d)\}$, which induces a continuous normal trace, $\boldsymbol{\sigma}n$, compare with $H(\mathrm{div}, \Omega)$ in Section A.1.3. Although this is a valid choice of spaces, constructing $H^{\,\mathrm{sym}}(\mathrm{div})$-conforming finite element spaces is tedious and requires a high polynomial degree.

Remark A.1.3 *As a result, so-called weakly symmetric methods were developed, where the symmetry of $\boldsymbol{\sigma}$ is broken and then enforced weakly by a Lagrange multiplier, leading to the construction of simpler elements.*

$\langle \mathrm{div}\boldsymbol{\sigma}, u\rangle$	$\boldsymbol{\sigma}$	u	trace $\boldsymbol{\sigma}$	trace u
$\langle \mathrm{div}\boldsymbol{\sigma}, u\rangle_{H^{-1}\times H^1}$	$L^2(\Omega, \mathbb{R}^{d\times d}_{\mathrm{sym}})$	$H^1(\Omega, \mathbb{R}^d)$	-	u
$\int_\Omega \mathrm{div}\boldsymbol{\sigma} \cdot u\, dx$	$H^{\,\mathrm{sym}}(\mathrm{div}, \Omega)$	$L^2(\Omega, \mathbb{R}^d)$	$\boldsymbol{\sigma}n$	-
$\langle \mathrm{div}\boldsymbol{\sigma}, u\rangle_{H(\mathrm{curl})^*\times H(\mathrm{curl})}$	$H(\mathrm{divdiv}, \Omega)$	$H(\mathrm{curl}, \Omega)$	$n^\top\boldsymbol{\sigma}n$	u_t

Table A.1: Depending on the interpretation of pairing $\langle \mathrm{div}\boldsymbol{\sigma}, u\rangle$ different regularity assumptions on $\boldsymbol{\sigma}$ and u are required yielding different well-defined traces.

The tangential-displacement normal normal-stress continuous element method (TDNNS) shifts the regularity half-half by requiring that $u \in H(\mathrm{curl},\Omega)$, i.e. with a tangential trace, and $\boldsymbol{\sigma} \in H(\mathrm{divdiv},\Omega) := \{\boldsymbol{\sigma} \in L^2(\Omega,\mathbb{R}^{d\times d}_{\mathrm{sym}}) \,|\, \mathrm{divdiv}\boldsymbol{\sigma} \in H^{-1}(\Omega)\}$. The norm is given by $\|\boldsymbol{\sigma}\|^2_{HDD} = \|\boldsymbol{\sigma}\|^2_{L^2} + \|\mathrm{divdiv}\boldsymbol{\sigma}\|^2_{H^{-1}}$. Then the duality pairing $\langle \mathrm{div}\boldsymbol{\sigma}, u\rangle_{H(\mathrm{curl})^*\times H(\mathrm{curl})}$ is well defined as there holds $\mathrm{div}(H(\mathrm{divdiv},\Omega)) \subset H(\mathrm{curl})^*$, the dual space of $H(\mathrm{curl})$. To see this, we need the following characterization of the dual space of $H(\mathrm{curl})$.

Lemma A.1.4 *There holds*

$$H(\mathrm{curl},\Omega)^* = H^{-1}(\mathrm{div},\Omega) := \{u \in H^{-1}(\Omega,\mathbb{R}^d) \,|\, \mathrm{div}u \in H^{-1}(\Omega)\}. \tag{A.1.19}$$

Proof: For an $u \in H_0(\mathrm{curl},\Omega)$ we use the regular decomposition $u = z + \nabla\varphi$ with $z \in H^1_0(\Omega,\mathbb{R}^d)$, $\varphi \in H^1_0(\Omega)$, and $\|z\|_{H^1} + \|\varphi\|_{H^1} \le c\|u\|_{H(\mathrm{curl})}$ to compute

$$\begin{aligned}\|f\|_{H(\mathrm{curl})^*} &= \sup_{u\in H_0(\mathrm{curl})} \frac{\langle f,u\rangle}{\|u\|_{H(\mathrm{curl})}} \simeq \sup_{z,\varphi} \frac{\langle f, z+\nabla\varphi\rangle}{\|\varphi\|_{H^1}+\|z\|_{H^1}} \simeq \sup_z \frac{\langle f,z\rangle}{\|z\|_{H^1}} + \sup_\varphi \frac{\langle \mathrm{div}f,\varphi\rangle}{\|\varphi\|_{H^1}} \\ &= \|\mathrm{div}f\|_{H^{-1}} + \|f\|_{H^{-1}} = \|f\|_{H^{-1}(\mathrm{div})}.\end{aligned}$$

□

Now there holds for $\boldsymbol{\sigma} \in H(\mathrm{divdiv},\Omega)$ that $\mathrm{div}\boldsymbol{\sigma} \in H^{-1}(\Omega,\mathbb{R}^d)$ as well as $\mathrm{divdiv}\boldsymbol{\sigma} \in H^{-1}(\Omega)$ such that $\mathrm{div}\boldsymbol{\sigma} \in H^{-1}(\mathrm{div},\Omega)$. In contrast to $H^{\mathrm{sym}}(\mathrm{div})$, the $H(\mathrm{divdiv})$ space only induces a continuous normal-normal trace, $\boldsymbol{\sigma}_{nn} := n^\top\boldsymbol{\sigma}n$, which enables the construction of simpler and lower-order finite elements, see [28]. If the functions are more regular at a triangulation, the duality pairing can be written in terms of element and face terms.

Lemma A.1.5 *Let $\boldsymbol{\sigma}$ be a symmetric piece-wise smooth tensor with $\boldsymbol{\sigma}_{nt} \in H^{\frac12}(\partial T)$ for all $T \in \mathcal{T}$ and normal-normal continuous. Then* $\mathrm{div}\boldsymbol{\sigma} \in H(\mathrm{curl},\Omega)^*$ *and*

$$\begin{aligned}\langle \mathrm{div}\boldsymbol{\sigma}, u\rangle_{H(\mathrm{curl})^*\times H(\mathrm{curl})} &= \sum_{T\in\mathcal{T}} \Big(\int_T \mathrm{div}\boldsymbol{\sigma}\cdot u\,dx - \int_{\partial T} \boldsymbol{\sigma}_{nt}u_t\,ds\Big) \\ &= \sum_{T\in\mathcal{T}} \Big(-\int_T \boldsymbol{\sigma} : \nabla u\,dx + \int_{\partial T} \boldsymbol{\sigma}_{nn}u_n\,ds\Big),\end{aligned} \tag{A.1.20}$$

where for the second identity we assumed that $u \in H(\mathrm{curl},\Omega)$ is piece-wise smooth and $u_n \in H^{\frac12}(\partial T)$.

Proof: We start with a smooth test function $\Psi \in C^\infty_0(\Omega,\mathbb{R}^d)$ and use the definition of distributions, split the domain into the triangles $T \in \mathcal{T}$, and integrate by parts back on each element

$$\langle \mathrm{div}\boldsymbol{\sigma},\Psi\rangle_{H(\mathrm{curl})^*\times H(\mathrm{curl})} = -\int_\Omega \boldsymbol{\sigma} : \nabla\Psi\,dx = -\sum_{T\in\mathcal{T}}\int_T \boldsymbol{\sigma} : \nabla\Psi\,dx = \sum_{T\in\mathcal{T}} \big(\int_T \mathrm{div}\boldsymbol{\sigma}\cdot\Psi\,dx - \int_{\partial T} \boldsymbol{\sigma}_n\cdot\Psi\,ds\big).$$

By splitting into normal and tangential components, $\boldsymbol{\sigma}_n\cdot\Psi = (\boldsymbol{\sigma}_{nn}n + \boldsymbol{P}_t\boldsymbol{\sigma}_n)\cdot(\Psi_n n + \boldsymbol{P}_t\Psi) = \boldsymbol{\sigma}_{nn}\Psi_n + \boldsymbol{P}_t\boldsymbol{\sigma}_n\cdot\boldsymbol{P}_t\Psi$, where $\boldsymbol{P}_t = \boldsymbol{I} - n\otimes n$ is the tangential projection, yields by abbreviating e.g. $\Psi_t := \boldsymbol{P}_t\Psi$ and reordering of the facet terms

$$\sum_{T\in\mathcal{T}}\int_{\partial T}\boldsymbol{\sigma}_n\cdot\Psi\,ds = \sum_{T\in\mathcal{T}}\int_{\partial T}\boldsymbol{\sigma}_{nn}\Psi_n + \boldsymbol{\sigma}_{nt}\cdot\Psi_t\,ds = \sum_{F\in\mathcal{F}\setminus\partial\Omega}\int_F [\![\boldsymbol{\sigma}_{nn}]\!]\Psi_n + [\![\boldsymbol{\sigma}_{nt}]\!]\cdot\Psi_t\,ds.$$

By using that $\boldsymbol{\sigma}_{nn}$ is continuous, $[\![\boldsymbol{\sigma}_{nn}]\!] = 0$, we obtain

$$\langle \mathrm{div}\boldsymbol{\sigma},\Psi\rangle_{H(\mathrm{curl})^*\times H(\mathrm{curl})} = \sum_{T\in\mathcal{T}}\Big(\int_T \mathrm{div}\boldsymbol{\sigma}\cdot\Psi\,dx - \int_{\partial T}\boldsymbol{\sigma}_{nt}\Psi_n\,ds\Big)$$

and

$$|\langle \mathrm{div}\boldsymbol{\sigma},\Psi\rangle_{H(\mathrm{curl})^*\times H(\mathrm{curl})}| \le \sum_{T\in\mathcal{T}} \|\mathrm{div}\boldsymbol{\sigma}\|_{L^2(T)}\|\Psi\|_{L^2(T)} + \|\boldsymbol{\sigma}_{nt}\|_{H^{\frac12}(\partial T)}\|\Psi_t\|_{H^{-\frac12}(\partial T)} \le C(\boldsymbol{\sigma})\|\Psi\|_{H(\mathrm{curl})}.$$

Thus, by density, we can extend the duality pairing formula to $\Psi \in H(\mathrm{curl}, \Omega)$. The second statement follows by integration by parts element-wise and noting that $\boldsymbol{\sigma}_n \cdot \Psi - \boldsymbol{\sigma}_{nt}\Psi_t = \boldsymbol{\sigma}_{nn}\Psi_n$. □

The so-called stress or Hellan–Herrmann–Johnson finite element space is defined by

$$\begin{aligned} M_h^k &:= \{\boldsymbol{\sigma}_h \in \mathcal{P}^k(\mathcal{T}, \mathbb{R}^{d\times d}_{\mathrm{sym}}) \,|\, [\![\boldsymbol{\sigma}_{h,nn}]\!]_F = 0 \text{ for all } F \in \mathcal{F}^{\mathrm{int}}\}, \\ M_{h,0}^k &:= \{\boldsymbol{\sigma}_h \in M_h^k \,|\, \boldsymbol{\sigma}_{h,nn} = 0 \text{ on } \partial\Omega\}. \end{aligned} \tag{A.1.21}$$

Here, the normal-normal jump is given by $[\![\boldsymbol{\sigma}_{h,nn}]\!]_F = \boldsymbol{\sigma}_{h,nn}|_{T_L} - \boldsymbol{\sigma}_{h,nn}|_{T_R}$. The functionals of M_h in the two-dimensional case are the normal-normal moments at the edges and moments over elements

$$\Psi_E(\boldsymbol{\sigma}) = \int_E J_E \, \boldsymbol{\sigma}_{nn} \, q \, ds \qquad q \in \mathcal{P}^k(E),\, E \in \mathcal{E}, \tag{A.1.22a}$$

$$\Psi_T(\boldsymbol{\sigma}) = \int_T J_T \, \boldsymbol{\sigma} : \boldsymbol{F}_T^{-\top} Q \boldsymbol{F}_T^{-1} \, dx \qquad Q \in \mathcal{P}^{k-1}(T, \mathbb{R}^{d\times d}_{\mathrm{sym}}),\, T \in \mathcal{T}, \tag{A.1.22b}$$

where J_E and J_T are the edge and element determinants and $\boldsymbol{F}_T$ the Jacobian of the transformation from the reference to the physical element, yielding the canonical interpolation operator $\mathcal{I}_h^{\mathrm{M_h},k} : C^0(\Omega, \mathbb{R}^{d\times d}) \to M_h^k$. The edge-based shape functions can be constructed based on barycentric coordinates

$$e_{ij} = \nabla\lambda_i^\perp \odot \nabla\lambda_j^\perp, \tag{A.1.23}$$

where $\odot$ is the symmetric dyadic product of the vectors $a \odot b = \frac{1}{2}(ab^\top + ba^\top)$ and $a^\perp$ denotes the rotation by $\frac{\pi}{2}$. High-order versions can be constructed by setting $e_{ij}q(\lambda_i - \lambda_j)$ where $q \in \mathcal{P}^l(E)$. Interior bubble shape functions are given by $e_{ij}\lambda_k p^l(x,y)$, $p(x,y) \in \mathcal{P}^l(T)$. The construction of shape functions in 3D is similar but more involved [25].

Example A.1.6 *On the reference triangle the barycentric coordinates are $\lambda_1 = x$, $\lambda_2 = y$, $\lambda_3 = 1-x-y$ and $\nabla\lambda_1^\perp = \begin{pmatrix}0\\1\end{pmatrix}$, $\nabla\lambda_2^\perp = \begin{pmatrix}-1\\0\end{pmatrix}$, $\nabla\lambda_3^\perp = \begin{pmatrix}1\\-1\end{pmatrix}$. The shape functions read $e_{12} = \nabla\lambda_1^\perp \odot \nabla\lambda_2^\perp = -\frac{1}{2}\begin{pmatrix}0 & 1\\1 & 0\end{pmatrix}$, $e_{13} = \begin{pmatrix}0\\1\end{pmatrix} \odot \begin{pmatrix}1\\-1\end{pmatrix} = \begin{pmatrix}0 & 0.5\\0.5 & -1\end{pmatrix}$, $e_{23} = \begin{pmatrix}-1 & 0.5\\0.5 & 0\end{pmatrix}$. With $n_1 = \begin{pmatrix}-1\\0\end{pmatrix}$, $n_2 = \begin{pmatrix}0\\-1\end{pmatrix}$, $n_3 = \frac{1}{\sqrt{2}}\begin{pmatrix}1\\1\end{pmatrix}$ there holds $n_1^\top e_{12} n_1 = n_2^\top e_{12} n_2 = 0$ and $n_3 \top e_{12} n_3 = -\frac{1}{2}$. Analogously, $n_1^\top e_{13} n_1 = n_3^\top e_{13} n_3 = 0$, $n_2^\top e_{13} n_2 = -1$ and $n_2^\top e_{23} n_2 = n_3^\top e_{23} n_3 = 0$, $n_1^\top e_{23} n_1 = -1$.*

To preserve the normal-normal degree of freedom during transformation from the reference to the physical element, a double Piola transformation is considered $\boldsymbol{\sigma} \circ \Phi = \frac{1}{J^2}\boldsymbol{F}\hat{\boldsymbol{\sigma}}\boldsymbol{F}^\top$. Then

$$\int_F J_F \boldsymbol{\sigma}_{nn} \, ds = \int_{\hat{F}} \underbrace{J_{\hat{F}}}_{=1} \hat{\boldsymbol{\sigma}}_{\hat{n}\hat{n}} \, d\hat{s}.$$

Remark A.1.7 *There does not hold $M_h^k \subset H(\mathrm{divdiv}, \Omega)$ as point evaluation is not a functional in $H^{-1}(\Omega)$ for dimensions higher than 1. The discrepancy is by an $\varepsilon > 0$ as $\mathrm{divdiv} M_h \subset H^{-1-\varepsilon}(\Omega)$.*

A.1.6 $H(\mathrm{curlcurl})$ and Regge finite elements

We define the following function space for $d = 2, 3$

$$H(\mathrm{curlcurl}, \Omega) := \{\boldsymbol{\varepsilon} \in L^2(\Omega, \mathbb{R}^{d\times d}_{\mathrm{sym}}) \,|\, \mathrm{curl}((\mathrm{curl}\,\boldsymbol{\varepsilon})^\top) \in H^{-1}(\Omega, \mathbb{R}^{(3d-3)\times(3d-3)}_{\mathrm{sym}})\}. \tag{A.1.24}$$

with norm $\|\boldsymbol{\varepsilon}\|^2_{H(\mathrm{curlcurl})} := \|\boldsymbol{\varepsilon}\|^2_{L^2} + \|\mathrm{curl}(\mathrm{curl}\,\boldsymbol{\varepsilon}^\top)\|^2_{H^{-1}}$. The differential operator $\mathrm{curl}((\mathrm{curl}\,\boldsymbol{\varepsilon})^\top)$ is called the incompatibility of $\boldsymbol{\varepsilon}$ and denoted by $\mathrm{inc}\,\boldsymbol{\varepsilon}$.

The Regge finite element space is given by

$$\mathcal{R}^k := \{\boldsymbol{\varepsilon} \in L^2(\Omega, \mathbb{R}^{d\times d}_{\mathrm{sym}}) \,|\, \text{ for all } T \in \mathcal{T}\, \boldsymbol{\varepsilon} \circ \Phi_T = \boldsymbol{F}^{-\top}\hat{\boldsymbol{\varepsilon}}\boldsymbol{F}^{-1}, \hat{\boldsymbol{\varepsilon}} \in \mathcal{P}^k(\hat{T}, \mathbb{R}^{d\times d}_{\mathrm{sym}}), \boldsymbol{\varepsilon} \text{ is tt-continuous } \}, \tag{A.1.25}$$

which is (like for the HHJ finite element space) a slightly non-conforming subspace of (A.1.24). Here the doubled covariant transformation is used for the mapping from the reference to the physical element. Then the tangential-tangential component is preserved

$$\int_E \frac{1}{J_E} \boldsymbol{\varepsilon}_{t_E t_E} \, dl = \int_{\hat{E}} \frac{1}{J_{\hat{E}}} \hat{\boldsymbol{\varepsilon}}_{\hat{t}_{\hat{E}} \hat{t}_{\hat{E}}} \, dl.$$

The canonical Regge interpolant $\mathcal{I}_h^{\mathcal{R},k} : C^0(\Omega, \mathbb{R}^{d\times d}_{\text{sym}}) \to \mathcal{R}^k$ is determined by the following functionals for a triangle

$$\Psi_E(\boldsymbol{\varepsilon}) = \int_E \frac{1}{J_E} \boldsymbol{\varepsilon} : p\, t_E \otimes t_E \, ds \qquad p \in \mathcal{P}^k(E), \tag{A.1.26a}$$

$$\Psi_T(\boldsymbol{\varepsilon}) = \int_T \frac{1}{J} \boldsymbol{\varepsilon} : FQF^\top \, dx \qquad Q \in \mathcal{P}^{k-1}(T, \mathbb{R}^{2\times 2}_{\text{sym}}). \tag{A.1.26b}$$

Regge finite elements seem to be the natural space for discretizing strain and metric tensors, which have the natural continuity condition of being tangential-tangential continuous (metric lengths and strain stretches).

The relation between Regge and HHJ finite elements is similar to the relation between $H(\text{curl})$-conforming and $H(\text{div})$-conforming elements. Elements in the HHJ space are normal-normal continuous whereas elements in the Regge space are tangential-tangential continuous.

A.2 Sobolev spaces and finite elements on surfaces

Before introducing finite element spaces on surfaces, we must define function spaces on manifolds and start with the integration by parts formula. A comprehensive introduction to finite elements on surfaces can be found, e.g. in [15].

Theorem A.2.1 (Integration by parts on manifolds) *Let $\mathcal{S}$ by an $n-1$-dimensional submanifold of $\mathbb{R}^n$ with smooth boundary $\partial\mathcal{S}$. Further let ν be the normal vector, μ the co-normal, and $f \in C^1(\overline{\mathcal{S}})$ a differentiable function up to the boundary. Then there holds with the mean curvature H*

$$\int_{\mathcal{S}} \nabla_{\mathcal{S}} f \, ds = \int_{\mathcal{S}} f \, H\nu \, ds + \int_{\partial\mathcal{S}} f\mu \, dl. \tag{A.2.1}$$

Proof: See e.g., [15, Theorem 2.10.]. □

Definition A.2.2 *The set of* square-integrable *functions on the surface $\mathcal{S}$ is defined as*

$$L^2(\mathcal{S}) := \{u : \mathcal{S} \to \mathbb{R} \,|\, \|u\|_{L^2(\mathcal{S})} < \infty\}. \tag{A.2.2}$$

A function $f \in L^2(\mathcal{S})$ is weakly differentiable*, $u = \nabla_{\mathcal{S}} f \in L^2(\mathcal{S}, \mathbb{R}^n)$, if for all $\Psi \in C_0^\infty(\mathcal{S}, \mathbb{R}^n)$ there holds*

$$\int_{\mathcal{S}} f \, \mathrm{div}_{\mathcal{S}}(\Psi) \, ds = -\int_{\mathcal{S}} u \cdot \Psi \, ds + \int_{\mathcal{S}} H f \, \Psi \cdot \nu \, ds \tag{A.2.3}$$

and the Sobolev space $H^1(\mathcal{S})$ is given by

$$H^1(\mathcal{S}) := \{u \in L^2(\mathcal{S}) \,|\, \nabla_{\mathcal{S}} u \in L^2(\mathcal{S}, \mathbb{R}^n)\}. \tag{A.2.4}$$

For vector-valued function spaces on surfaces, we first define

$$L^2(\mathcal{S}, T\mathcal{S}) := \{u \in L^2(\mathcal{S}, \mathbb{R}^n) \,|\, u \cdot \nu = 0\}, \tag{A.2.5a}$$

$$L^2(\mathcal{S}, T\mathcal{S} \times T\mathcal{S}) := \{\boldsymbol{\sigma} \in L^2(\mathcal{S}, \mathbb{R}^{n\times n}) \,|\, \boldsymbol{\sigma}\nu = \nu^\top \boldsymbol{\sigma} = 0\} \tag{A.2.5b}$$

as the set of square-integrable tangential vector and matrix fields on $\mathcal{S}$ and then

$$H(\mathrm{div}, \mathcal{S}) := \{u \in L^2(\mathcal{S}, T\mathcal{S}) \,|\, \mathrm{div}_{\mathcal{S}}(u) \in L^2(\mathcal{S})\}, \tag{A.2.6a}$$

$$H(\mathrm{curl}, \mathcal{S}) := \{u \in L^2(\mathcal{S}, T\mathcal{S}) \,|\, \mathrm{curl}_{\mathcal{S}}(u) \in L^2(\mathcal{S})\}, \tag{A.2.6b}$$

and analogously $H(\mathrm{divdiv}, \mathcal{S})$.

The finite element spaces introduced in Section A.1 fall into two categories:

1. Spaces where the trace of a 3D element results in a 2D element of the same space.
2. Spaces where the trace of a 3D element does not lead to a valid 2D element of the same space.

The spaces H^1 and $H(\mathrm{curl})$ belong to the first class, whereas L^2, $H(\mathrm{div})$, and $H(\mathrm{divdiv})$ are contained in the second category.

Nevertheless, we generally describe how 2D flat elements can be mapped onto surfaces. Therefore, let $\hat{T} \subset \mathbb{R}^2$ be the reference element and $\Phi_T : \hat{T} \to \mathcal{T} \subset \mathbb{R}^3$ the mapping onto a surface element described above, i.e., Φ_T can be seen as an embedding ($\nabla\Phi_T \in \mathbb{R}^{3\times 2}$ has full rank).

Let $\hat{u}$ be an H^1-conforming finite element on $\hat{T}$. Then, we map it onto the surface with $u \circ \Phi_T := \hat{u}$. The L^2-conforming elements follow the same idea, see Figure A.1. Thus, we can define

$$Q_h^k(\mathcal{T}) := \{u \in L^2(\mathcal{T}) \,|\, \text{ for all } T \in \mathcal{T}\, \exists \hat{u} \in \mathcal{P}^k(\hat{T}) : \, u|_T \circ \Phi_T = \hat{u}\}, \tag{A.2.7}$$

$$U_h^k(\mathcal{T}) := \{u \in H^1(\mathcal{T}) \,|\, \text{ for all } T \in \mathcal{T}\, \exists \hat{u} \in \mathcal{P}^k(\hat{T}) : \, u|_T \circ \Phi_T = \hat{u}, \, u \text{ continuous}\}. \tag{A.2.8}$$

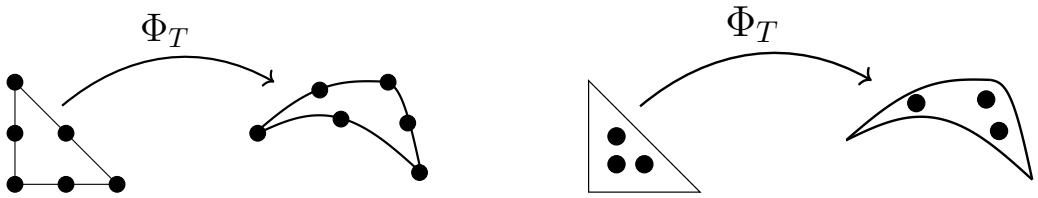

Figure A.1: Mapping of H^1- and L^2-conforming elements from reference triangle onto a curved physical surface element.

To preserve the normal or tangential continuity of $H(\mathrm{div})$- or $H(\mathrm{curl})$-conforming finite elements, the Piola and Covariant transformations are adapted

$$u \circ \Phi_T := \frac{1}{J}\boldsymbol{F}\hat{u}, \qquad \boldsymbol{F} = \nabla\Phi_T \in \mathbb{R}^{3\times 2}, \quad J = \sqrt{\det(\boldsymbol{F}^\top \boldsymbol{F})}, \tag{A.2.9}$$

$$v \circ \Phi_T = (\boldsymbol{F}^\dagger)^\top \hat{v}, \qquad \boldsymbol{F}^\dagger = (\boldsymbol{F}^\top \boldsymbol{F})^{-1}\boldsymbol{F}^\top, \tag{A.2.10}$$

with the Moore–Penrose pseudo inverse $\boldsymbol{F}^\dagger$. Therefore

$$\mathcal{N}_{II}^k(\mathcal{T}) := \{u \in H(\mathrm{curl},\mathcal{T}) \mid \text{ for all } T \in \mathcal{T}\ \exists \hat{u} \in \mathcal{P}^k(\hat{T},\mathbb{R}^2) :\ u|_T \circ \Phi_T = (\boldsymbol{F}^\dagger)^\top \hat{u}, [\![u_t]\!]_F = 0 \text{ for all } F \in \mathcal{F}^{\mathrm{int}}\}, \tag{A.2.11}$$

$$BDM^k(\mathcal{T}) := \{u \in H(\mathrm{div},\mathcal{T}) \mid \text{ for all } T \in \mathcal{T}\ \exists \hat{u} \in \mathcal{P}^k(\hat{T},\mathbb{R}^2) :\ u|_T \circ \Phi_T = \frac{1}{J}\boldsymbol{F}\hat{u}, [\![u_\mu]\!]_F = 0 \text{ for all } F \in \mathcal{F}^{\mathrm{int}}\}. \tag{A.2.12}$$

In the same spirit, the transformation rule for $H(\mathrm{divdiv})$ elements on surfaces is given by

$$\boldsymbol{\sigma} \circ \Phi_T := \frac{1}{J^2}\boldsymbol{F}\hat{\boldsymbol{\sigma}}\boldsymbol{F}^\top, \quad \hat{\boldsymbol{\sigma}} \in \mathcal{P}^k(\hat{T},\mathbb{R}^{2\times 2}_{\mathrm{sym}}). \tag{A.2.13}$$

The finite element space $M_h^k(\mathcal{T})$ is defined accordingly. To simplify notation we neglect the dependency of $\mathcal{T}$, if there is no chance of confusion.

Note that $\boldsymbol{F}$ in (A.2.9) acts as a push forward of the tangent vector field $\hat{u}$, if $\mathbb{R}^2$ is identified as a sub-manifold of $\mathbb{R}^3$. Thus, the transformed u is a tangent vector field on the surface. Further $\boldsymbol{\sigma}_h \in M_h$ acts on the tangent space of the surface, i.e., $\boldsymbol{\sigma}_h : \mathcal{T} \to T\mathcal{T} \times T\mathcal{T}$ and $\boldsymbol{\sigma}_h\nu = \nu^\top\boldsymbol{\sigma}_h = 0$.

The definitions of the facet space (3.5.2) and normal-facet space (3.5.3) on surfaces, denoted by $\Gamma_h^k(\mathcal{T})$ and $\Lambda_h^k(\mathcal{T})$, follow immediately. Note that for the normal-facet space, the Piola transformation must transform the involved co-normal vector.

Bibliography

[1] Douglas N. Arnold and Richard S. Falk. Asymptotic analysis of the boundary layer for the Reissner–Mindlin plate model. *SIAM Journal on Mathematical Analysis*, 27(2):486–514, 1996.

[2] Douglas N. Arnold and Johnny Gúzman. Local L^2-bounded commuting projections in FEEC, 2021.

[3] John M Ball. Convexity conditions and existence theorems in nonlinear elasticity. *Archive for Rational Mechanics and Analysis*, 63(4):337–403, 1976.

[4] Marcel Berger. *A Panoramic View of Riemannian Geometry*. Springer, Heidelberg, 2003.

[5] Dietrich Braess. *Finite Elements: Theory, Fast Solvers, and Applications in Solid Mechanics*. Cambridge University Press, Cambridge, 3rd edition, 2007.

[6] Dietrich Braess, Stefan Sauter, and Christoph Schwab. On the justification of plate models. *Journal of Elasticity*, 103(1):53–71, 2011.

[7] Carsten Carstensen and Georg Dolzmann. An a priori error estimate for finite element discretizations in nonlinear elasticity for polyconvex materials under small loads. *Numerische Mathematik*, 97(1):67–80, 2004.

[8] D. Chapelle and K.J. Bathe. Fundamental considerations for the finite element analysis of shell structures. *Computers & Structures*, 66(1):19–36, 1998.

[9] Philippe G Ciarlet. *Mathematical Elasticity. Vol. I: Three-Dimensional Elasticity*, volume 20. North-Holland, Amsterdam, 1988.

[10] Philippe G. Ciarlet. An introduction to differential geometry with applications to elasticity. *Journal of Elasticity*, 78-79(1):1–215, 2005.

[11] M. I. Comodi. The Hellan–Herrmann–Johnson method: Some new error estimates and postprocessing. *Mathematics of Computation*, 52(185):17–29, 1989.

[12] Eugene Cosserat and François Cosserat. Théorie des corps déformables. *Nature*, 81(67), 1909.

[13] Manfredo P. do Carmo. *Differential Geometry of Curves and Surfaces*. Prentice Hall, Inc., Englewood Cliffs, New Jersey, 1976.

[14] Georges Duvant and Jacques Louis Lions. *Inequalities in Mechanics and Physics*, volume 219 of *Grundlehren der mathematischen Wissenschaften*. Springer-Verlag, Berlin Heidelberg, 1 edition, 1976.

[15] Gerhard Dziuk and Charles M. Elliott. Finite element methods for surface PDEs. *Acta Numerica*, 22:289–396, 2013.

[16] Noel J. Hicks. *Notes on Differential Geometry*. Van Nostrand, 1965.

[17] W.T. Koiter. A consistent first approximation in the general theory of thin elastic shells. In W.T. Koiter, editor, *The theory of thin elastic shells*, pages 12–33. North-Holland, Amsterdam, 1960.

[18] Raz Kupferman and Jake P. Solomon. A Riemannian approach to reduced plate, shell, and rod theories. *Journal of Functional Analysis*, 266(5):2989–3039, 2014.

[19] Patrick Le Tallec. Numerical methods for nonlinear three-dimensional elasticity. volume 3 of *Handbook of Numerical Analysis*, pages 465–622. Elsevier, 1994.

[20] John M Lee. *Introduction to Riemannian manifolds*, volume 176. Springer, 2 edition, 2018.

[21] Jerrold E Marsden and T. J. R. Hughes. *Mathematical foundations of elasticity*. Dover Publication, Inc, New York, 1994.

[22] L. S. D. Morley. The constant-moment plate-bending element. *Journal of Strain Analysis*, 6(1):20–24, 1971.

[23] Jean-Marie Morvan. *Generalized curvatures*. Springer, 2008.

[24] PM Naghdi. The theory of shells. In S Flügge, editor, *Handbuch der Physik*, volume VI/2. Springer-Verlag, Berlin and New York, 1972.

[25] A. Pechstein and J. Schöberl. Tangential-displacement and normal-normal-stress continuous mixed finite elements for elasticity. *Math. Models Methods Appl. Sci.*, 21(8):1761–1782, 2011.

[26] A. Pechstein and Joachim Schöberl. The TDNNS method for Reissner–Mindlin plates. *Numerische Mathematik*, 137(3):713–740, 2017.

[27] R. S. Rivlin and J. L. Ericksen. Stress-deformation relations for isotropic materials. *Journal of Rational Mechanics and Analysis*, 4:323–425, 1955.

[28] Astrid Sinwel. *A new family of mixed finite elements for elasticity*. PhD thesis, Johannes Kepler Universität Linz, 2009.

[29] Michael Spivak. *A comprehensive introduction to differential geometry*, volume 1. Publish or Perish, Inc., Houston, Texas, 3 edition, 1999.

[30] Jakob Steiner. Über parallele Flächen. *Monatsber. Preuss. Akad. Wiss*, 2:114–118, 1840.

[31] Loring W. Tu. *Differential Geometry: Connections, Curvature, and Characteristic Classes*. Springer Science+Business Media, New York, NY, 2017.

[32] Peter Wriggers. *Nonlinear finite element methods*. Springer Science & Business Media, Heidelberg, 1 edition, 2008.